# Development of Three-limb, Full-mobility Parallel-kinematics Machines

#### $Wei\ Li$



Supervisor: Prof. Jorge Angeles

Department of Mechanical Engineering

McGill University, Montreal

Canada

April 2018

### **ABSTRACT**

Parallel-kinematics machines (PKMs) have been studied extensively because of their significantly higher performance in terms of accuracy, rigidity and load-carrying capacity over serial robots. However, they suffer from limited workspace, multiple singularities and coupled motion, which makes their design and analysis especially challenging. These issues have motivated extensive research on PKMs. In this dissertation, two novel classes of six-degree-of-freedom (dof) PKMs are proposed, namely, the 3-CPS and 3-CCC topologies. Their kinematics, singularity and workspace analyses, together with their optimum design, were conducted. Both classes of PKMs bear some common features. In particular, they both have three limbs, which yields less interference and larger workspace, when compared with the six-limb Stewart-Gough class. Moreover, all motors are mounted on the base, greatly reducing the inertia load of the system, while providing higher load-carrying capacity and better dynamics performance, which makes them quite suitable for high-speed operations. Furthermore, the two classes bear their own features, as discussed in detail herein.

The dissertation spans three topics. The first pertains to the kinematics, singularity and workspace analyses plus optimum design of the 3- $\underline{C}PS$  PKM, dubbed the SDelta—for six-dof Delta robot. It is shown that the given robot offers a large workspace with a proper choice of design variables. Moreover, we developed a novel method for its singularity analysis, which is applicable to a large number of parallel robots. Next, the SDelta optimum design for maximum dexterity is conducted. The axes of its six actuated wrenches intersecting pairwise, an expression for the inverse of the  $6 \times 6$  robot forward Jacobian matrix (FJM) is found symbolically. Based on this expression, we formulate an optimization problem of the robot geometry for maximum dexterity. It is shown that the SDelta can achieve a local minimum condition number close to unity.

The second topic is the design for isotropy of a large class of six-dof PKMs whose six

actuated wrenches intersect pairwise, thus covering numerous instances such as three-limb six-dof PKMs with one passive spherical joint in each limb, including the SDelta. The inverse of the FJM of the SDelta, derived here in symbolic form, turns out to be applicable to this class of PKMs. This result has a significant theoretical value, quite useful in singularity analysis, design for isotropy and optimization. In this dissertation, we elaborate on the application of the expression for the above-mentioned inverse to the optimum design of this class of PKMs. With this approach, we not only provide closed-form expressions for the optimum parameters for isotropy within this class, but also propose the concept of quasi isotropy, under which the robot, with a suitable design, can attain postures "close" to isotropy. This greatly increases the range of choice of the shape of the moving platform (MP) and the location of the operation point, while maintaining high dexterity. The latter is required, e.g., when a gripper or another tool is attached to the MP triangle.

The last topic is the analysis and optimum design of the 3-CCC PKM class. Firstly, its design for isotropy is investigated, based on which we find the conditions yielding the existence of a continuous set of isotropic postures. This feature is quite advantageous and probably unique for six-dof PKMs. Moreover, the forward-displacement of the same class, singularity and workspace analyses are conducted, which reveal many interesting features. For example, the associated forward-displacement solution allows for a simple formulation, which can be cast in closed-form; the rotation and translation motions of the MP are decoupled, the PKM singularity condition being determined solely by the MP orientation, and occurring only under large-amplitude rotations. Besides, this class bears a large workspace volume.

Due to the low inertia load of the proposed designs, they are capable of providing large accelerations, making them quite suitable for high-speed operations. This feature also makes them suitable for generating shaking operations (i.e., small-amplitude, high-frequency motions)—a major application we target, where large accelerations are needed. This operation can be used, for example, for inertia-parameter identification. Besides, the special features of the proposed architectures, especially the second, make them suitable for many other applications such as motion simulators, parallel manipulators, micro-manipulators, machine-tools, and medical devices.

## RÉSUMÉ

Les robots parallèles ont fait l'objet de nombreuses études en raison de leurs excellentes performances en matière de précision, de rigidité et de capacité de charge, qui sont supérieures à celles des robots sériels. Toutefois, la conception et l'analyse de ces robots sont compliquées par leur espace de travail limité, leurs singularités multiples et leur couplage rotation-translation, justifiant par là-même les recherches dans ce domaine. Cette thèse présente deux robots parallèles novateurs à six degrés de liberté, de topologie 3-CPS et 3-CCC. Leur cinématique, leur singularité, leur espace de travail et leur conception optimale sont étudiés. Les deux topologies partagent un certain nombre de caractéristiques : chacune a trois membres, ce qui réduit les interférences et élargit l'espace de travail, contrairement à la topologie Stewart-Gough à six membres. En outre, tous les moteurs sont montés à la base du robot, ce qui réduit l'inertie, augmente la capacité de charge et améliore les performances dynamiques du système, le rendant particulièrement bien adapté aux opérations à haute vitesse. Les deux topologies ont aussi leurs propres caractéristiques, exposées en détail dans cette thèse.

La thèse comporte trois volets. Le premier porte sur la cinématique, la singularité, l'espace de travail, et la conception optimale des robots parallèles à topologie 3-CPS, surnommés le SDelta—robot Delta à six degrés de liberté. Nous démontrons que ce robot a un vaste espace de travail lorsque ses variables sont adéquatement choisies lors de sa conception. Nous proposons également une nouvelle méthode d'analyse de singularité applicable à un grand nombre de robots parallèles. Nous présentons ensuite la configuration optimale du SDelta en vue d'une dextérité maximale. Les axes des six torseurs statiques motorisés se coupant deux à deux, nous obtenons une expression symbolique pour l'inverse de la matrice jacobienne 6 × 6 dite directe. Cette expression permet de formuler un problème d'optimisation de la géométrie du robot afin d'obtenir la dextérité maximale. On constate que le minimum local

du conditionnement numérique du SDelta est voisin de l'unité.

Le deuxième volet est la conception axée sur l'isotropie d'un grand nombre de robots parallèles à six degrés de liberté dont les couples mobiles se coupent deux à deux, ce qui est le cas de nombreux robots parallèles à trois membres et six degrés de liberté qui ont un joint sphérique passif dans chaque membre, comme le SDelta. L'inverse de la matrice jacobienne du SDelta montre qu'elle est applicable à ce type de robot parallèle. La valeur théorique de ce résultat est très utile pour l'analyse des singularités, pour la conception axée sur l'isotropie et pour l'optimisation. Nous appliquons l'expression de l'inverse dont il est question plus haut à la conception optimale de ce type de robots parallèles. Cette approche nous permet d'obtenir non seulement des expressions symboliques des paramètres d'isotropie pour ce type de robots, mais aussi de proposer le concept de quasi isotropie dans lequel le robot sous conception peut atteindre des positions «voisines »de l'isotropie. Elle élargit aussi considérablement la gamme des configurations de la plate-forme mobile et l'emplacement du point d'opération tout en conservant une excellente dextérité. La dextérité est effectivement nécessaire lorsqu'une pince ou un autre outil est fixé au triangle de la plate-forme mobile.

Le dernier volet porte sur l'analyse et la conception optimale des robots parallèles de type 3-CCC. Nous débutons par la conception axée sur l'isotropie d'où nous tirons les conditions qui mènent à un ensemble continu de positions isotropiques, ce qui est avantageux et probablement unique dans les robots parallèles à six degrés de liberté. En outre, nous analysons le problème dit direct du déplacement de ces robots, leurs singularités et leur espace de travail, ce qui donne des résultats intéressants. Ainsi, la solution relative au déplacement direct fait appel à une formulation simple qui peut être exprimée sous forme symbolique; les mouvements de rotation et de translation de la plate-forme sont découplés, la condition de singularité des robots parallèles étant alors seulement déterminée par l'orientation de la plate-forme et ne se produisant que dans des rotations de grande amplitude. De plus, ce type de robot a un grand espace de travail.

En raison de la faible inertie découlant de la conception proposée, ces robots peuvent fournir de fortes accélérations, ce qui les rend utiles dans les opérations à haute vitesse. Ils sont également intéressants pour générer des secousses (mouvements de faible amplitude à haute fréquence)—une application que nous visons, dans laquelle des fortes accélérations sont

nécessaires. Cette opération peut servir, par exemple, à identifier les paramètres d'inertie des corps solides. En outre, les architectures proposées, notamment la seconde, permettent d'utiliser ces robots dans des appareils aussi divers que les simulateurs de mouvements, les manipulateurs parallèles, les micro-manipulateurs, les machines outil et les appareils médicaux.

#### ACKNOWLEDGEMENTS

Firstly, I would like to express my most sincere gratitude to my supervisor, Prof. Jorge Angeles. Starting as a fast-track student with little research experience, I faced numerous challenges during my PhD studies, which I could never have overcome without his unreserved guidance. I would like to thank him for introducing me to the charming world of scientific research, which led to my determination of embarking on this path. Moreover, I would like to express my gratitudes to Profs. Jozsef Kövecses and Michael Kokkolaras, for serving as my Ph.D. Committee and their valuable comments. Furthermore, I would like to acknowledge the support from the McGill Engineering Doctoral Award and the Chinese Scholarship Council (CSC) for their financial support.

I would like to express my gratitudes to Drs. Xiaoqing Ma, Ting Zou, and Xiaowei Shan, former members of the *Robotic Mechanical Systems Laboratory* (RMSL), who have provided me not only plenty of help on my research but also a lot of good memories of working together. Special thanks to the group members Messrs. Thomas Friedlaender, Nate He, Mathew Shaker and Guillaume Sauze for their help in my course work, and to my friends, Dr. Yunlong Tang and Mr. Sheng Yang, for their valuable suggestions for my research and career. Most importantly, I would like to thank my parents, Zhenfa Li and Shuxin Dong, for their endless support all over my life.

#### CLAIMS OF ORIGINALITY

The main original contributions of this thesis are listed below:

- 1. Two novel six-dof PKM classes are proposed, one with a 3-CPS, the other with a 3-CCC topology. Both bear a three-limb architecture, yielding less interference and larger workspace when compared with their six-limb counterparts. Moreover, all six motors are located on the base, greatly reducing the inertia load of the system, which yields a higher load-carrying capacity and better dynamics performance. These features make these robots quite suitable for high-speed operations and the major application we target, shaking operations. Moreover, these PKMs bear various other special features, which will be introduced below, making the proposed architectures, especially the second, suitable for many other applications such as motion simulators, parallel manipulators, micromanipulators, machine-tools, medical devices, etc.
- 2. The forward-displacement, singularity and workspace analyses are conducted for the 3-<u>CPS PKM</u>. Furthermore, the optimization for maximum dexterity is conducted, which shows that it can achieve a local minimum condition number close to unity. These results indicate that it offers both large workspace and good dexterity with a proper choice of design variables.
- 3. A new formulation of the singularity analysis, based on a geometric interpretation of singularity, is proposed, which is applicable to a large class of six-dof PKMs whose six actuated-wrench axes intersect pairwise.
- 4. The inverse of the robot forward Jacobian matrix is found symbolically for this class. This expression has a significant theoretical value, highly useful in applications such as singularity analysis, design for isotropy and optimization.
- 5. The design for isotropy of the said class of PKMs is investigated. Closed-form relations among the design parameters are provided that yield isotropy.

- 6. The concept of quasi isotropy is proposed, which indicates robot postures whereby the six columns of the forward Jacobian matrix are mutually orthogonal, even though of slightly different Euclidean norms. The introduction of this concept greatly increases the range of choices of the shape of the moving platform (MP) and the location of the operation point while maintaining high dexterity, which is required, e.g., when a gripper or any other tool is attached to the MP triangle.
- 7. The design for isotropy is conducted for the 3-CCC PKM, indicating that there exists a continuous set of isotropic poses within the workspace of the 3-CCC PKM, which feature is quite advantageous and rare, probably unique, for six-dof PKMs. The conditions yielding this feature are studied in detail.
- 8. The forward-displacement, singularity and workspace analyses for the 3-<u>CCC PKM</u>, from which many other interesting features of this class were found.

# TABLE OF CONTENTS

A	ostra	ict —	1
$\mathbf{R}_{0}$	ésum	é	iii
A	ckno	wledgements	vii
C	laim	of Originality	ix
Li	${f st}$ of	Figures	$\mathbf{x}\mathbf{v}$
$\mathbf{A}$	bbre	viations	xix
N	omen	nclature	xx
1	Intr	Introduction	
	1.1	Motivation and Background	1
	1.2	Forward Displacement Analysis	4
	1.3	Singularity Analysis	5
	1.4	Workspace	6
	1.5	Performance Evaluation and Optimum Design	7
	1.6	The Organization of the Thesis	9
2	Arc	hitectures of the Two PKM Classes	11
	2.1	The 3- <u>CPS</u> Architecture	12
	2.2	The 3- $\underline{\mathbf{C}}$ CC Architecture	14
3	$\mathrm{Th}\epsilon$	e 3- <u>C</u> PS PKM	15
	3.1	Kinematics	15

		3.1.1	The Forward Jacobian and Drive Jacobian Matrices	10
		3.1.2	The Actuator Jacobian Matrix	18
		3.1.3	Redefinition of the Actuator Jacobian and the Drive Jacobian	19
	3.2	The F	orward-displacement Analysis	20
	3.3	Singul	arity Analysis	21
		3.3.1	Singularities of the Serial Jacobian Matrices	21
		3.3.2	Type-I Singularity	22
		3.3.3	Type-II Singularity	22
		3.3.4	Case Study: the Fixed-orientation Singularity Locus	25
	3.4	Works	pace Analysis	27
		3.4.1	The Geometrical Method for Workspace Quantification	27
		3.4.2	Case Study	29
	3.5	Singul	arity and Workspace Analyses—A Discussion	31
	3.6	The C	ptimum Design of the 3- <u>C</u> PS PKM for Maximum Dexterity	33
		3.6.1	Derivation of the Inverse of the Forward Jacobian Matrix	34
		3.6.2	Unconstrained Dexterity Maximization	39
			3.6.2.1 Derivation of the Norm of the Forward Jacobian	40
			3.6.2.2 Derivation of the Norm of the Inverse of the Forward Jacobian	41
			3.6.2.3 Solving the Optimization Problem at a Symmetric Posture .	42
			3.6.2.4 Some Remarks	45
		3.6.3	Discussion of the Optimization Results	46
4	${f Th}$	e Desi	gn for Isotropy of a Class of Six-dof PKMs	49
	4.1	The K	inematics Jacobian Matrix and Its Symbolic Inverse	50
		4.1.1	The Kinematics Relations	50
		4.1.2	The Symbolic Inverse of the Forward Jacobian	52
	4.2	The Is	otropic Design	54
		4.2.1	The Operation Point Lying in the MP Triangle	57
		4.2.2	The Operation Point Lying Outside of the MP Triangle	64
		4.2.3	The Isotropy of the Inverse Jacobian Matrix	68

5	$Th\epsilon$	e 3- <u>C</u> C	C Parallel-Kinematics Machine	71
	5.1	Kinen	natics	72
		5.1.1	The Derivation of the Jacobian Matrix	72
		5.1.2	The Inverse Jacobian and Actuator Jacobian	80
		5.1.3	Introducing the Characteristic Length	8.
	5.2	The Is	sotropic Design	83
		5.2.1	Geometric Conditions for Isotropy	83
		5.2.2	Realization of the Isotropic Design	85
			5.2.2.1 The Design of the Base Platform	85
			5.2.2.2 Design of the Moving Platform	86
			5.2.2.3 The Feasible Set of Characteristic Points	87
			5.2.2.4 Several Typical Layouts of the Proposed PKM	89
			5.2.2.5 Enumeration of Several Representative Designs	92
		5.2.3	Discussion	94
	5.3	The F	Forward-displacement Analysis	95
		5.3.1	The Orientation Problem	95
		5.3.2	The Positioning Problem	100
		5.3.3	Case Study	102
	5.4	Singu	larity Analysis	104
		5.4.1	Limb Singularity	105
		5.4.2	The Singularity of the Forward Jacobian Matrix	108
		5.4.3	The Singularity Analysis of the Inverse Jacobian	108
		5.4.4	Case Study	109
	5.5	Works	space Analysis	110
		5.5.1	The Geometrical Method for Workspace Quantification	110
		5.5.2	Case Study	111
	5.6	Forwa	ard-Displacement, Singularity and Workspace	
		Analy	rses—A Discussion	112

6 Closing Remarks and Recommendations		sing Remarks and Recommendations for Future Research	115	
	6.1	Conclusions	115	
	6.2	Recommendations for Future Research	117	
$R\epsilon$	efere	nces	119	
Aŗ	f Appendix			
	A.1	The Three-Cosine Theorem	129	
	A.2	The Coefficients of the Resultant Polynomial for the Forward-Kinematics of		
		the 3- <u>C</u> CC PKM	129	

# LIST OF FIGURES

1.1	An example of Stewart-Gough platform (reproduced from [1])	2
2.1	Architecture of the SDelta Robot	12
2.2	An embodiment of the C-drive	12
2.3	Graph of the SDelta robot	13
2.4	Graph of the C-drive	13
2.5	An example of a 3-CCC PKM	14
2.6	Graph of the 3- $\underline{\mathrm{CCC}}$ PKM	14
3.1	Notation for the kinematic chain of the $j$ th limb of the SDelta Robot	16
3.2	Dimensions of the SDelta Robot: (a) top view; (b) front view	16
3.3	The workspace and singularity loci of the SDelta at the reference orientation	
	(a) Design I (b) Design II	26
3.4	The workspace and singularity loci of the SDelta with the orientation ${f q}=$	
	$[0,0,1]^T$ and $\theta=15^\circ$ (a) Design I (b) Design II	26
3.5	The workspace and singularity loci of the SDelta with the orientation ${f q}=$	
	$[0,1,0]^T$ and $\theta=15^\circ$ (a) Design I (b) Design II	27
3.6	Illustration of the workspace formulation based on the geometric method $$ . $$	28
3.7	The workspace of the SDelta under the reference orientation (a) Design I (b)	
	Design II	30
3.8	The workspace of the SDelta with the orientation $\mathbf{q} = [0,0,1]^T$ and $\theta = 15^\circ$	
	(a) Design I (b) Design II	30
3.9	The workspace of the SDelta with the orientation $\mathbf{q} = [0, 1, 0]^T$ and $\theta = 15^\circ$	
	(a) Design I (b) Design II	30
3 10	The workspace volume w r t the ratio of $a/b$ under different orientations	31

3.11	Alternative layouts of the three C-drives	32
3.12	Inverse condition number of the robot vs. $\beta$ and $\gamma$ , (a) $\beta \in (-1,1), \gamma \in (-2,2)$	
	(b) $\beta \in (-1,7), \gamma \in (-2,2)$	45
3.13	(a) Condition number of the SDelta Robot vs. $\beta$ and $\gamma$ , using the unique	
	characteristic length for the architecture (b) the difference between (a) and	
	previous calculation shown in Fig. 3.12	46
3.14	An example of the SDelta indicating its large orientation capacity when the	
	centroid of the MP is close to the BP plane	47
4.1	Architecture of the SDelta Robot	51
4.2	The wrench axes $\mathcal{G}_j$ , $\mathcal{E}_j$ , their common perpendicular $\mathcal{F}_j$ , and vector $\mathbf{p}_j$ of the	
	jth limb of the S Delta Robot	51
4.3	The layout of $\mathbf{f}_j$ in the MP plane $(\Pi_4)$ and the definition of $\theta_j$ (top view)	57
4.4	The definition of $\epsilon_j$ and $\gamma_j$ , in plane $\Pi_j$	57
4.5	One of the two layouts of $\Pi_j$ , $\mathbf{e}_j$ and $\mathbf{g}_j$ that may render isotropy	61
4.6	The directions of $\mathbf{f}_j$ coinciding with the three edges of the the tetrahedron .	61
4.7	An example of an isotropic Stewart-Gough platform with the operation point	
	at the centroid of the MP triangle	63
4.8	An example of an isotropic Stewart-Gough platform with the operation point	
	lying outside of the plane of the MP triangle	63
5.1	The determination of the BP and MP using $\mathbf{d}_i,  \mathbf{c}_0$ and $\mathbf{p}_i $	86
5.2	The surface of feasible points of isotropy within a cube of edge length $\ell$	91
5.3	The surface of feasible points of isotropy within a cube of edge length $1.5\ell$ .	91
5.4	An example of an isotropic design for Layout I	94
5.5	An example of an isotropic design for Layout II	94
5.6	An example of an isotropic design for Layout III	94
5.7	An example an the isotropic design for Layout IV	94
5.8	The architecture of a 3 $\underline{C}$ CC PKM for case study	102
5.9	The layouts corresponding to those solutions in the case study of the forward	
	kinematics	104

5.10	Singularity of the 3- <u>CCC PKM</u> (a) the curve for limb singularity (b) the limb	
	singularity and that of ${\bf K}$	110
5.11	The workspace of the $3-\underline{C}CC$ PKM (a) under the reference orientation (b)	
	with the orientation $\mathbf{e} = [1,0,0]^T$ and $\phi = 15^\circ$ (c) $\mathbf{e} = [0,0,1]^T$ and $\phi = 15^\circ$	
	(d) $\mathbf{e} = [1/\sqrt{3}, 1/\sqrt{3}, 1/\sqrt{3}]^T$ and $\phi = 15^{\circ}$	112
A 1	The illustration of the three-cosine theorem	129

# LIST OF ABBREVIATIONS

PKM Parallel-kinematics machine

BP, MP Base platform and moving platform

FJM Forward Jacobian matrix

dof degree of freedom

SGP Stewart-Gough platform

FDP forward displacement problem

DfI design for isotropy

R, P, H, C, U and S joints revolute, prismatic, screw, cylindrical, universal

and spherical joints

OP operation point

ERP Euler-Rodrigues parameters

#### NOMENCLATURE

- Forward Jacobian Matrix: the coefficient of the twist in the kinematic relation between twist array and motor-rate array. Represented as **K**.
- Inverse Jacobian Matrix: the coefficient of the motor-rate array in the foregoing kinematic relation. Represented as J.
- Actuator Jacobian Matrix: the matrix that maps the motor-rate array into the sixdimensional array of C-drive rates. Represented as  $\mathbf{J}_m$ .
- Drive Jacobian Matrix: the matrix that maps each column of the actuator Jacobian matrix into the corresponding column of the inverse Jacobian matrix. Represented as **D**.
- Quasi Isotropy: the property of a PKM to attain postures whereby a) its forward and inverse Jacobian matrices attain condition numbers "slightly above" unity and b) the columns of each of the two Jacobian matrices are mutually orthogonal.

#### Chapter 1

#### INTRODUCTION

#### 1.1 Motivation and Background

A parallel-kinematics machine (PKM) is defined as a multi-degree-of-freedom (multi-dof) articulated mechanical system composed of one moving platform (MP) and one base platform (BP), connected by at least two serial limbs [2]. Compared to their serial counterparts, PKMs offer a significantly higher performance in terms of accuracy, rigidity and load-carrying capacity, thereby leading to a wide variety of applications such as motion simulators, parallel manipulators, haptic devices, micro-manipulators, six-axis force/torque sensors and machinetools [2,3]. On the other hand, PKMs suffer of drawbacks such as limited workspace, multiple singularities, coupled motion and complex-control requirements. As a result, numerous researchers are working on PKMs research and development.

Early works on six-dof PKMs are found mostly around the Stewart-Gough platform (SGP) [4,5], whose MP and BP are connected via six limbs, as shown in Fig. 1.1. This number, however, results in severe interference, complex singularity loci and limited workspace. Despite these shortcomings, most six-dof PKMs in industry still utilize this structure nowadays. Various researchers have proposed alternative structures with a lower number of limbs and different actuation schemes. Among these, three-limb, six-dof symmetric PKMs are probably the most promising candidates in applications where six-dof mobility, homogeneous performance and relatively large workspaces are required [6,7].

Numerous three-limb six-dof PKMs can be found in the literature [7–17]. However, when the number of limbs is smaller than six, each limb has to be actuated by more than one motor; hence, most of these designs have some motors mounted on moving links. The presence of

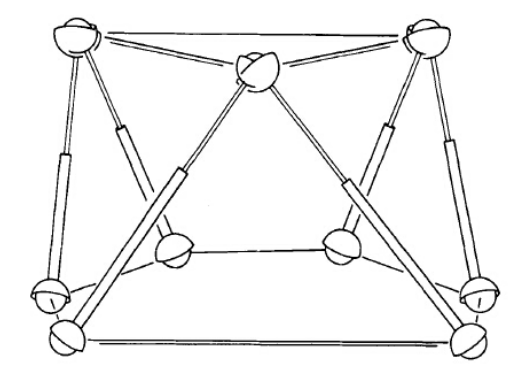


Figure 1.1: An example of Stewart-Gough platform (reproduced from [1])

floating motors leads to a waste of installed power<sup>1</sup>; moreover, the load-carrying capacity and dynamic performance are compromised. Thus, PKMs with all actuators located on the base are preferred, as they are capable of producing large accelerations, making them especially suitable for high-speed operations and the major application we target—shaking operations, to be introduced presently. Several designs with all the motors mounted on the base have been proposed. For example, Sorli et al. [10] used three double-parallelogram mechanisms to realize this goal, but this design resorted to many extra components, which led to extra interference. Chen et al. [11] proposed a six-dof haptic device using two-dof planetary-belt systems; these systems unavoidably introduce belt slip and flexibility, thus making them unsuitable for high-speed or high-torque applications. One major problem with these designs is that most of the actuation systems either are extremely complex or introduce many extra moving parts, thereby exacerbating the link interference, while limiting the workspace. Many other parallel robots carrying three limbs have been proposed [7,12–16], either failing to have all actuators mounted on the base or achieving this at the expense of a complex actuation system.

In this dissertation, two architectures are proposed, with all their motors mounted on the base, which is realized upon introducing a simple two-dof cylindrical actuator, the C-Drive [18]. This feature yields lower inertia load, higher load-carrying capacity and better dynamic performance, making them suitable for high-speed and shaking operations—the major application we target. Shaking operations, i.e., small-amplitude, high-frequency motions, can be used, e.g., for rigid-body inertia-parameter identification. A rigid body bears 10 inertia

<sup>&</sup>lt;sup>1</sup>Increased load for the motors mounted on the BP.

parameters, usually listed as mass, position vector of the centre of mass, and the symmetric, positive-definite inertia tensor [19]. Alternatively, rather than the position vector of the centre of mass, the moment of mass can be considered, namely, the product of the mass times the foregoing position vector<sup>2</sup>. With the growing demand for high-speed and high-precision operations, the precise knowledge of the inertia properties of a rigid body is becoming more and more important, which can be used in many applications, e.g., for high-speed operations and model-based control, among others.

Inertia-parameter identification is based on the dynamics model: the specimen, a rigid body, undergoes a prescribed trajectory, and the histories of the acceleration and the wrench exerted on the specimen are recorded. If we insert these data into the dynamics model, a system of linear equations in the inertia parameters is obtained, from which these parameters can be estimated. While various approaches for inertia-parameter identification have been proposed, they suffer from various drawbacks, the accuracy of their results being mediocre; a comprehensive comparison is available in the literature [19].

A key issue for the identification process is the type of motion the specimen undergoes. Even though numerous attempts have been made in the identification in the time domain—mostly based on large-amplitude motion, the identification results are usually unsatisfactory. Indeed, the excitation frequency range for such a motion is narrow, which renders the test incapable of providing sufficient excitation to all the six dof of the specimen motion. On the other hand, small-amplitude, high-frequency (shaking) operations about all six directions of the motion space is advantageous due to their capacity of providing sufficient excitation to the specimen along all six directions. This increases the signal-to-noise ratio. Moreover, these operations generate data over a broad frequency range. These features are essential for increasing the accuracy of the identification process. Approaches based on small-amplitude vibrations can be found in the literature, see, e.g., [20–23]. However, due to the limitation of the current equipment, the frequency they can achieve is mostly low, which limits the acceleration generated on the specimen. Hence, novel equipment that can provide small-amplitude, high-frequency shaking operations is needed.

<sup>&</sup>lt;sup>2</sup>As pointed out by Professor J.R. Forbes, the internal examiner

Six-dof PKMs are naturally suitable for this task due to their high load-carrying capacity, accuracy and stiffness. Attempts of using six-dof PKMs for identification have been made based on the Stewart-Gough Platform [22, 23]. However, the complex singularity locus, limited workspace and coupled motion impose difficulties in this process. Two architectures are proposed in this dissertation, both with all their motors mounted on the base, greatly reducing the inertia load of the system, thereby making them capable of providing higher acceleration (excitation), which is essential for inertia-parameter identification. Moreover, these PKMs have some other interesting features, especially the 3-CCC class<sup>3</sup>, which offers: simple forward-displacement model; decoupled rotation and translation; simple singularity; a large workspace and high dexterity, making this class more attractive for the task at hand. These features also make the class of interest promising in some other applications, such as motion generation, to cite just one. For example, high-frequency operations are needed in flight simulators to emulate the disturbances brought about by turbulence with high fidelity. Other applications can be cited, also motivated by flight simulation, e.g., high-amplitude rotations of the MP, as needed in airplane acrobatics.

It is noteworthy that this dissertation focuses on kinematics analysis and design, dynamics lying outside of its scope. Next, we provide a literature survey on the approaches for the analyses and optimization related to the kinematics.

#### 1.2 Forward Displacement Analysis

The forward displacement problem (FDP) consists in determining the pose of the MP of a PKM given its actuated joint variables, which is essential in path-planning and feedback control. The FDP of PKMs involves solving a system of nonlinear equations, which is usually quite complex, leading to a 40th-degree polynomial in the case of the most general Stewart-Gough platform [24]. According to Merlet [3], methods of analysis mainly resort to polynomial continuation [25], Gröbner bases [26] and dialytic elimination [27, 28]. Polynomial continuation is capable of providing, numerically, all the solutions of the given problem, which can be used to solve very large systems, its main disadvantage being its high compu-

 $<sup>^3</sup>$ In this dissertation, R, P, H, C , U and S denote revolute, prismatic, screw, cylindrical, universal and spherical joints, respectively, underlined symbols denoting an actuated joint.

tational complexity. Gröbner bases offer currently the fastest method to solve the forward displacement problem in a guaranteed manner [29], but this approach can be applied only when the coefficients of the equations are rational. Regarding dialytic elimination, the system of algebraic<sup>4</sup> equations is reduced to one univariate polynomial equation upon eliminating one unknown at a time. Elimination methods allow for the study of the properties of the solutions, even though they generally require ad hoc algebraic manipulations.

Besides the above methods, several other approaches have been proposed. Boudreau [30] proposed a novel method based on genetic algorithms, but these are quite time consuming. Merlet [29] proposed a new method based on interval analysis. This method is claimed to be safer in terms of producing the correct solutions corresponding to the current assembly mode. Some other pertinent approaches can be found in the literature [31,32].

#### 1.3 Singularity Analysis

Singularity is one of the major issues arising in PKM analysis and design. Unlike serial mechanisms, PKMs possess complex singularity sets<sup>5</sup> within their workspace. At singular configurations, a PKM will lose or gain degrees of freedom instantaneously, while losing either stiffness or mobility, or encountering extreme internal forces, thereby leading to uncontrollable motion, poor performance and even damage of the mechanism. Due to the complex characteristics of the singularity locus, it is quite challenging to achieve a good understanding of the singularity set with the purpose of avoiding it. Singularity analysis has thus been a central topic in PKM analysis for a long time. This section provides a review of the different approaches reported for singularity analysis.

According to Merlet [3], there exist four general approaches for singularity analysis, based on: screw theory; Grassmann geometry; differential geometry; and the rank-deficiency condition of the Jacobian matrices. Hunt proposed a general framework for singularity analysis using screw theory [33]. Kumar [34] developed a general method for kinematics and singularity analysis by means of the reciprocal-twist and wrench systems. Later, a more systematic method was proposed by Merlet [35], who used Grassmann geometry to identify singular

<sup>&</sup>lt;sup>4</sup>i.e., mutivariate polynomials.

<sup>&</sup>lt;sup>5</sup>Also referred to as singularity surface in the literature.

configurations, and introduced a series of simple geometric rules by which he found all the singularity configurations known at that time. Merlet's work [35] is a major contribution to this subject, as it provides a powerful and systematic tool for singularity analysis. However, although it is generally possible to identify the geometric conditions for singular configurations by the rules introduced by Merlet, it may be difficult to express the geometric conditions algebraically. These are essential for obtaining the expression for the singularity locus, as needed for graphic-visualization and real-time control purposes. Park et al. [36] proposed a differential-geometric method for the analysis of singularities of closed-loop chains. As for methods based on the rank-deficiency of the Jacobian matrices, one may obtain the equations of the singularity set by equating the determinant of the Jacobian matrices to zero, but this approach encounters a major challenge of computational cost, since the corresponding characteristic polynomials are extremely cumbersome. Numerical algorithms have been proposed based on these observations [37, 38].

Besides the above general methods, several approaches have been proposed for the singularity analysis of a specific class of PKMs [39–43], i.e., six-dof PKMs whose six actuated-wrench axes intersect pairwise. This covers a large number of PKMs—see, for example, [41, 44]—and the SDelta investigated in this dissertation. The singularity condition of this class of PKMs lends itself to a straightforward geometrical interpretation, besides a simpler formulation [44–46]. Based on this interpretation, we propose a novel formulation to derive one single, simple expression for the singularity condition, applicable to this large class of PKMs.

#### 1.4 Workspace

Workspace is one of the most important attributes of PKMs. Since the workspace for a six-dof PKM is embedded in a six-dimensional space that cannot be represented graphically, one usually investigates its 3D subsets by fixing three of the six Cartesian coordinates of the MP, such as the constant-orientation workspace, reachable workspace, dexterous workspace, orientation workspace, etc. [3]. Merlet [3] classified the pertinent methods into geometrical [47,48], discretization [13,49–51] and numerical [52–54].

Geometrical methods offer some advantages: they are usually much faster, more accurate

and simpler to implement for some applications, such as calculating the workspace volume [3]. Their main disadvantage is that their complexity heavily depends on the structure of the PKM and the types of constraints that need to be considered. Examples are provided by Gosselin [55], Merlet [56] and Bonev et al. [48]. Discretization methods have been favoured for their simplicity and capacity of handling all the constraints [49, 51]. These methods, however, face several problems: they are quite demanding computationally; their accuracy depends on the fineness of the grid, while their computation time grows exponentially with the "grid resolution"; it is hard to treat cases involving voids inside the workspace. As for numerical methods, there exist two typical principles: the first is based on the rank-deficiency of the Jacobian matrix of the system of equations describing the constraints on the workspace boundary [52, 53]. Given that the range of motions of a R joint is finite—not so that of P joints, if one makes abstraction of the joint physical limitations—these joints define motions of MP points with a zero velocity component normal to the workspace boundary, an observation on which the second principle is based [57].

Besides the above methods, some researchers have introduced several ad-hoc methods. For example, Merlet et al. [58] proposed general algorithms based on interval analysis, which can be applied to different structures, even though they are also computationally expensive. Bohigas et al. [59] proposed a method using the branch-and-prune technique. Johnson et al. [60] proposed a method that produces a set of two-dimensional cross-sections of the workspace region with the aid of CAD software, which does not require any analytical work. Some researchers utilized optimization algorithms to find the workspace, such as Snyman et al. [61].

In this dissertation, a geometric approach is used for the two classes due to its accuracy, efficiency and convenience in terms of workspace volume computation.

#### 1.5 Performance Evaluation and Optimum Design

Different applications may impose requirements on different aspects, such as workspace volume, dexterity, stiffness and accuracy; in order to evaluate the performance in these aspects, various indices have been proposed [62]. Among these, the most widely used include

dexterity, manipulability, isotropy, workspace volume, etc. A comprehensive review of performance indices appeared recently [63].

Dexterity characterizes the accuracy of the robot and the homogeneity of the motion of the MP along different directions of the six-dimensional Cartesian space [62,63]; as a result, dexterity analysis is crucial in robot design and analysis. Dexterity can be characterized by the condition number of the kinematic Jacobian matrix [64], a dimensionless scalar ranging from 1 to infinity. The lower the condition number, the higher the dexterity. Furthermore, when the condition number of the Jacobian matrices can achieve their minimum, i.e., unity, the corresponding dexterity reaches its maximum, under which the robot at hand is called isotropic. Since the six rows (columns) of the Jacobian matrices are orthogonal at isotropic postures<sup>6</sup>, the positioning accuracy of the robot along all six directions of the Cartesian space is a maximum [62,63,65]. When isotropy is achievable for a given PKM, the optimization problem can be formulated in a different form, which offers an alternative and more efficient way for the optimization.

The design for isotropy of serial robots has been discussed in the literature [65–67]. In the case of parallel robots, two Jacobians come into play<sup>7</sup>, the isotropy conditions being more challenging than serial robots. Examples of isotropic designs can be found in the literature [68–71].

It was found that the SDelta does not allow an isotropic design. Hence, an optimization for maximal dexterity is conducted based on the condition number. However, based on the expression of the inverse of the *forward Jacobian* matrix, derived for the SDelta, a novel approach is proposed for the design for isotropy (DfI) of a large class of PKMs. Lastly, it is found that the 3-CCC PKM not only allows for isotropy, but in fact, allows for a continuous locus of isotropy, which is quite advantageous and rare for PKMs. The conditions yielding this feature are investigated in detail.

<sup>&</sup>lt;sup>6</sup>This statement presupposes a *normalization* of the Jacobian, by means of the robot *characteristic length*, so as to render all the Jacobian entries dimensionally homogeneous.

<sup>&</sup>lt;sup>7</sup>In a PKM, in general, two Jacobian matrices occur in the kinematics model, relating the moving-platform twist with the array of actuator rates. The one multiplying the former is termed the *forward Jacobian* [68], that multiplying the latter, the *inverse Jacobian*.

#### 1.6 The Organization of the Thesis

Chapter 1 includes the motivation and background of this dissertation: Firstly, an introduction of PKMs is given, followed by a review of the existing three-limb six-dof PKMs, while highlighting the advantages of designs with all the motors mounted on the base. Next, the significance of inertia-parameter identification and the drawbacks of approaches based on large-amplitude motion are given, from which it is apparent that shaking operations, one major application we target, is quite advantageous for this task. Lastly, the approaches for the kinematics, singularity and workspace analyses of PKMs, and the literature survey on their optimum design, are provided. It is noteworthy that this dissertation only focuses on the design and analysis based on the kinematics; the dynamics analysis and optimization are out of the scope of this dissertation.

Chapter 2 is dedicated to the description of the architectures of the two proposed PKMs. Their design philosophy, topology, actuation scheme and features are discussed.

Chapter 3 is devoted to the analysis and optimum design of the SDelta robot. Firstly, its kinematics, singularity and workspace analyses are provided. Its forward-displacement analysis leads to a system of three quadratic equations in three unknowns, which admits up to eight solutions, or half the number of those admitted by the simplest SGP<sup>8</sup>. Next, we developed a novel method for its singularity analysis, which is also applicable to a large number of parallel robots. Furthermore, the workspace is analyzed via a geometric method. Next, the optimal design of the SDelta is conducted. Due to the special structure of its Jacobian matrix, we find the inverse of the robot forward Jacobian matrix symbolically, based on which we formulate an optimization problem of the robot for maximum dexterity. Drawing from the optimization results, we offer some guidelines on the choices of the optimum design parameters. It is shown that the SDelta can achieve a local minimum condition number close to unity. The above results indicate that the given robot has the potential to offer both large workspace and good dexterity with a proper choice of design variables.

Chapter 4 is devoted to the design for isotropy of a large class of PKMs, i.e., six-dof

<sup>&</sup>lt;sup>8</sup>Six limbs laid out so that their axes intersect pairwise at the BP and the MP, with different pairs of each platform, common in flight simulators.

PKMs whose six actuated wrenches intersect pairwise, covering numerous PKMs such as all the three-limb six-dof PKMs with one passive spherical joint in each limb, including the SDelta. The inverse of the Jacobian matrix of the SDelta, derived in Chapter 3 turns out to be applicable to this large class of PKMs, which is found to be highly attractive in many applications, e.g., singularity analysis, design for isotropy and optimization. In this chapter, the application of this symbolic expression to the optimum design of this large class of PKMs is introduced, where we provide closed-form expressions of the geometric conditions that yield isotropic architectures. We also propose the concept of quasi isotropy, under which a condition number close to unity is possible, while the six rows of the Jacobian matrix are orthogonal; hence, the performance under such configurations is close to isotropy. This greatly increases the range of the choices of the shape of the MP and the location of the operation point, which is required, e.g., when a gripper or another tool is attached to the MP.

Chapter 5 is devoted to the optimum design and analysis of the 3-CCC PKM. Firstly, its design for isotropy is investigated, based on which we find the conditions on the design parameters leading to the existence of a continuous set of isotropic postures. This feature is quite advantageous and rare for six-dof PKMs. Furthermore, the forward-displacement, singularity and workspace analyses of the proposed PKM are conducted, which reveal many interesting features. For example, the pertinent forward-displacement problem allows for a simple formulation, which can be solved in closed-form; the rotation and translation motions of the MP are decoupled; the singularity is determined solely by the MP orientation, and occurring only under large-amplitude rotations. This class bears a reasonably large workspace volume, among other features.

Chapter 6 summarizes the work of this dissertation, offers some recommendations for future work, and concludes the thesis.

#### Chapter 2

#### ARCHITECTURES OF THE TWO PKM CLASSES

Upon consideration of the drawbacks of the existing PKMs, summarized in the Introduction, three design principles are proposed in this dissertation:

- Three-limb, six-dof symmetric PKMs are preferred, in light of their advantages over their six-limb counterparts, namely, lower interference and hence, larger workspace.
- Designs with base-mounted motors are required, since travelling motors significantly increase the inertia load of the system, thereby affecting the load-carrying capacity and dynamic response of the robot. This requirement can be met by means of multi-dof actuators, such as cylindrical [18], planar motors [72], spherical actuators [73], among others, with their own advantages and disadvantages in terms of stiffness, accuracy and availability. However, actuators of this kind are not yet readily available off the shelf, as many are still at the development phase. Here we utilize a novel cylindrical actuator that we have been developing over the last four years in McGill University's Robotic Mechanical Systems Laboratory.
- Designs with fewer components are preferred, in order to reduce interference and simplify their dynamics characteristics. Hence, multi-dof joints are preferable, such as universal (U), cylindrical (C), and spherical (S). S joints, moreover, can be generated by an assembly of U and R joints, which is simpler to implement while offering a larger range of motion.

Taking these considerations into account, we propose two topologies, namely,  $3-\underline{CPS}$  and 3-CCC.

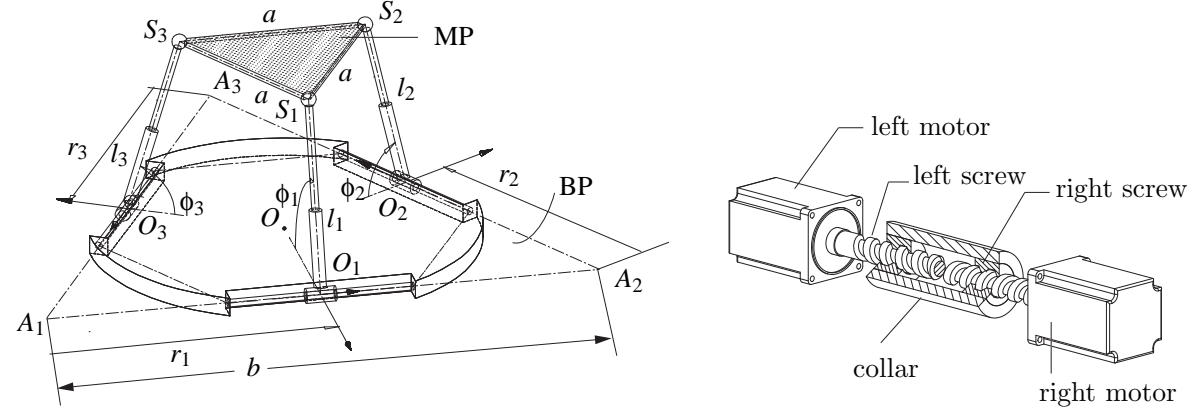


Figure 2.1: Architecture of the SDelta Robot

Figure 2.2: An embodiment of the C-drive

#### 2.1 The 3-CPS Architecture

The first architecture, dubbed the SDelta Robot—for the six-dof Delta robot<sup>1</sup>, bears a 3-CPS topology, each C joint being realized with a two-dof cylindrical actuator, dubbed the C-Drive [18], as shown in Figs. 2.1 and 2.2. First and foremost, what distinguishes the SDelta from other three-limb (or three-loop) parallel robots is its topology, as it is based on three parallel actuation mechanisms, each with a RHHR topology [18], as displayed in Figs. 2.3 and 2.4. In these figures, 0 denotes the BP, while the closed subchain 0-1-2-3-0 denotes one of the three actuation mechanisms, one on each side of the equilateral triangle of Fig. 2.3. In these subchains, 2 is the driving link of one limb, 5 and 8 those of the two other limbs. Moreover, 1 and 3 denote the left-hand and the right-hand screws, driven by corresponding rotary motors. Moreover, 10, 11 and 12 denote the links of the passive C-joints making up each limb, which are coupled to the MP (13) by means of spherical joints [75].

As stated in the Introduction, each limb has to carry two motors for a three-limb six-dof PKM, and hence, most current designs have travelling motors, which limits the robot performance. Here, we introduce a parallel substructure in each serial limb, i.e., the two-dof cylindrical actuator, the C-drive [18], as shown in Fig. 2.2, to locate all the motors on the base for the proposed PKM. As stated previously, this drive carries one single-loop closed kinematic chain of the  $\underline{R}\underline{H}\underline{H}\underline{R}$  type; the two H joints, of identical pitches p but of opposite hands, lead to a  $2\times 2$  constant, isotropic Jacobian matrix of the drive mechanism, which is the simplest possible. The C-drive operates as a differential: when the two motors turn in

<sup>&</sup>lt;sup>1</sup>The original, three-dof Delta Robot, was patented by R. Clavel, EPFL, Switzerland [74].

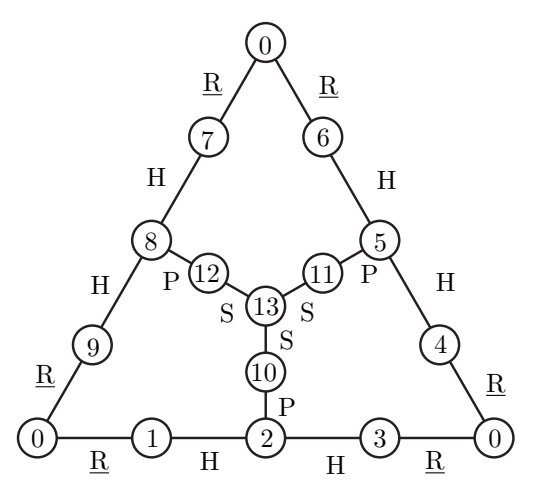


Figure 2.3: Graph of the SDelta robot

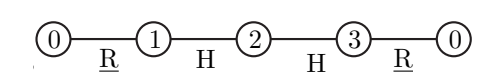


Figure 2.4: Graph of the C-drive

the same sense<sup>2</sup> at the same rate, the collar undergoes a pure rotation; when the two motors turn in opposite senses at the same rate, the collar undergoes a pure translation. Each limb is thus driven in both translation along a given direction and rotation about an axis parallel to the same direction. Now, regarding the embodiment of the limb kinematic chains, in light of manufacturability issues, we do not recommend the use of a <u>CPS</u> chain, which is used in the thesis as a simple description of the topology of each of the three limbs. We recommend, instead, its <u>CCU</u> equivalent, since the P joint suffers of what is known as the "sticky-drawer effect" [76].

The SDelta Robot has the advantage that its architecture is simple, with fewer components than other three-limb designs, which reduces the complexity of its architecture and hence, simplifies its dynamics model and its control. This simplicity also reduces the potential interference among the limbs, thus resulting in a larger workspace. Moreover, mounting all motors on the base reduces the inertial load on the system, thereby making it suitable for high-speed operations, and the major application we target—shaking operations. A similar topology, a 3-PRPS limb kinematic chain, was proposed by Behi [8], whose first two joints form a C-joint; in this design, however, the two prismatic joints in each limb are actuated, and hence, each limb has one floating motor, thereby increasing significantly the inertia load of the system.

<sup>&</sup>lt;sup>2</sup>As viewed from the same side of the drive layout.

## 2.2 The 3-CCC Architecture

Next, we propose a second architecture with all the motors mounted on the base, which bears a 3-CCC topology, as shown in Figs. 2.5 and 2.6.

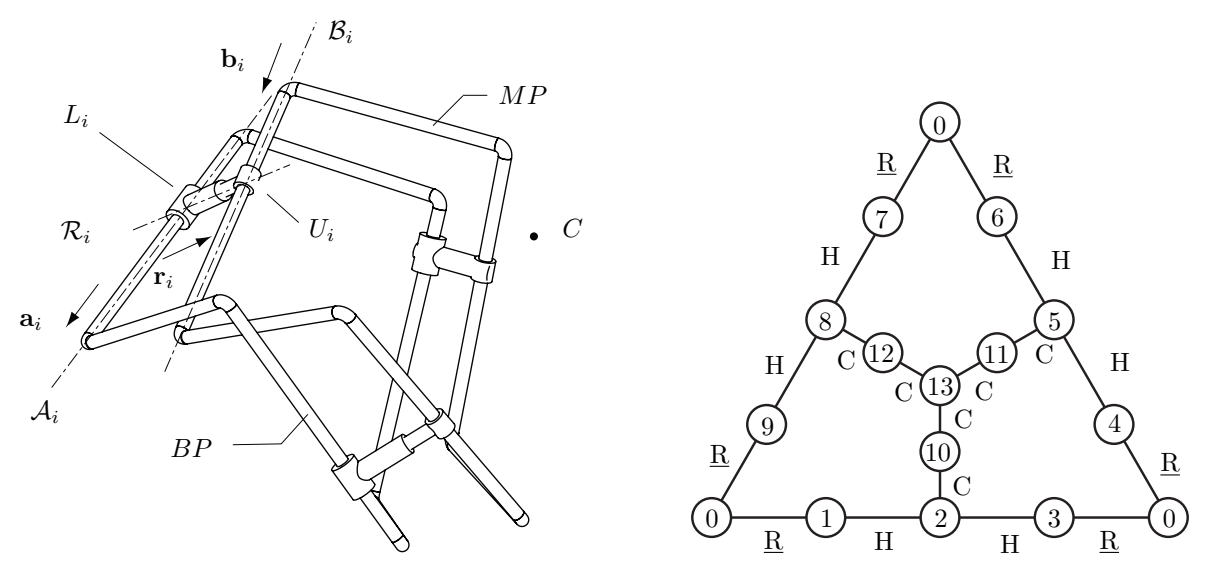


Figure 2.5: An example of a 3-CCC PKM

Figure 2.6: Graph of the 3-CCC PKM

The 3-CCC PKM consists of one BP, one MP, and three limbs, each limb consisting, in turn, of three C joints. The axes  $\mathcal{A}_i$ , for i=1,2,3, of the three C joints on the base are actuated in our case, in order to have only stationary motors; moreover, the axes  $\mathcal{B}_i$ , for i=1,2,3, of the three distal cylindrical joints are fixed to the MP; the axes of the middle cylindrical joints, denoted  $\mathcal{R}_i$ , connect the two cylindrical joints on the BP and MP, each limb having six degrees of freedom. Again, the three C joints on the base are actuated via the C-Drive introduced previously, in order to fix all the motors to the base.

In the chapters that follow, the kinematics, singularity and workspace analyses, along with the optimization of these two architectures, are reported, from which their various special features are revealed. Furthermore, the design for isotropy of a large class of PKMs is conducted in Chapter 4 based on the inverse of the *forward Jacobian* matrix, derived for the SDelta in Chapter 3.

## Chapter 3

## THE 3-CPS PKM

The work pertaining to the 3-<u>CPS PKM</u> is described in this chapter. Firstly, its kinematics relations (velocity level) are derived, as needed for simulation and control. Next, its forward-displacement, singularity and workspace analyses are conducted for two given sets of design parameters. These analyses reveal its performance on different aspects, which are essential for robot evaluation, simulation and control. Lastly, the optimization of the dexterity index, i.e., minimization of the condition number of the Jacobian matrix, is conducted. The optimization offers guidelines on how to choose the design parameters to obtain maximum dexterity.

## 3.1 Kinematics

The architecture of the SDelta Robot and the C-Drive are displayed in Figs. 2.1 and 2.2, where the MP and the BP are represented by equilateral triangles, of sides a and b, respectively, while the three vertices of the BP are labeled  $A_i$ , for i = 1, 2, 3. Moreover, the architecture of one of its limbs is illustrated in Fig. 3.1. Let  $\mathbf{c}$  be the position vector of the operation point C on the moving platform<sup>1</sup>, under the assumption that point O on the BP is the origin of the fixed coordinate frame,  $\mathbf{t} = [\boldsymbol{\omega}^T, \dot{\mathbf{c}}^T]^T$  the twist of the MP, with  $\boldsymbol{\omega}$  denoting the angular velocity of the MP, and  $\dot{\mathbf{c}}$  the velocity of C. Furthermore,  $\dot{\boldsymbol{\psi}} = [\dot{\psi}_{L1}, \dot{\psi}_{R1}, \dot{\psi}_{L2}, \dot{\psi}_{R2}, \dot{\psi}_{L3}, \dot{\psi}_{R3}]^T$  represents the array of six motor rates, three to the right (R), three to the left (L) of point  $O_j$  of the C-Drive collar in Fig. 3.1, for j = 1, 2, 3. Then we need to find the mapping between  $\mathbf{t}$  and  $\dot{\boldsymbol{\psi}}$ . It is known [47] that the array of actuated-joint rates  $\dot{\boldsymbol{\psi}}$  and the MP twist are related by two Jacobian matrices,  $\mathbf{K}$  and  $\mathbf{J}$ , termed the forward and the inverse Jacobian matrices, respectively, namely,

$$\mathbf{Kt} = \mathbf{J}\dot{\boldsymbol{\psi}} \tag{3.1}$$

<sup>&</sup>lt;sup>1</sup>Depicted in Fig. 3.1 as the centroid C of the equilateral triangle  $S_1S_2S_3$ .

However, since each C-drive of the SDelta Robot carries two screw pairs, the derivation of its Jacobian matrices is not as straightforward. We thus introduce a new array:

$$\dot{\boldsymbol{\phi}} = [\dot{\phi}_1, \, \dot{r}_1, \, \dot{\phi}_2, \, \dot{r}_2, \, \dot{\phi}_3, \, \dot{r}_3]^T \tag{3.2}$$

where  $\dot{\phi}_j$  and  $\dot{r}_j$  represent the turning and the sliding rates of the collar of the *j*th C-drive, for j = 1, 2, 3. Now we can express Eq. (3.1) in the form

$$\mathbf{Kt} = \mathbf{D}\dot{\boldsymbol{\phi}}, \quad \dot{\boldsymbol{\phi}} = \mathbf{J}_m \dot{\boldsymbol{\psi}} \tag{3.3}$$

with matrices  $\mathbf{K}$ ,  $\mathbf{D}$  and  $\mathbf{J}_m$  as yet to be displayed, the latter two referred to as the *drive* Jacobian and the actuator Jacobian, respectively. Therefore, the inverse Jacobian matrix  $\mathbf{J}$  can be expressed as the product of the drive Jacobian and the actuator Jacobian, namely,

$$\mathbf{J} = \mathbf{DJ}_m \tag{3.4}$$

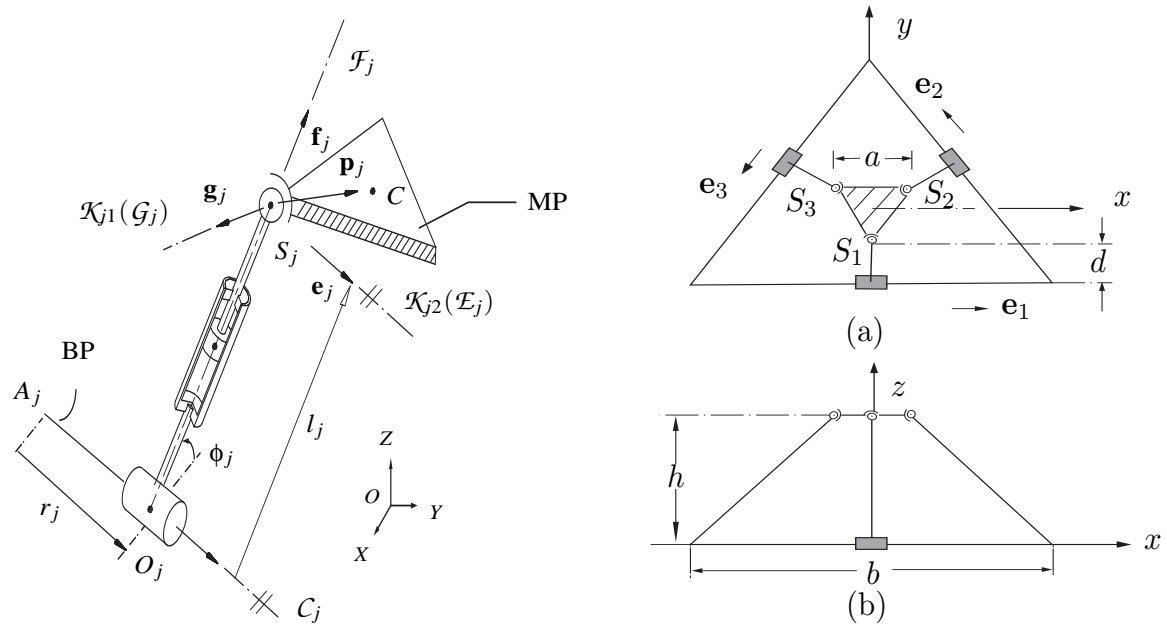


**Figure 3.1:** Notation for the kinematic chain of **Figure 3.2:** Dimensions of the SDelta Robot: (a) the *j*th limb of the SDelta Robot top view; (b) front view

#### 3.1.1 The Forward Jacobian and Drive Jacobian Matrices

Firstly we introduce our notation: Vector  $\mathbf{p}_j$  is defined as that joining the spherical joint centre  $S_j$  with the operation point C, while  $\mathbf{e}_j$  and  $\mathbf{f}_j$ , for j = 1, 2, 3, all shown in Fig. 3.1,

represent the unit vectors parallel to the jth C-drive axis  $C_j$  and the jth-limb axis  $\mathcal{F}_j$ ;  $\mathbf{g}_j$  is defined as the unit vector along  $\mathbf{e}_j \times \mathbf{f}_j$ , with  $\mathbf{e}_j$  and  $\mathbf{f}_j$  at right angles by design. Therefore,  $\{\mathbf{e}_j, \mathbf{f}_j, \mathbf{g}_j\}$  is an orthonormal, right-handed triad, as illustrated in Fig. 3.1.

Matrices  $\mathbf{K}$  and  $\mathbf{D}$  relate the MP twist with the array of the turning and sliding rates of the collars of the three C-drives. These Jacobian matrices can be conveniently derived based on screw theory [77, 78]. It is known that every joint in the robot bears an axis, either a "finite" line or a line at infinity, associated with a corresponding array of Plücker coordinates. In this vein, let us assume that the *i*th joint variable of  $\boldsymbol{\phi}$  is associated with the *j*th joint of the *k*th limb; then, the *i*th row of  $\mathbf{K}$  must be a screw reciprocal [64] to the Plücker array of all the axes in the *k*th limb, but the one associated with the *j*th joint. Moreover, it is recalled that a "finite" line can be regarded as a screw of zero pitch, while a line at infinity as an infinite-pitch screw. Furthermore,

- 1. Two zero-pitch screws are reciprocal when they are coplanar.
- 2. Two screws of infinite pitch are always reciprocal to each other.
- 3. A zero-pitch screw is reciprocal to an infinite-pitch screw when their directions are orthogonal.

From these rules, it becomes apparent that the line  $\mathcal{K}_{j1}$ —associated with the wrench corresponding to the rotational degree of freedom of the jth C-drive—must pass through  $S_j$ , with its direction vector normal to  $\mathbf{e}_j$  and  $\mathbf{f}_j$ , i.e., along  $\mathbf{g}_j$ , as shown in Fig. 3.1. Moreover, line  $\mathcal{K}_{j2}$ —associated with the wrench corresponding to the translational degree of freedom of the jth C-drive—is found to pass through  $S_j$  and is parallel to the axis of the jth C-drive  $\mathcal{C}_j$ , as shown, again, in Fig. 3.1. Based on the above analysis, we can obtain the  $\mathbf{K}$  matrix as

$$\mathbf{K} = \begin{bmatrix} (\mathbf{g}_1 \times \mathbf{p}_1)^T & \mathbf{g}_1^T \\ (\mathbf{e}_1 \times \mathbf{p}_1)^T & \mathbf{e}_1^T \\ (\mathbf{g}_2 \times \mathbf{p}_2)^T & \mathbf{g}_2^T \\ (\mathbf{e}_2 \times \mathbf{p}_2)^T & \mathbf{e}_2^T \\ (\mathbf{g}_3 \times \mathbf{p}_3)^T & \mathbf{g}_3^T \\ (\mathbf{e}_3 \times \mathbf{p}_3)^T & \mathbf{e}_3^T \end{bmatrix}$$

$$(3.5)$$

Under this notation,  $\mathbf{g}_j$  and  $\mathbf{e}_j$  represent the unit vectors parallel to lines  $\mathcal{K}_{j1}$  and  $\mathcal{K}_{j2}$ , respectively, for j = 1, 2, 3. We will henceforth denote  $\mathcal{K}_{j1}$  and  $\mathcal{K}_{j2}$  as  $\mathcal{G}_j$  and  $\mathcal{E}_j$ , respectively, for simplicity, as shown in Fig. 3.1, their Plücker arrays being  $\mathbf{k}_{j1} = \left[\mathbf{g}_j^T, (\mathbf{g}_j \times \mathbf{p}_j)^T\right]^T$  and  $\mathbf{k}_{j2} = \left[\mathbf{e}_j^T, (\mathbf{e}_j \times \mathbf{p}_j)^T\right]^T$ .

Once **K** is available, **D** is straightforward to derive, as it turns out to be a diagonal matrix, whose *i*th component is the reciprocal product of the line corresponding to the *i*th row of **K** and that associated with the joint of the *i*th component of  $\phi$ . **D** is found to bear the form

$$\mathbf{D} = \operatorname{diag}(l_1, 1, l_2, 1, l_3, 1) \tag{3.6}$$

with  $l_i$  representing the length of the *i*th limb, thereby deriving the *forward* and the *drive* Jacobian matrices, **K** in Eq. (3.5) and **D** in Eq. (3.6).

#### 3.1.2 The Actuator Jacobian Matrix

Let  $\mathbf{J}_m$ , the matrix relating the array of six motor rates with the array of the turning and sliding rates of the collars of the three C-drives, be termed the *actuator Jacobian*. The Jacobian matrix  $\mathbf{J}_C$ , of one C-drive [18], relates the speeds of the two screws with the turning and sliding rates of the collar, namely:

$$\dot{\boldsymbol{\gamma}}_C = \mathbf{J}_C \dot{\boldsymbol{\psi}}_C \tag{3.7}$$

with

$$\dot{\boldsymbol{\gamma}}_C = \begin{bmatrix} \dot{\phi} \\ \dot{r} \end{bmatrix}, \ \mathbf{J}_C = \begin{bmatrix} 1/2 & 1/2 \\ p/4\pi & -p/4\pi \end{bmatrix}, \ \dot{\boldsymbol{\psi}}_C = \begin{bmatrix} \dot{\psi}_L \\ \dot{\psi}_R \end{bmatrix}$$
 (3.8)

where  $\dot{\gamma}_C$  and  $\dot{\psi}_C$  represent the two-dimensional speed arrays of the collar and of the screws, respectively,  $\dot{\psi}_L$ ,  $\dot{\psi}_R$  the angular speeds of the left- and the right-hand screws of the C-drive, respectively, and hence, of the motors. Moreover,  $\dot{\phi}$  and  $\dot{r}$  represent the rotational and translational speeds of the collar of the C-drive, while p is the pitch of the screws of the three C-drives.

It is noteworthy that the three C-drives are identical, the above relation thus applying to all of them. Apparently, then,  $\mathbf{J}_m$  is a block-diagonal matrix for the three C-drives:

$$\mathbf{J}_m = \operatorname{diag}(\mathbf{J}_C, \mathbf{J}_C, \mathbf{J}_C) \tag{3.9}$$

thereby deriving relation (3.3).

#### 3.1.3 Redefinition of the Actuator Jacobian and the Drive Jacobian

If the rates of the C-drive are redefined as  $\dot{\gamma}_C = [\dot{\phi}, 2\pi \dot{r}/p]^T$ , then, we can rewrite Eq. (3.7) as

$$\dot{\boldsymbol{\gamma}}_C = \mathbf{J}_C \dot{\boldsymbol{\psi}}_C$$
, with  $\mathbf{J}_C = \begin{bmatrix} 1/2 & 1/2 \\ 1/2 - 1/2 \end{bmatrix}$ ,  $\dot{\boldsymbol{\psi}}_C = \begin{bmatrix} \dot{\psi}_L \\ \dot{\psi}_R \end{bmatrix}$  (3.10)

In this vein, we redefine  $\mathbf{J}_m$  as

$$\mathbf{J}_m = \operatorname{diag}(\mathbf{J}_C, \mathbf{J}_C, \mathbf{J}_C) \tag{3.11}$$

which is a constant isotropic matrix because  $\mathbf{J}_C$  in Eq. (3.10) is isotropic<sup>2</sup>. Correspondingly,  $\mathbf{D}$  is redefined as

$$\mathbf{D} = \operatorname{diag}\left(l_1, \frac{p}{2\pi}, l_2, \frac{p}{2\pi}, l_3, \frac{p}{2\pi}\right)$$
 (3.12)

in order to preserve the equality in Eq. (3.4). Finally, the **J** matrix becomes

$$\mathbf{J} = \mathbf{DJ}_m \tag{3.13}$$

where  $\mathbf{D}$ , as displayed in Eq. (3.12), is a diagonal matrix whose entries have all units of length, while  $\mathbf{J}_m$  is a 6 × 6 dimensionless block-diaongal isotropic matrix, as displayed in Eq. (3.11).

So far we have established the kinematics relation of the SDelta at the velocity level,

 $<sup>^2</sup>$ A non-singular square matrix is isotropic if it is a) dimensionally homogeneous and b) its inverse is proportional to its transpose. For rectangular matrices, change non-singular to full rank and inverse to generalized inverse.

from which the relevant Jacobian matrices are available. Next, we provide its forward-displacement, singularity and workspace analyses.

## 3.2 The Forward-displacement Analysis

The architecture of the SDelta Robot is shown in Figs. 2.1 and 3.1, where the MP and the BP are represented by equilateral triangles, of sides a and b, respectively [75]. The elimination method suggested by Nanua et al. [79] is adopted for its forward-displacement analysis. In the foregoing paper, the authors analyzed a class of Stewart-Gough platform<sup>3</sup> with three pairs of concurrent limbs, ending up with a 16th-degree resolvent polynomial; in our case, the forward-displacement problem leads to a simpler model, namely, an octic polynomial. Given that the displacement of the actuated joints (i.e., the three C-Drives) are known, while the lengths of the limbs,  $l_j$  for j=1,2,3, are not yet determined, we can regard the three C-Drives as "locked", thereby yielding an equivalent 3-dof 3-PS PKM. The forward-displacement analysis of a 3-PS mechanism has been investigated by Parenti-Castelli and Innocenti [80]; in this vein, we denote denote the position vector of point  $S_j$ , the centre of the spherical joint of the jth limb, as  $s_j$ , for j=1,2,3, the relations below readily following:

$$\|\mathbf{s}_2 - \mathbf{s}_1\|^2 = \|\mathbf{s}_3 - \mathbf{s}_2\|^2 = \|\mathbf{s}_1 - \mathbf{s}_3\|^2 = a^2$$
 (3.14)

In the forward-displacement analysis, the sliding  $r_j$  of the jth C joint and its rotation  $\phi_j$  are prescribed, the pose of the MP being unknown. The MP pose is found upon locating points  $S_j$ , which is possible when the limb lengths  $l_j$  are known, their computation being outlined below. Proceeding exactly as Nanua et al. did [79], three quadratic equations in the three

<sup>&</sup>lt;sup>3</sup>The simplest version of the SGP, whose limbs are laid out so that their axes intersect pairwise at the BP and the MP, with different pairs of each platform, common in flight simulators.

limb lengths  $l_j$  are derived:

$$l_{1}^{2} + l_{2}^{2} - \sqrt{3}(b - r_{1})\cos\phi_{2}l_{2} + [(\cos\phi_{1}\cos\phi_{2} - 2\sin\phi_{1}\sin\phi_{2})l_{2} - \sqrt{3}r_{2}\cos\phi_{1}]l_{1}$$

$$+ r_{1}r_{2} - br_{2} - a^{2} + b^{2} - 2br_{1} + r_{1}^{2} + r_{2}^{2} = 0 \qquad (3.15a)$$

$$l_{2}^{2} + l_{3}^{2} - \sqrt{3}(b - r_{2})\cos\phi_{3}l_{3} + [(\cos\phi_{2}\cos\phi_{3} - 2\sin\phi_{2}\sin\phi_{3})l_{3} - \sqrt{3}r_{3}\cos\phi_{2}]l_{2}$$

$$+ r_{2}r_{3} - br_{3} - a^{2} + b^{2} - 2br_{2} + r_{2}^{2} + r_{3}^{2} = 0 \qquad (3.15b)$$

$$l_{3}^{2} + l_{1}^{2} - \sqrt{3}(b - r_{3})\cos\phi_{1}l_{1} + [(\cos\phi_{1}\cos\phi_{3} - 2\sin\phi_{1}\sin\phi_{3})l_{1} - \sqrt{3}r_{1}\cos\phi_{3}]l_{3}$$

$$+ r_{3}r_{1} - br_{1} - a^{2} + b^{2} - 2br_{3} + r_{3}^{2} + r_{1}^{2} = 0 \qquad (3.15c)$$

The Bezout number [81] of a system of multivariable polynomial equations is defined as the product of the degrees of the individual equations, which is the number of roots admitted by the resolvent (monovariate) polynomial<sup>4</sup> of the system. In our case, this number is  $2^3 = 8$ , half the number of the solutions of the forward-displacement problem admitted by the (six-limb) simplest SGP with triangular BP and MP.

The said octic resolvent polynomial can be derived by dyalitic elimination [64] if all roots are needed. For purpose of control, a numerical method (Newton-Raphson) is recommended.

## 3.3 Singularity Analysis

The singularities of parallel robots pertain to 1) those occurring in the serial Jacobian matrices  $\mathbf{J}_j$  of any of the limbs and 2) those occurring in matrices  $\mathbf{K}$  and  $\mathbf{D}$ . The latter are known as type-I (for  $\mathbf{K}$ ) and type-II for ( $\mathbf{D}$ ) singularities [47].

## 3.3.1 Singularities of the Serial Jacobian Matrices

The limb singularity occurs when the Plücker array of the axes of the six joints of the jth limb become linearly dependent, under which the PKM encounters a loss of mobility. Since each limb of the SDelta Robot has a decoupled architecture—i.e., a spherical joint coupling the MP with each limb—the singularity analysis of its Jacobian matrices is straightforward.

<sup>&</sup>lt;sup>4</sup>This is the monovariate polynomial equation obtained after eliminating all but one of the unknowns from the given system.

The pertinent singularities can be classified into wrist and shoulder singularities: Wrist singularities occur when the three wrist axes become coplanar [64]. This means that the axes of the three concurrent revolute joints are coplanar. Furthermore, the shoulder singularity, according to screw theory, hanppens only when a) a wrist singularity does not occur, and b) there exists one line  $\mathcal{L}_j$  passing through  $S_j$  that intersects the C-Drive axis  $\mathcal{C}_j$ , and is normal to  $\mathbf{e}_j$  and  $\mathbf{f}_j$ . This can only happen when the length of the jth limb is zero, which is physically impossible for the SDelta architecture. Hence, the shoulder singularity does not occur for this architecture.

## 3.3.2 Type-I Singularity

Since **D** is a diagonal matrix, it becomes singular when any of its diagonal entries vanishes. From Eq. (3.12) it can be readily seen that this happens when the length of one of the limbs is zero, which is, again, physically impossible in general. This condition is the same as that for the shoulder singularity of serial Jacobian matrices, and hence, excluded.

## 3.3.3 Type-II Singularity

This occurs when **K** becomes singular, and the robot gains extra mobility. The singularity of three-limb PKMs with one passive S joint at each limb end has been investigated extensively, based on: screw theory [39]; passive joint velocities [40]; instability analysis [41]; the pure condition [42]; and the characteristic tetrahedron [43]. An approach proposed for the 6-3 Stewart-Gough platform can also be applied to this class of PKMs [82]. Moreover, the singularity of a more general class of PKMs, namely, three-limb PKMs whose limbs, each, includes a passive S joint somewhere, has also been investigated based on passive joint velocities [45] and Grassmann-Cayley algebra [44,46]. It has been shown that the singularity of this class of robots yields a straightforward geometrical interpretation, namely, the four planes—three planes composed of the three pairs of intersecting wrench axes plus the plane of the MP triangle—share at least one common point [44–46]. Starting from this geometric condition, we propose a simple formulation for the singularity condition without involving any determinant calculation [40–43,45] or passive joint velocities [40,45].

We have obtained K as shown in Eq. (3.5), whose six rows can be regarded as the Plücker

coordinates [64] of six actuated-wrench axes, intersecting pairwise at the centre of the three spherical joints. Hence, **K** becomes singular when the four planes—three planes composed of the three pairs of intersecting actuated-wrench axes together with the plane of the MP triangle—share at least one common point [41–46]. We denote the plane defined by the intersecting lines  $\mathcal{E}_j$ ,  $\mathcal{G}_j$  as  $\Pi_j$ , its normal as  $\mathbf{n}_j$ , for j=1,2,3. It is noteworthy that  $\mathbf{n}_j=\mathbf{f}_j$  for the SDelta Robot, but this does not hold for a general six-dof PKM whose actuated-wrench axes intersect pairwise, hence, we use  $\mathbf{n}_j$  for generality. Moreover, we denote the MP plane as  $\Pi_4$ , its normal as  $\mathbf{n}_4$ . Next we conduct the singularity analysis based on this geometrical interpretation.

First, denote the intersecting line between  $\Pi_j$  and  $\Pi_4$  as  $\mathcal{L}_j$ , for j=1,2,3; it is noteworthy that  $\mathcal{L}_j$  passes through  $S_j$ , and lies in the common plane  $\Pi_4$ ; the foregoing geometrical condition is then equivalent to requiring that the three lines  $\mathcal{L}_j$ , for j=1,2,3, share common points. In this way, we can reduce the analysis to the plane  $\Pi_4$ . Furthermore, let us denote the intersecting point of  $\mathcal{L}_1$  with  $\mathcal{L}_2$  and with  $\mathcal{L}_3$  as  $R_2$  and  $R_3$ , respectively; then, the condition leads to requiring that the position vectors of  $R_2$  and  $R_3$  be identical.

Let  $\mathbf{l}_j$  denote a vector parallel to  $\mathcal{L}_j$ ; then,  $\mathbf{l}_j$  must be normal to both  $\mathbf{n}_j$  and  $\mathbf{n}_4$ . We do not require  $\mathbf{l}_j$  to be of unit norm here, and hence, we can assign

$$\mathbf{l}_j = \mathbf{n}_j \times \mathbf{n}_4 \quad j = 1, 2, 3 \tag{3.16}$$

Furthermore, upon defining the position vector of the common point as  $\boldsymbol{\xi}$ , we have

$$\boldsymbol{\xi} = \eta_1 \mathbf{l}_1 - \mathbf{p}_1 = \eta_2 \mathbf{l}_2 - \mathbf{p}_2 = \eta_3 \mathbf{l}_3 - \mathbf{p}_3 \tag{3.17}$$

where  $\eta_j$ , j = 1, 2, 3, are as yet to be determined. From the above relations, we have

$$\eta_1 \mathbf{l}_1 - \eta_2 \mathbf{l}_2 = \mathbf{p}_1 - \mathbf{p}_2 \tag{3.18a}$$

$$\eta_1 \mathbf{l}_1 - \eta_3 \mathbf{l}_3 = \mathbf{p}_1 - \mathbf{p}_3 \tag{3.18b}$$

Next we cross-multiply both sides of Eq. (3.18a) with  $l_2$ , those of Eq. (3.18b) with  $l_3$ , which

leads to

$$\eta_1 \mathbf{l}_1 \times \mathbf{l}_2 = (\mathbf{p}_1 - \mathbf{p}_2) \times \mathbf{l}_2 \tag{3.19a}$$

$$\eta_1 \mathbf{l}_1 \times \mathbf{l}_3 = (\mathbf{p}_1 - \mathbf{p}_3) \times \mathbf{l}_3 \tag{3.19b}$$

It can be seen that both sides of Eqs. (3.19a) and (3.19b) are parallel to the z-axis of the MP frame. Next, upon dot-multiplying the LHS of Eq. (3.19a) with the RHS of Eq. (3.19b), then equating this product with that of the corresponding sides of Eqs. (3.19a) and (3.19b), we obtain

$$(\mathbf{l}_1 \times \mathbf{l}_2) \cdot [(\mathbf{p}_1 - \mathbf{p}_3) \times \mathbf{l}_3] = (\mathbf{l}_1 \times \mathbf{l}_3) \cdot [(\mathbf{p}_1 - \mathbf{p}_2) \times \mathbf{l}_2]$$
(3.20)

where the common factor  $\eta_1$  has been eliminated. Moreover, plugging Eq. (3.16) into Eq. (3.20), after some manipulations, leads to

$$[(\mathbf{n}_3 - \mathbf{n}_3 \cdot \mathbf{n}_4 \mathbf{n}_4) \cdot (\mathbf{p}_1 - \mathbf{p}_3)][(\mathbf{n}_2 \times \mathbf{n}_1) \cdot \mathbf{n}_4] = [(\mathbf{n}_2 - \mathbf{n}_2 \cdot \mathbf{n}_4 \mathbf{n}_4) \cdot (\mathbf{p}_1 - \mathbf{p}_2)][(\mathbf{n}_3 \times \mathbf{n}_1) \cdot \mathbf{n}_4]$$
(3.21)

Furthermore, it is noted that  $\mathbf{n}_4$  is normal to  $\mathbf{p}_i - \mathbf{p}_j$ , for  $i, j = 1, 2, 3, i \neq j$ ; we can thus simplify Eq. (3.21) to obtain

$$[\mathbf{n}_3 \cdot (\mathbf{p}_1 - \mathbf{p}_3)][(\mathbf{n}_2 \times \mathbf{n}_1) \cdot \mathbf{n}_4] = [\mathbf{n}_2 \cdot (\mathbf{p}_1 - \mathbf{p}_2)][(\mathbf{n}_3 \times \mathbf{n}_1) \cdot \mathbf{n}_4]$$
(3.22)

which is the singularity condition sought. It is observed that, when represented in the MP frame,  $\mathbf{p}_j$  and  $\mathbf{n}_4$  in Eq. (3.22) become constant, which reduces the computational cost greatly. As a result, we choose to express all the vectors in the MP frame. Then, we only need to find  $\mathbf{n}_j$ , for j=1,2,3, in the MP frame. It is noteworthy that, for the SDelta robot,  $\mathbf{n}_j$  is nothing but  $\mathbf{f}_j$ , and hence, parallel to the axis of the jth limb; moreover, its norm does not affect the relation in Eq. (3.22). Assuming that the perpendicular foot of  $S_j$  on the axis of the jth C-drive is  $O_j$ , as shown in Figs. 3.1, we can use  $\overrightarrow{O_jS_j}$  to substitute  $\mathbf{n}_j$  in Eq. (3.22), where

$$\overrightarrow{O_jS_j} = (\mathbf{1} - \mathbf{e}_j \mathbf{e}_j^T) \overrightarrow{A_jS_j} = (\mathbf{1} - \mathbf{e}_j \mathbf{e}_j^T) (\overrightarrow{CS_j} - \overrightarrow{CA_j})$$
(3.23)

which yields

$$[\overrightarrow{O_jS_j}]_{\mathcal{M}} = \mathbf{Q}^T (\mathbf{1} - [\mathbf{e}_j]_{\mathcal{B}} [\mathbf{e}_j]_{\mathcal{B}}^T) \{ [\mathbf{c}]_{\mathcal{B}} - [\overrightarrow{OA_j}]_{\mathcal{B}} - \mathbf{Q}[\mathbf{p}_j]_{\mathcal{M}} \}$$
(3.24)

in which only  $\mathbf{Q}$  and  $\mathbf{c}$  are variable, with  $\mathbf{Q}$  representing the rotation matrix of the MP, which is the  $3 \times 3$  identity matrix under the reference pose. Then we can use  $\overrightarrow{O_jS_j}$  to substitute  $\mathbf{n}_j$  in Eq. (3.22), for j=1,2,3.

It can be readily verified that this equality also holds even if some of the four planes  $\Pi_j$  are coincident, or when some of the three intersecting lines  $\mathcal{L}_j$  coincide.

## 3.3.4 Case Study: the Fixed-orientation Singularity Locus

Since the singularity locus of a six-dof PKM is impossible to visualize, its fixed-orientation subset has been mostly investigated in the literature, which means that the orientation, i.e., the  $\mathbf{Q}$  matrix, is fixed. Further,  $\overrightarrow{O_jS_j}$  is linear in  $\mathbf{c}$ , while  $(\mathbf{n}_j \times \mathbf{n}_1) \cdot \mathbf{n}_4$  is quadratic in  $\mathbf{c}$ , for j = 2, 3; it then follows that Eq. (3.22) yields a cubic surface in  $\mathbf{c}$ . A numerical example is given below for illustration.

Apparently, the design parameters impact on the singularity distribution and the workspace. Hence, we plot these items for two typical sets of design variables, namely, the sides of the MP and the BP are assumed to obey the relation a/b = 0.2 for Design I and a/b = 1 for Design II, respectively. Furthermore, we define the reference pose of the MP as that under which the operation point C coincides with O in the BP, while the MP orientation is as shown in Fig. 3.2, with the BP and MP planes coincident.

Several typical orientations are selected, under which the singularity loci are plotted as the surfaces shown in Figs. 3.3 to 3.5, with the open and closed surfaces representing the singularity locus and the corresponding workspace boundary, respectively. In these figures, the orientation is given by the numerical values of the vector  $\mathbf{q}$  and angle  $\theta$  of the rotation matrix  $\mathbf{Q}$  that carries the BP from its reference to its current attitude.

It is observed that, when the MP rotates about the Z-axis, the singularity is characterized by three vertical planes, which can be analyzed by means of Grassmann geometry: at the reference orientation, the three wrench axes  $\mathcal{E}_i$ , for i = 1, 2, 3, corresponding to the three

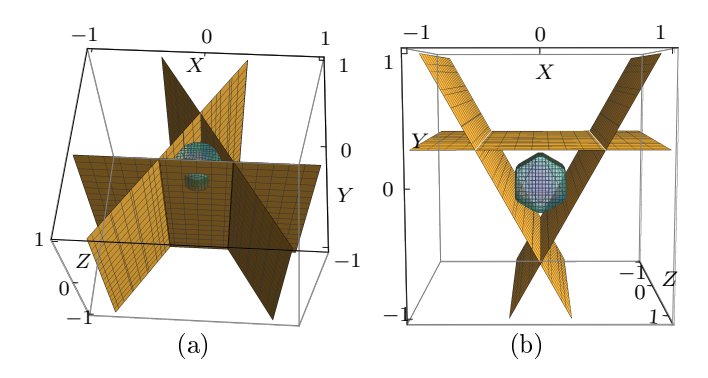


Figure 3.3: The workspace and singularity loci of the SDelta at the reference orientation (a) Design I (b) Design II

C-Drive axes, lie all in a horizontal plane. Then, when the middle link of the *i*th limb is vertical, the wrench line corresponding to  $\mathbf{g}_i$  lies also in the same horizontal plane, these four lines becoming a linear variety [35] of rank 3, which leads to a singular configuration. Hence, the three planes can be found when the MP translates to a configuration in which  $S_i$  lies in the vertical plane that passes through the *i*th C-Drive axis. Furthermore, when the MP undergoes a rotation about the Z-axis, the three lines  $\mathcal{E}_i$  are still in the same horizontal plane, which again, leads to three vertical singularity planes; this is simple to characterize. However, when the MP rotates about some other axes, the singularity surface has, generally, a complex shape.

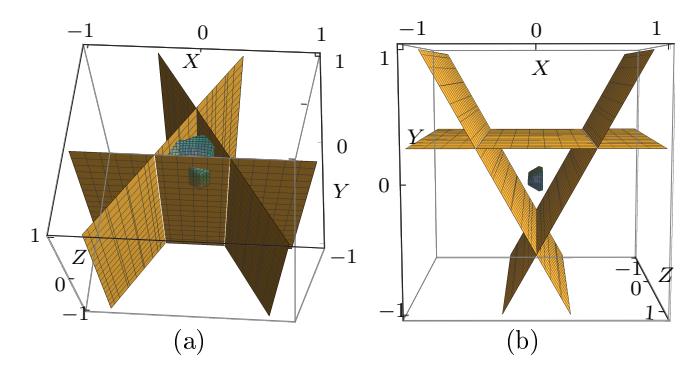


Figure 3.4: The workspace and singularity loci of the SDelta with the orientation  $\mathbf{q} = [0, 0, 1]^T$  and  $\theta = 15^{\circ}$  (a) Design I (b) Design II

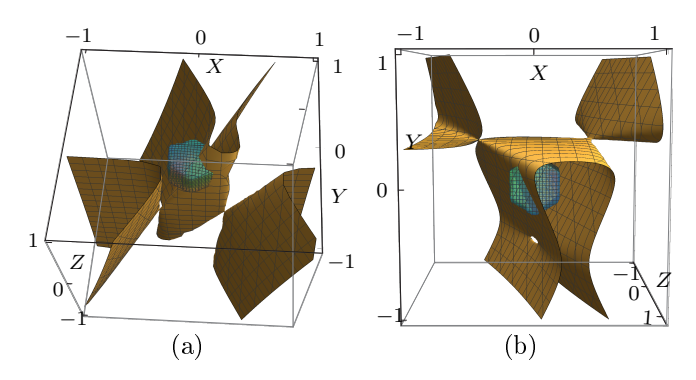


Figure 3.5: The workspace and singularity loci of the SDelta with the orientation  $\mathbf{q} = [0, 1, 0]^T$  and  $\theta = 15^{\circ}$  (a) Design I (b) Design II

## 3.4 Workspace Analysis

In this section we investigate the fixed-orientation position workspace to have a general idea of the workspace volume. We consider only the limits of the active and passive joints first, then verify whether singularities exist within the workspace thus obtained.

## 3.4.1 The Geometrical Method for Workspace Quantification

We developed a geometrical method capable of obtaining the three-dimensional position workspace systematically, targeting its graphical display and workspace-volume evaluation with computer-algebra software, which lends itself also to workspace optimization via mathematical programming. The basic principle of the construction of the fixed-orientation workspace follows: We find the feasible workspace of the MP under the constraint of only the *i*th limb (i.e., we assume that the two other limbs are disconnected and regard the robot as a serial chain), denoted as  $W_i$ ; then, the workspace of interest will be the intersection of  $\{W_i\}_{1}^{3}$ . Next, we explain the procedure for finding  $W_i$ .

Since the orientation of the MP is fixed for the fixed-orientation workspace, the centre of the spherical joint  $S_i$  undergoes the same motion as the operation point C. Hence, we firstly find the "position workspace" of  $S_i$ —denoted  $W_{Si}$ . Considering the stroke of the C-drive, denoted  $r_s$ , the upper and lower bounds of the limb length, denoted  $l_{min}$  and  $l_{max}$ , the position of  $S_i$  is found to lie within the region between two co-axial cylinders of radii  $l_{min}$  and  $l_{max}$ , respectively, whose height is the stroke  $r_s$ , as shown in Fig. 3.6(a).

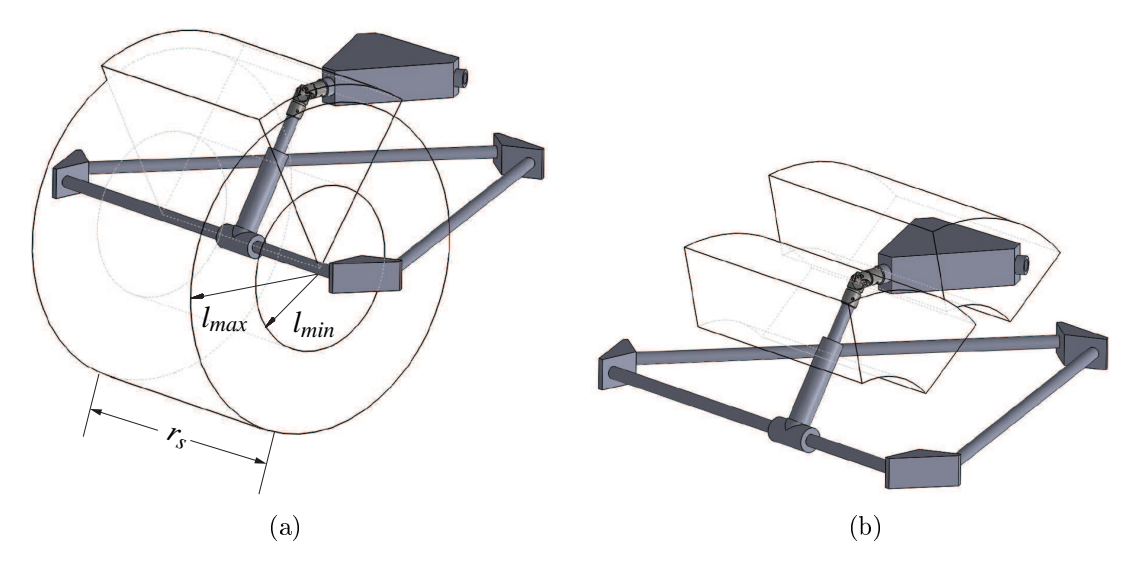


Figure 3.6: Illustration of the workspace formulation based on the geometric method

Furthermore, we consider the constraint of the S joint, which we assume to be realized by a ball-and-socket joint, whose working-angle range can be modelled as a cone [3], its maximum denoted  $\delta_{max}$ . Apparently, the translation of the MP along the direction  $\mathbf{e}_i$  of the axis of the C-drive, or along the direction  $\mathbf{f}_i$  of the ith limb, will not change the relative orientation of the two links connected by the spherical joint; only the translation of the MP in the direction of  $\mathbf{g}_i$  will change the foregoing relative orientation, which corresponds to the rotation of the C-drive. Hence, the motion of the S joint has a limit only on the feasible range of the angle of rotation of the C-drive; this limit remains constant when  $S_i$  translates in the direction of  $\mathbf{e}_i$  or  $\mathbf{f}_i$ . This means that, when we further consider the limits of the S joint, we will no longer have a cylindrical shape, but a pie slice, as shown, again, in Fig. 3.6(a), whose angular range can be derived from the projection of the cone onto the plane normal to  $\mathbf{e}_i$ . Until now, we have found  $\mathcal{W}_{si}$ ; it is a simple matter to translate this region by  $\mathbf{p}_i$ to find  $W_i$ , the feasible region of the operation point under the constraint of the *i*th limb, as shown in Fig. 3.6(b). Once all the three regions  $\{W_i\}_1^3$  are available, their intersection yields the fixed-orientation workspace sought. Researchers usually discretize one of the three coordinates, e.g., the Z-coordinate, then find the workspace shape on different layers. With the aid of computer-algebra, this kind of intersection operation of geometrical objects can be handled directly; the software in use also provides the workspace volume and the visulization of its boundary.

## 3.4.2 Case Study

The fixed-orientation worksapce is provided for the robot, again, with two sets of design parameters:

$$a = 0.2b, l_{min} = 0.45b, l_{max} = 0.85b, \text{ and } a = b, l_{min} = 0.6b, l_{max} = 1.13b$$
 (3.25)

where  $l_{min}$  and  $l_{max}$  represent the minimum and maximum lengths of each limb; It is noteworthy that we choose different  $l_{min}$  and  $l_{max}$  values in order to keep the height of the MP similar at the reference pose for the two sets of different design parameters. Moreover, we assume the maximum angle attained by the S joint to be  $\delta_{max} = 45^{\circ}$ ; then, the workspace under the reference orientation is plotted in Fig. 3.7 for each case, yielding volume values of  $0.049b^3$  and  $0.067b^3$ , respectively. The workspace is also evaluated under several other orientations, as shown in Figs. 3.8 and 3.9, with the volumes  $0.045b^3$ ,  $0.007b^3$ ,  $0.047b^3$ ,  $0.042b^3$ , respectively. It is, however, noteworthy that the singularity surface sometimes crosses the workspace for the given set of design parameters and selected orientation, as shown in Figs. 3.3 to 3.5, similar to the case of the Stewart-Gough platform [83].

Finally, in order to reveal the effect of the ratio a/b on the workspace volume (V), we plot V vs. a/b, in the range of 0.2 to 1.5, which we deem to be sufficient in general applications. Moreover, even though we used different  $l_{min}$  and  $l_{max}$  values for Designs I and II, in order to make the height of the MP similar at the reference pose, we fix them here in order to reveal the effect of solely the ratio a/b; more specifically,  $l_{min} = 0.55b$ ,  $l_{max} = b$ . Then, the workspace volumes are, again, plotted under the three different orientations, i.e., the reference orientation, the orientation  $\mathbf{q} = [0,0,1]^T$  with  $\theta = 15^\circ$  and  $\mathbf{q} = [0,1,0]^T$  with  $\theta = 15^\circ$ , respectively, as shown in Fig. 3.10. Apparently, the workspace volume V under the reference orientation remains largely unchanged for different values of a/b; however, V decreases significantly when the MP is rotated about the Z-axis; when the MP is rotated about other directions, the workspace volume can either decrease or increase. It is noteworthy that the above workspace volume is different from those of Designs I and II, indicating that the range of the passive limb length affects the workspace as well.

The above result indicates that, when the range of the passive limb length is fixed, the

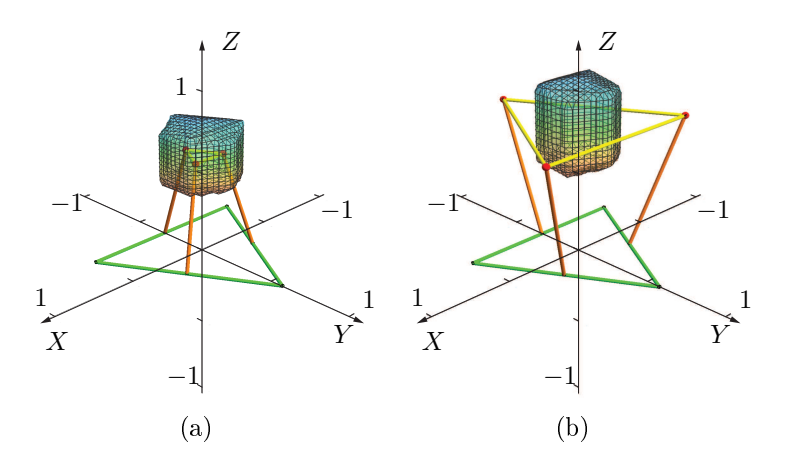
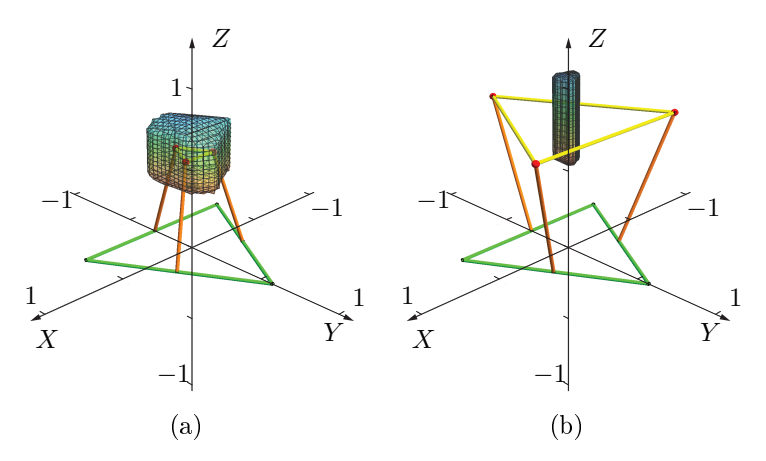
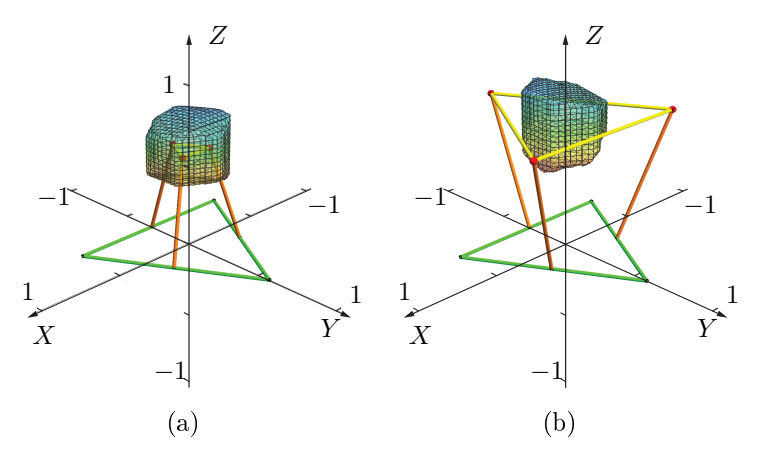


Figure 3.7: The workspace of the SDelta under the reference orientation (a) Design I (b) Design II



**Figure 3.8:** The workspace of the SDelta with the orientation  $\mathbf{q} = [0, 0, 1]^T$  and  $\theta = 15^\circ$  (a) Design I (b) Design II



**Figure 3.9:** The workspace of the SDelta with the orientation  $\mathbf{q} = [0, 1, 0]^T$  and  $\theta = 15^\circ$  (a) Design I (b) Design II

workspace volume generally decreases as the ratio a/b increases; however, for a larger MP, (e.g., a = b), the robot allows for a larger range of the passive limb length<sup>5</sup>, which can end up with a bigger workspace volume.

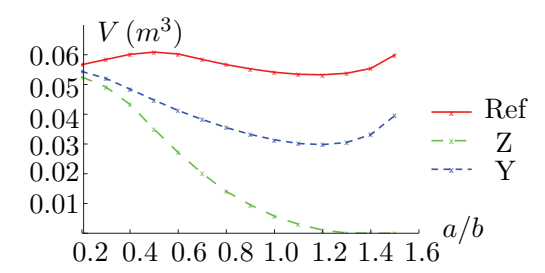


**Figure 3.10:** The workspace volume w.r.t. the ratio of a/b, under different orientations

## 3.5 Singularity and Workspace Analyses—A Discussion

From the above figures, for which two sets of arbitrarily chosen design parameters are used, it is apparent that singularity locus and workspace are greatly affected by the ratio a/b and the range of the limb length. Interestingly, when the MP finds itself at the reference orientaion, the singularity locus is the union of three vertical planes, each corresponding to a set of postures under which one of the three points  $S_j$  lies in the vertical plane passing through the axis of the jth C-Drive, for j = 1, 2, 3. As a result, |a - b/2| must be as large as possible, in order to make the distance from  $S_j$  to the vertical plane passing through the axis of the jth C-Drive as large as possible, the singularity surface becoming farther from the desired workspace region. Furthermore, when the MP rotates about the Z-axis, the singularity surface is still the union of three vertical planes. As the MP rotates about an axis other than the Z-axis, the singularity surfaces generally show the tendency to both rotate about this axis, and deform in such a way that their shapes become more complex<sup>6</sup>.

As for the workspace volume, it is greatly affected not only by the ratio a/b but also by the range of the limb length: the workspace volume increases as the stroke of each limb increases; moreover, as the average of  $l_{min}$  and  $l_{max}$  increases, the "centre" of the workspace region lies higher and the workspace volume generally becomes larger.

<sup>&</sup>lt;sup>5</sup>In Designs I and II, we assume that  $l_{max} \approx 2l_{min}$  and  $l_{ref} \approx (l_{max} + l_{min})/2$ , where  $l_{ref}$  represents the limb length at the reference pose; moreover, the reference height of the MP was kept similar in Designs I and II to make a reasonable comparison, which ends up with different  $l_{min}$  and  $l_{max}$  values.

<sup>&</sup>lt;sup>6</sup>The complexity of a surface can be quantified in terms of the curvature distribution [84].

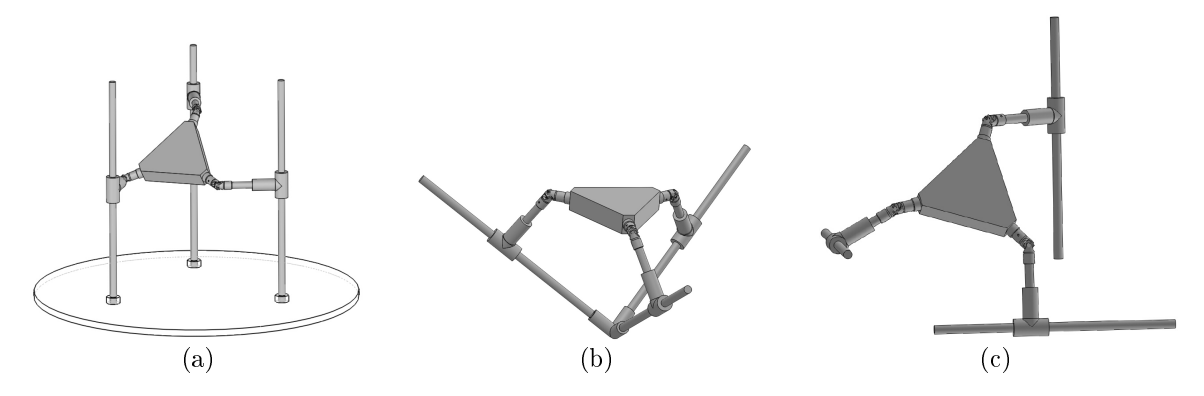


Figure 3.11: Alternative layouts of the three C-drives

The singularity locus sometimes crosses the workspace, which is undesirable; we believe that this is due to the three C-Drive axes becoming coplanar, which yields the three singularity planes at the reference orientation. As a result, other layouts of the three C-Drives may be explored, such as those with three vertical axes, three intersecting orthogonal axes or three skew orthogonal axes, as shown in Figs. 3.11. These alternatives have the potential to provide a larger singularity-free workspace. For example, for the layout with three vertical axes, it allows for a larger stroke of the three intermediate P joints for the same footprint<sup>7</sup>; moreover, the workspace can be extended along the vertical axis as long as we increase the C-drive lengths. These features yield a larger workspace, although this platform is mostly suitable for small workpieces, due to the possible interference among the three guideways and a large workpiece.

So far we have completed the forward-displacement, singularity and workspace analyses of the SDelta, which are essential in the robot evaluation, simulation and control. Next, its optimization based on a dexterity index is provided, which offers guidelines on how to choose the design parameters for high dexterity.

<sup>&</sup>lt;sup>7</sup>Here "footprint" means the area the robot occupies.

# 3.6 The Optimum Design of the 3-<u>CPS PKM</u> for Maximum Dexterity

According to one typical dictionary<sup>8</sup> definition, dexterity: the ability to use your hands skillfully. In robotics the term has been adopted to indicate the precision capability of a robotic manipulator to execute a positioning task [64]. Two measures have been adopted: the condition number [66] and manipulability, the absolute value of the determinant [85] of the Jacobian matrix. These two indices are intended to measure, roughly speaking, the distance of a robot posture, given by the joint angles, from singularity. The absolute value of the Jacobian determinant depends on the size of the robot, and hence, favors large robots; the former, when the Jacobian matrix has been normalized by means of a characteristic length, is dimensionless, besides being the measure adopted within numerical analysis [86] community for the same purpose. For these reasons, the condition number appears as a sound measure of dexterity, and hence, we adopt it in this dissertation. The condition number  $\kappa$  is a dimensionless scalar ranging from 1 to infinity, which, when calculated based on the Frobenius norm<sup>9</sup>,  $\|\cdot\|_F$ , represented as  $\kappa_F$ , takes the form [64]

$$\kappa_F(\mathbf{K}) = \frac{1}{n} \sqrt{\|\mathbf{K}\|_F^2 \|\mathbf{K}^{-1}\|_F^2} = \frac{1}{n} \sqrt{\text{tr}(\mathbf{K}\mathbf{K}^T)\text{tr}[(\mathbf{K}\mathbf{K}^T)^{-1}]}, \quad n = 6$$
 (3.26)

It is known that the lower the condition number, the higher the dexterity.

Furthermore, the reciprocal of the condition number of the Jacobian matrix is adopted here to quantify the dexterity. Since  $\mathbf{D}$  is diagonal, its condition number can be readily monitored as the ratio of the largest absolute value to the smallest absolute value of its non-zero entries, which is well bounded, since the limb extensions are designed to be always positive. Moreover, as  $\mathbf{J}_m$  is orthogonal, it is isotropic. Hence, we only look at matrix  $\mathbf{K}$  here. Given that the entries of the Jacobian matrices bear different units, we introduce a pertinent characteristic length L [68] to resolve this dimensional inhomogeneity. To this end,

<sup>&</sup>lt;sup>8</sup>Merriam-Webster Learner's Dictionary.

<sup>&</sup>lt;sup>9</sup>This norm is chosen because it yields an *analytic function* of the condition number, and hence, is infinitely many times differentiable [67]. Moreover, it can be readily shown that the Frobenius norm of a matrix is immutable to a multiplication of the matrix by an orthogonal matrix. As well, the same norm is *invariant* under a change of frame.

we redefine both the twist and matrix  $\mathbf{K}$  in their dimensionally homogeneous forms:

$$\mathbf{t}_{h} = \begin{bmatrix} \dot{\boldsymbol{\omega}} \\ \dot{\mathbf{c}}/L \end{bmatrix}, \quad \mathbf{K}_{h} = \begin{bmatrix} (\mathbf{g}_{1} \times \mathbf{p}_{1})^{T} & L\mathbf{g}_{1}^{T} \\ (\mathbf{e}_{1} \times \mathbf{p}_{1})^{T} & L\mathbf{e}_{1}^{T} \\ (\mathbf{g}_{2} \times \mathbf{p}_{2})^{T} & L\mathbf{g}_{2}^{T} \\ (\mathbf{e}_{2} \times \mathbf{p}_{2})^{T} & L\mathbf{e}_{2}^{T} \\ (\mathbf{g}_{3} \times \mathbf{p}_{3})^{T} & L\mathbf{g}_{3}^{T} \\ (\mathbf{e}_{3} \times \mathbf{p}_{3})^{T} & L\mathbf{e}_{3}^{T} \end{bmatrix}$$

$$(3.27)$$

which yields  $\mathbf{K}_h \mathbf{t}_h = \mathbf{K} \mathbf{t}$ , the latter appearing in Eq. (3.3). The characteristic length [64] is defined as the value L that minimizes the condition number of  $\mathbf{K}_h$ , as yet to be determined.

Next, the optimum design of the SDelta is conducted based on the condition number of the Jacobian matrix  $\mathbf{K}$ . From Eq. (3.26), it is apparent that the expression for  $\mathbf{K}^{-1}$  is needed when a symbolic formulation is sought. Next, the inverse of the robot forward Jacobian matrix is found symbolically. After that, we formulate an optimization problem based on its condition number, for maximum dexterity. Drawing from the optimization results, we offer some guidelines on choosing the optimum design parameters.

#### 3.6.1 Derivation of the Inverse of the Forward Jacobian Matrix

The axes of the six actuated wrenches of a large class of six-dof PKMs intersect pairwise, including most of the three-limb PKMs whose each limb includes a passive spherical joint<sup>10</sup> [39,75]. Next, we derive a symbolic expression for the inverse of the forward Jacobian matrix for this class of PKMs, an instance being the SDelta, illustrated in Fig. 2.1. Due to the special layout of the six actuated wrenches, the Jacobian matrix **K** of such robots always bears the form of Eq. (3.5), with  $\mathbf{e}_j$  and  $\mathbf{g}_j$  representing the unit vectors associated with the jth pair of intersecting wrench axes, for j = 1, 2, 3; unlike the case of the SDelta, these vectors are, in general, not necessarily normal to each other. In order to make the derivation below general, in the remainder of this subsection we redefine  $\mathbf{f}_j$ , such that  $\mathbf{f}_j \equiv \mathbf{g}_j \times \mathbf{e}_j$ , for j = 1, 2, 3, which is not necessarily a unit vector; moreover, the expression of  $\mathbf{K}^{-1}$  below does not require the operation point C to be the centroid of triangle  $S_1S_2S_3$  in this subsection.

<sup>&</sup>lt;sup>10</sup>Numerous examples of such PKMs can be found in [41, 44].

As a matter of fact, C need not even be a point of the plane of the triangle  $S_1S_2S_3$ .

We denote  $\mathbf{K}^{-1}$  as  $\overline{\mathbf{K}}$ , i.e.,  $\mathbf{K}\overline{\mathbf{K}} = \mathbf{1}$ , where  $\mathbf{1}$  represents the  $6 \times 6$  identity matrix. If the first column of  $\overline{\mathbf{K}}$  is denoted by  $\overline{\mathbf{k}}_1$ , then

$$\mathbf{K}\overline{\mathbf{k}}_1 = \boldsymbol{\iota}_1 \tag{3.28}$$

with  $\iota_1$  representing a six-dimensional vector array, whose first entry is unity, all other entries vanishing. Next,  $\overline{\mathbf{k}}_1$  is defined as the six-dimensional array

$$\overline{\mathbf{k}}_1 = \begin{bmatrix} \mathbf{u}_1 \\ \mathbf{m}_1 \end{bmatrix} \tag{3.29}$$

where  $\mathbf{u}_1$  and  $\mathbf{m}_1$  represent three-dimensional vectors, as yet to be determined. Then, the inner product of the last five rows of  $\mathbf{K}$  with  $\overline{\mathbf{k}}_1$  must vanish. The inner product of the third and fourth rows of  $\mathbf{K}$  with  $\overline{\mathbf{k}}_1$  leads to

$$(\mathbf{m}_1 - \mathbf{u}_1 \times \mathbf{p}_2)^T \mathbf{g}_2 = 0, \quad (\mathbf{m}_1 - \mathbf{u}_1 \times \mathbf{p}_2)^T \mathbf{e}_2 = 0$$
(3.30)

which imply that  $\mathbf{m}_1 - \mathbf{u}_1 \times \mathbf{p}_2$  is parallel to  $\mathbf{g}_2 \times \mathbf{e}_2$ , i.e., to  $\mathbf{f}_2$ ; hence,  $(\mathbf{m}_1 - \mathbf{u}_1 \times \mathbf{p}_2) = k_2 \mathbf{f}_2$  or, equivalently,

$$\mathbf{m}_1 = k_2 \mathbf{f}_2 + \mathbf{u}_1 \times \mathbf{p}_2 \tag{3.31}$$

where  $k_2$  represents a scalar, as yet to be found. Similarly, from the inner product of the fifth and sixth rows of  $\mathbf{K}$  with  $\overline{\mathbf{k}}_1$ , we have

$$\mathbf{m}_1 = k_3 \mathbf{f}_3 + \mathbf{u}_1 \times \mathbf{p}_3 \tag{3.32}$$

with  $k_3$ , as well, to be determined. Equations (3.31) and (3.32) yield

$$\mathbf{u}_1 \times (\mathbf{p}_2 - \mathbf{p}_3) = -k_2 \mathbf{f}_2 + k_3 \mathbf{f}_3 \tag{3.33}$$

from which we can conclude that  $\mathbf{u}_1$ ,  $\mathbf{p}_2 - \mathbf{p}_3$  and  $\mathbf{f}_2 \times \mathbf{f}_3$  are coplanar. Thus, we can assume

 $\mathbf{u}_1$  to be a linear combination of the last two vectors, i.e.,

$$\mathbf{u}_1 = w_1(\mathbf{p}_2 - \mathbf{p}_3) + w_2(\mathbf{f}_2 \times \mathbf{f}_3) \tag{3.34}$$

with  $w_1$  and  $w_2$  to be determined. After plugging Eq. (3.34) into Eq. (3.33) and some straightforward manipulations, we obtain

$$w_2\{[\mathbf{f}_2^T(\mathbf{p}_2 - \mathbf{p}_3)]\mathbf{f}_3 - [\mathbf{f}_3^T(\mathbf{p}_2 - \mathbf{p}_3)]\mathbf{f}_2\} = -k_2\mathbf{f}_2 + k_3\mathbf{f}_3$$
(3.35)

and hence,

$$k_2 = w_2 \mathbf{f}_3^T (\mathbf{p}_2 - \mathbf{p}_3), \quad k_3 = w_2 \mathbf{f}_2^T (\mathbf{p}_2 - \mathbf{p}_3)$$
 (3.36)

Relations (3.31), (3.34) and (3.36) guarantee that the inner product of the last four rows of  $\mathbf{K}$  with  $\overline{\mathbf{k}}_1$  do vanish,  $w_1$  and  $w_2$  being free parameters. Next, we find the ratio of  $w_1$  to  $w_2$  from the vanishing of the inner product of the second row of  $\mathbf{K}$  with  $\overline{\mathbf{k}}_1$ , which leads to

$$(\mathbf{p}_1 \times \mathbf{u}_1 + \mathbf{m}_1)^T \mathbf{e}_1 = 0 \tag{3.37}$$

After plugging Eqs. (3.31), (3.34) and (3.36) into Eq. (3.37) and some straightforward simplifications, we obtain

$$w_1[(\mathbf{p}_1 - \mathbf{p}_2) \times (\mathbf{p}_2 - \mathbf{p}_3)]^T \mathbf{e}_1 + w_2\{(\mathbf{p}_1 - \mathbf{p}_2) \times (\mathbf{f}_2 \times \mathbf{f}_3) + [\mathbf{f}_3^T(\mathbf{p}_2 - \mathbf{p}_3)]\mathbf{f}_2\}^T \mathbf{e}_1 = 0$$
 (3.38)

from which we can find the ratio of  $w_1$  to  $w_2$ . Let us denote the coefficients of  $w_1$  and  $w_2$  as<sup>11</sup>

$$s_1 = [(\mathbf{p}_1 - \mathbf{p}_2) \times (\mathbf{p}_2 - \mathbf{p}_3)]^T \mathbf{e}_1 \equiv 2s_\Delta \mathbf{n}^T \mathbf{e}_1, \ s_2 = \{(\mathbf{p}_1 - \mathbf{p}_2) \times (\mathbf{f}_2 \times \mathbf{f}_3) + [\mathbf{f}_3^T (\mathbf{p}_2 - \mathbf{p}_3)]\mathbf{f}_2\}^T \mathbf{e}_1 \equiv \mathbf{r}_1^T \mathbf{e}_1$$

$$(3.39)$$

where  $s_{\Delta}$  represents the area of the MP triangle  $S_1S_2S_3$ , **n** is the unit vector normal to the MP triangle, its direction defined according to Eqs. (3.39), while  $\mathbf{r}_1$  is defined as

$$\mathbf{r}_1 = \{ [(\mathbf{p}_1 - \mathbf{p}_3)^T \mathbf{f}_3] \mathbf{f}_2 - [(\mathbf{p}_1 - \mathbf{p}_2)^T \mathbf{f}_2] \mathbf{f}_3 \}$$
 (3.40)

<sup>&</sup>lt;sup>11</sup>Rather than working with the ratio  $w_1/w_2$ , or  $w_2/w_1$  for that matter, in which either of the two variables can vanish, we keep both in the balance of the paper.

The simplest way of assigning values to  $w_1$  and  $w_2$  is, thus,

$$w_1 = -s_2 = -\mathbf{r}_1^T \mathbf{e}_1, \quad w_2 = s_1 = 2s_\Delta \mathbf{n}^T \mathbf{e}_1 \tag{3.41}$$

In this way, we can represent vectors  $\mathbf{u}_1$  and  $\mathbf{m}_1$  as

$$\mathbf{u}_1 = -\mathbf{r}_1^T \mathbf{e}_1(\mathbf{p}_2 - \mathbf{p}_3) + 2s_\Delta \mathbf{n}^T \mathbf{e}_1(\mathbf{f}_2 \times \mathbf{f}_3), \quad \mathbf{m}_1 = w_2(\mathbf{f}_2^T \mathbf{p}_2)\mathbf{f}_3 - w_2(\mathbf{f}_3^T \mathbf{p}_3)\mathbf{f}_2 + w_1\mathbf{p}_2 \times \mathbf{p}_3$$
(3.42)

Furthermore, if we define  $\mathbf{h}_1$  as

$$\mathbf{h}_1 = (\mathbf{f}_2^T \mathbf{p}_2) \mathbf{f}_3 - (\mathbf{f}_3^T \mathbf{p}_3) \mathbf{f}_2 \tag{3.43}$$

then,

$$\mathbf{m}_1 = 2s_{\Delta}(\mathbf{n}^T \mathbf{e}_1)\mathbf{h}_1 - (\mathbf{r}_1^T \mathbf{e}_1)\mathbf{p}_2 \times \mathbf{p}_3$$
(3.44)

Now we can guarantee that  $\overline{\mathbf{k}}_1$  is orthogonal to the last five rows of  $\mathbf{K}$ . However, its inner product with the first row of  $\mathbf{K}$  must be unity; hence, the last step is to calculate this inner product, denoted as  $t_1$ . Then, the scaled  $\overline{\mathbf{k}}_1$  can be expressed as

$$\overline{\mathbf{k}}_{s1} = \frac{1}{t_1} \begin{bmatrix} \mathbf{u}_1 \\ \mathbf{m}_1 \end{bmatrix} \tag{3.45}$$

which satisfies  $\mathbf{K}\mathbf{\bar{k}}_{s1} = \boldsymbol{\iota}_1$ , with  $\boldsymbol{\iota}_1$  introduced in Eq. (3.28). Finally,  $t_1$  is derived as

$$t_1 = (\mathbf{g}_1 \times \mathbf{p}_1)^T \mathbf{u}_1 + \mathbf{g}_1^T \mathbf{m}_1 = (\mathbf{p}_1 \times \mathbf{u}_1 + \mathbf{m}_1)^T \mathbf{g}_1$$
(3.46)

which, after routine algebraic manipulations, reduces to

$$t_1 = 2s_{\Delta}(\mathbf{f}_1 \times \mathbf{r}_1) \cdot \mathbf{n} \tag{3.47}$$

We have obtained so far the first column of  $\overline{\mathbf{K}}$  (i.e., of  $\mathbf{K}^{-1}$ ). Next we derive the remaining columns of  $\overline{\mathbf{K}}$ . First, we express  $\overline{\mathbf{K}}$  as

$$\overline{\mathbf{K}} = \begin{bmatrix} \overline{\mathbf{k}}_{s1} & \overline{\mathbf{k}}_{s2} & \overline{\mathbf{k}}_{s3} & \overline{\mathbf{k}}_{s4} & \overline{\mathbf{k}}_{s5} & \overline{\mathbf{k}}_{s6} \end{bmatrix}$$
(3.48)

Following the form of  $\overline{\mathbf{k}}_{s1}$ , as given by Eq. (3.45), we can set

$$\overline{\mathbf{k}}_{sj} = \frac{1}{t_j} \begin{bmatrix} \mathbf{u}_j \\ \mathbf{m}_j \end{bmatrix}, \quad j = 2, \dots, 6$$
(3.49)

For example, for the first column of  $\overline{\mathbf{K}}$ ,

$$\mathbf{r}_{1} = [(\mathbf{p}_{1} - \mathbf{p}_{3})^{T} \mathbf{f}_{3}] \mathbf{f}_{2} - [(\mathbf{p}_{1} - \mathbf{p}_{2})^{T} \mathbf{f}_{2}] \mathbf{f}_{3}$$

$$\mathbf{h}_{1} = (\mathbf{f}_{2}^{T} \mathbf{p}_{2}) \mathbf{f}_{3} - (\mathbf{f}_{3}^{T} \mathbf{p}_{3}) \mathbf{f}_{2}$$

$$\mathbf{u}_{1} = -\mathbf{r}_{1}^{T} \mathbf{e}_{1} (\mathbf{p}_{2} - \mathbf{p}_{3}) + 2s_{\Delta} \mathbf{n}^{T} \mathbf{e}_{1} (\mathbf{f}_{2} \times \mathbf{f}_{3})$$

$$\mathbf{m}_{1} = 2s_{\Delta} (\mathbf{n}^{T} \mathbf{e}_{1}) \mathbf{h}_{1} - (\mathbf{r}_{1}^{T} \mathbf{e}_{1}) \mathbf{p}_{2} \times \mathbf{p}_{3}$$

$$t_{1} = 2s_{\Delta} (\mathbf{f}_{1} \times \mathbf{r}_{1}) \cdot \mathbf{n}$$

$$(3.50)$$

Due to the symmetries in the structure of  $\mathbf{K}$ , we can find the second column of  $\overline{\mathbf{K}}$  by simply exchanging the roles of  $\mathbf{e}_1$  and  $\mathbf{g}_1$  in Eqs.  $(3.50)^{12}$ :

$$\mathbf{u}_{2} = -(\mathbf{r}_{1}^{T}\mathbf{g}_{1})(\mathbf{p}_{2} - \mathbf{p}_{3}) + 2s_{\Delta}(\mathbf{n}^{T}\mathbf{g}_{1})(\mathbf{f}_{2} \times \mathbf{f}_{3})$$

$$\mathbf{m}_{2} = 2s_{\Delta}(\mathbf{n}^{T}\mathbf{g}_{1})\mathbf{h}_{1} - (\mathbf{r}_{1}^{T}\mathbf{g}_{1})\mathbf{p}_{2} \times \mathbf{p}_{3}$$

$$t_{2} = -2s_{\Delta}(\mathbf{f}_{1} \times \mathbf{r}_{1}) \cdot \mathbf{n}$$

$$(3.51)$$

and hence,

$$t_2 = -t_1 (3.52)$$

Moreover, we can find the third and fifth columns of  $\overline{\mathbf{K}}$  upon exchanging subscripts 1, 2, 3 with 2, 3, 1 or 3, 1, 2 in Eqs. (3.50), respectively, and the fourth and sixth columns of  $\overline{\mathbf{K}}$  upon exchanging subscript 1, 2, 3 with 2, 3, 1 or 3, 1, 2 in Eqs. (3.51), respectively. It is noteworthy that the corresponding subscripts in all the terms within  $\mathbf{r}_j$  and  $\mathbf{h}_j$  have to be exchanged as well.

Furthermore, it is found that we only need to calculate the denominator once because

$$t_1 = t_3 = t_5 = -t_2 = -t_4 = -t_6 \tag{3.53}$$

<sup>&</sup>lt;sup>12</sup>Consistently,  $\mathbf{f}_1$  should be substituted by  $-\mathbf{f}_1$ , but it is readily verified that this does not affect the result;  $\mathbf{n}$ , which does not involve  $\mathbf{e}_1$  or  $\mathbf{g}_1$ , is not affected, either.

Now we prove the above statement: If we denote the edge joining the *i*th and *j*th S joint centre as  $\mathbf{s}_{ij} = \overrightarrow{S_iS_j}$ , then,  $\mathbf{p}_i - \mathbf{p}_j = \mathbf{s}_{ij}$ ; moreover,

$$2s_{\Delta}(\mathbf{r}_{1} \times \mathbf{n}) = [(\mathbf{s}_{13}^{T}\mathbf{f}_{3})\mathbf{f}_{2} - (\mathbf{s}_{12}^{T}\mathbf{f}_{2})\mathbf{f}_{3}] \times (\mathbf{s}_{12} \times \mathbf{s}_{13}) = (\mathbf{s}_{13}^{T}\mathbf{f}_{3})(\mathbf{s}_{23}^{T}\mathbf{f}_{2})\mathbf{s}_{12} - (\mathbf{s}_{12}^{T}\mathbf{f}_{2})(\mathbf{s}_{23}^{T}\mathbf{f}_{3})\mathbf{s}_{13}$$
(3.54)

and hence,

$$t_{1} = 2s_{\Delta}(\mathbf{r}_{1} \times \mathbf{n}) \cdot \mathbf{f}_{1} = [(\mathbf{s}_{13}^{T}\mathbf{f}_{3})(\mathbf{s}_{23}^{T}\mathbf{f}_{2})\mathbf{s}_{12} - (\mathbf{s}_{12}^{T}\mathbf{f}_{2})(\mathbf{s}_{23}^{T}\mathbf{f}_{3})\mathbf{s}_{13}] \cdot \mathbf{f}_{1}$$

$$= -(s_{12}^{T}\mathbf{f}_{1})(\mathbf{s}_{23}^{T}\mathbf{f}_{2})(\mathbf{s}_{31}^{T}\mathbf{f}_{3}) + (\mathbf{s}_{12}^{T}\mathbf{f}_{2})(\mathbf{s}_{23}^{T}\mathbf{f}_{3})(\mathbf{s}_{31}^{T}\mathbf{f}_{1})$$
(3.55)

If we exchange, for example, subscripts 1, 2, 3 with 2, 3, 1, respectively, while noticing that  $\mathbf{s}_{ij} = -\mathbf{s}_{ji}$ , we obtain

$$t_{3} = [(\mathbf{s}_{21}^{T}\mathbf{f}_{1})(\mathbf{s}_{31}^{T}\mathbf{f}_{3})\mathbf{s}_{23} - (\mathbf{s}_{23}^{T}\mathbf{f}_{3})(\mathbf{s}_{31}^{T}\mathbf{f}_{1})\mathbf{s}_{21}] \cdot \mathbf{f}_{2}$$

$$= -(s_{12}^{T}\mathbf{f}_{1})(\mathbf{s}_{23}^{T}\mathbf{f}_{2})(\mathbf{s}_{31}^{T}\mathbf{f}_{3}) + (\mathbf{s}_{12}^{T}\mathbf{f}_{2})(\mathbf{s}_{23}^{T}\mathbf{f}_{3})(\mathbf{s}_{31}^{T}\mathbf{f}_{1}) = t_{1}$$
(3.56)

Similarly, relation (3.53) follows. Finally, if we define  $t = t_1$ , then  $\overline{\mathbf{K}}$  can be written as

$$\overline{\mathbf{K}} = \frac{1}{t} \begin{bmatrix} \mathbf{u}_1 & -\mathbf{u}_2 & \mathbf{u}_3 & -\mathbf{u}_4 & \mathbf{u}_5 & -\mathbf{u}_6 \\ \mathbf{m}_1 & -\mathbf{m}_2 & \mathbf{m}_3 & -\mathbf{m}_4 & \mathbf{m}_5 & -\mathbf{m}_6 \end{bmatrix}$$
(3.57)

Interestingly, Eq. (3.55) is the same as the expression for the singularity loci of three-limb PKMs with three passive spherical joints derived by Yang et al. [40]. This makes sense because, when  $\mathbf{K}$  becomes singular, its inverse does not exist, which happens when and only when t=0. From the mixed-product form of t—i.e.,  $t_1$  in expression (3.47)—we obtain a more compact form of the singularity loci, which should yield a more efficient evaluation of the singularity loci of any six-dof three-limb PKM with three passive S joints.

## 3.6.2 Unconstrained Dexterity Maximization

Next, we employ the expression for  $\mathbf{K}^{-1}$  derived in the previous subsection to conduct the optimization for the SDelta based on a dexterity index. Firstly, we formulate the optimization

problem: The architecture parameters  $\alpha$  and  $\gamma$  are defined as

$$\alpha = \frac{a}{b} \quad \gamma = \frac{h}{b} \tag{3.58}$$

where a and b are the lengths of the sides of the MP and BP equilateral triangles, respectively, while h is the height of the MP plane at the reference pose<sup>13</sup>, as shown in Fig. 3.2. Moreover, the pose of the MP is given by its orientation  $\mathbf{Q} \in \mathbb{R}^{3\times3}$  and the position vector  $\mathbf{c}$  of the operation point C. Next, the rotation matrix  $\mathbf{Q}$  is represented by  $\mathbf{q}$  and  $\theta$ , the unit vector parallel to the axis of rotation and the angle of rotation, respectively; then, the set of design variables is defined as:

$$\mathbf{x} = \begin{bmatrix} b & L & \mathbf{q} & \mathbf{c} & \alpha & \gamma & \theta \end{bmatrix}^T \in \mathbb{R}^{11} \tag{3.59}$$

where L is the *characteristic length* [68], as yet to be found. Then, the optimization problem can be formulated as

$$f(\mathbf{x}) = \frac{1}{n^2} \|\mathbf{K}\|_F^2 \|\mathbf{K}^{-1}\|_F^2 \to \min_{\mathbf{x}}$$
s.t.  $b, \alpha, L > 0$  (3.60)

In order to solve this problem, we next derive  $\|\mathbf{K}\|_F^2$  and  $\|\mathbf{K}^{-1}\|_F^2$ , which carry simpler expressions than  $\|\mathbf{K}\|_F$  and  $\|\mathbf{K}^{-1}\|_F$ .

#### 3.6.2.1 Derivation of the Norm of the Forward Jacobian

When deriving the condition number of the forward Jacobian matrix, its homogeneous form, as per Eq. (3.27), is needed, which was obtained upon introducing the characteristic length [68] L. L can be found, together with the other entries of the design vectors  $\mathbf{x}$  of

<sup>13</sup>It is noteworthy that h is actually the component of the position vector  $\mathbf{c}$  of the operation point along the z axis  $(c_z)$  in the BP frame at the reference pose.

Eq. (3.59), upon solution of problem (3.60). To this end,  $\|\mathbf{K}_h\|_F^2$  is readily derived as

$$\|\mathbf{K}_{h}\|_{F}^{2} = \sum_{j=1}^{3} [L^{2}(\|\mathbf{g}_{j}\|_{2}^{2} + \|\mathbf{e}_{j}\|_{2}^{2}) + (\mathbf{g}_{j} \times \mathbf{p}_{j})^{T}(\mathbf{g}_{j} \times \mathbf{p}_{j}) + (\mathbf{e}_{j} \times \mathbf{p}_{j})^{T}(\mathbf{e}_{j} \times \mathbf{p}_{j})$$

$$= \sum_{j=1}^{3} [2L^{2} + (\mathbf{p}_{j}^{T}\mathbf{p}_{j}\mathbf{g}_{j} - \mathbf{p}_{j}^{T}\mathbf{g}_{j}\mathbf{p}_{j})^{T}\mathbf{g}_{j} + (\mathbf{p}_{j}^{T}\mathbf{p}_{j}\mathbf{e}_{j} - \mathbf{p}_{j}^{T}\mathbf{e}_{j}\mathbf{p}_{j})^{T}\mathbf{e}_{j}]$$

$$= \sum_{j=1}^{3} [2L^{2} + 2\|\mathbf{p}_{j}\|_{2}^{2} - (\mathbf{p}_{j}^{T}\mathbf{g}_{j})^{2} - (\mathbf{p}_{j}^{T}\mathbf{e}_{j})^{2}]$$
(3.61)

Since  $\{\mathbf{e}_j, \mathbf{f}_j, \mathbf{g}_j\}_1^3$  are orthonormal for the SDelta, and the operation point is located at the centroid of the MP triangle,  $\|\mathbf{K}_h\|_F^2$  simplifies to

$$\|\mathbf{K}_h\|_F^2 = 6L^2 + \sum_{j=1}^3 \left(\frac{a}{\sqrt{3}}\right)^2 + \sum_{j=1}^3 (\mathbf{p}_j^T \mathbf{f}_j)^2 = 6L^2 + \alpha^2 b^2 + \sum_{j=1}^3 (\mathbf{p}_j^T \mathbf{f}_j)^2$$
(3.62)

where  $\mathbf{p}_j$  and  $\mathbf{f}_j$  are functions of  $\mathbf{x}$ .

#### 3.6.2.2 Derivation of the Norm of the Inverse of the Forward Jacobian

We recall the expressions of  $\mathbf{K}^{-1}$  and  $\mathbf{K}_h$  displayed in Eqs. (3.57) and (3.27). Since we multiplied the right block of  $\mathbf{K}$  by L, the lower block of  $\mathbf{K}^{-1}$  should be divided by L correspondingly, namely,

$$\overline{\mathbf{K}}_h = \frac{1}{t} \begin{bmatrix} \mathbf{u}_1 & -\mathbf{u}_2 & \mathbf{u}_3 & -\mathbf{u}_4 & \mathbf{u}_5 & -\mathbf{u}_6 \\ \mathbf{m}_1/L & -\mathbf{m}_2/L & \mathbf{m}_3/L & -\mathbf{m}_4/L & \mathbf{m}_5/L & -\mathbf{m}_6/L \end{bmatrix}$$
(3.63)

If we further consider the geometry of the robot under study, as shown in Fig. 2.1, where both the MP and the BP are equilateral triangles, of sides a and b, respectively, and the operation point C is selected as the centroid of triangle  $S_1S_2S_3$ , then,  $\mathbf{u}_1$ ,  $\mathbf{u}_2$  and  $\mathbf{m}_1$ ,  $\mathbf{m}_2$  can

be further simplified as

$$\mathbf{u}_{1} = -\left(\mathbf{r}_{1}^{T}\mathbf{e}_{1}\right)\left(\mathbf{p}_{2} - \mathbf{p}_{3}\right) + \frac{\sqrt{3}}{2}a^{2}(\mathbf{n}^{T}\mathbf{e}_{1})\left(\mathbf{f}_{2} \times \mathbf{f}_{3}\right)$$

$$\mathbf{u}_{2} = -\left(\mathbf{r}_{1}^{T}\mathbf{g}_{1}\right)\left(\mathbf{p}_{2} - \mathbf{p}_{3}\right) + \frac{\sqrt{3}}{2}a^{2}(\mathbf{n}^{T}\mathbf{g}_{1})\left(\mathbf{f}_{2} \times \mathbf{f}_{3}\right)$$

$$\mathbf{m}_{1} = \frac{\sqrt{3}}{6}a^{2}\left[3(\mathbf{n}^{T}\mathbf{e}_{1})\mathbf{h}_{1} - \left(\mathbf{r}_{1}^{T}\mathbf{e}_{1}\right)\mathbf{n}\right]$$

$$\mathbf{m}_{2} = \frac{\sqrt{3}}{6}a^{2}\left[3(\mathbf{n}^{T}\mathbf{g}_{1})\mathbf{h}_{1} - \left(\mathbf{r}_{1}^{T}\mathbf{g}_{1}\right)\mathbf{n}\right]$$

$$(3.64a)$$

Next, we partition  $\overline{\mathbf{K}}_h$  into three  $6 \times 2$  blocks, and denote the Euclidean norm of the jth block as  $d_j$ , which leads to

$$d_1^2 = \frac{1}{t_1^2} [\|\mathbf{u}_1\|_2^2 + \|\mathbf{u}_2\|_2^2 + \frac{1}{L^2} (\|\mathbf{m}_1\|_2^2 + \|\mathbf{m}_2\|_2^2)]$$
(3.65)

where  $\|\mathbf{u}_1\|_2^2 + \|\mathbf{u}_2\|_2^2$  and  $\|\mathbf{m}_1\|_2^2 + \|\mathbf{m}_2\|_2^2$  are derived as

$$\|\mathbf{u}_{1}\|_{2}^{2} + \|\mathbf{u}_{2}\|_{2}^{2} = a^{2}[(\mathbf{r}_{1}^{T}\mathbf{e}_{1})^{2} + (\mathbf{r}_{1}^{T}\mathbf{g}_{1})^{2}] + \frac{3}{4}a^{4}[(\mathbf{n}^{T}\mathbf{e}_{1})^{2} + (\mathbf{n}^{T}\mathbf{g}_{1})^{2}]\|\mathbf{f}_{2} \times \mathbf{f}_{3}\|_{2}^{2} - 2\sqrt{3}a^{2}(\mathbf{r}_{1}^{T}\mathbf{e}_{1}\mathbf{n}^{T}\mathbf{e}_{1} + \mathbf{r}_{1}^{T}\mathbf{g}_{1}\mathbf{n}^{T}\mathbf{g}_{1})\mathbf{s}_{23}^{T}(\mathbf{f}_{2} \times \mathbf{f}_{3})$$
(3.66)

and

$$\|\mathbf{m}_{1}\|_{2}^{2} + \|\mathbf{m}_{2}\|_{2}^{2} = \frac{a^{4}}{12} \{9[(\mathbf{n}^{T}\mathbf{e}_{1})^{2} + (\mathbf{n}^{T}\mathbf{g}_{1})^{2}]\|\mathbf{h}_{1}\|_{2}^{2} + (\mathbf{r}_{1}^{T}\mathbf{e}_{1})^{2} + (\mathbf{r}_{1}^{T}\mathbf{g}_{1})^{2} - 6(\mathbf{r}_{1}^{T}\mathbf{e}_{1}\mathbf{n}^{T}\mathbf{e}_{1} + \mathbf{r}_{1}^{T}\mathbf{g}_{1}\mathbf{n}^{T}\mathbf{g}_{1})\mathbf{h}_{1}^{T}\mathbf{n}\}$$
(3.67)

Thus,  $\|\mathbf{K}^{-1}\|_F^2$  can be expressed as

$$\|\mathbf{K}^{-1}\|_F^2 = \sum_{j=1}^3 d_j^2 \tag{3.68}$$

with  $d_j$  defined in Eq. (3.65), for j = 1, similar expressions following for j = 2, 3.

#### 3.6.2.3 Solving the Optimization Problem at a Symmetric Posture

The evaluation of the condition number under arbitrary postures is cumbersome, since the dimension of the corresponding design space is 11; it is thus desirable to limit the design space to a more manageable subspace. Due to the symmetric architecture of the robot under study, the minimum condition number is most likely to be found at a symmetric posture. Apparently, such a posture occurs when the centroid of the MP lies right above that of the BP, and the MP has the reference orientation shown in Fig. 3.2, i.e.,  $\theta = 0$  and  $c_x = c_y = 0$ , where  $c_x$  and  $c_y$  represent the components of  $\mathbf{c}$  along the x and y axes in the BP frame. Now the set of design variables becomes<sup>14</sup>

$$\mathbf{x} = \begin{bmatrix} b & \alpha & \gamma & L \end{bmatrix}^T \tag{3.69}$$

Moreover, Eqs. (3.62) and (3.68), evaluated in this subspace, are simplified dramatically:

$$\|\mathbf{K}\|_{F}^{2} = 6L^{2} + \alpha^{2}b^{2} + \frac{4\alpha^{4}b^{2} - 4\alpha^{3}b^{2} + \alpha^{2}b^{2}}{4\alpha^{2} - 4\alpha + 12\gamma^{2} + 1}$$

$$= \frac{2(12L^{2}\alpha^{2} - 12L^{2}\alpha + 36L^{2}\gamma^{2} + 3L^{2} + 4\alpha^{4}b^{2} - 4\alpha^{3}b^{2} + 6\alpha^{2}b^{2}\gamma^{2} + \alpha^{2}b^{2})}{4\alpha^{2} - 4\alpha + 12\gamma^{2} + 1}$$
(3.70)

and

$$\|\mathbf{K}^{-1}\|_{F}^{2} = \frac{60 L^{2} \alpha^{2} - 60 L^{2} \alpha + 288 L^{2} \gamma^{2} + 15 L^{2} + 20 \alpha^{4} b^{2} - 20 \alpha^{3} b^{2} + 12 \alpha^{2} b^{2} \gamma^{2} + 5 \alpha^{2} b^{2}}{3 L^{2} \alpha^{2} b^{2} (4 \alpha^{2} - 4 \alpha + 1)}$$

$$(3.71)$$

Furthermore, defining  $\rho$  as the ratio L/b, the objective function becomes

$$f(\mathbf{x}) = \frac{1}{36} \|\mathbf{K}\|_F^2 \|\mathbf{K}^{-1}\|_F^2 = \kappa_F^2(\mathbf{K}) = \frac{N}{D}$$
 (3.72)

where

$$N = N_4 \rho^4 + N_2 \rho^2 + N_0, \quad D = 54(1 - 2\alpha)^2 \alpha^2 [(1 - 2\alpha)^2 + 12\gamma^2] \rho^2$$
 (3.73)

with

$$N_{0} = \alpha^{4}[(1 - 2\alpha)^{2} + 6\gamma^{2}][5 + 20(-1 + \alpha)\alpha + 12\gamma^{2}]$$

$$N_{2} = 3\alpha^{2}[(1 - 2\alpha)^{2} + 12\gamma^{2}][5 + 20(-1 + \alpha)\alpha + 12\gamma^{2}]$$

$$+ 3\alpha^{2}[(1 - 2\alpha)^{2} + 6\gamma^{2}][5 + 20(-1 + \alpha)\alpha + 96\gamma^{2}]$$

$$N_{4} = 9[(1 - 2\alpha)^{2} + 12\gamma^{2}][5 + 20(-1 + \alpha)\alpha + 96\gamma^{2}]$$
(3.74)

<sup>&</sup>lt;sup>14</sup>We should use  $c_z$  instead of  $\gamma$  as one of the design parameters, but here we use  $\gamma$ , the height of the MP plane at the reference posture of Fig. 3.2 as one of the design variables instead, for conciseness.

which are free of b and L. Moreover, by inspection, it is found that  $\rho$  always appears at even powers, and  $\alpha$  mostly appears as  $2\alpha - 1$ . For these reasons, we define

$$\lambda = \rho^2, \quad \beta = 2\alpha - 1 \tag{3.75}$$

Then we redefine the vector of design variables as  $\mathbf{x} = [\beta, \gamma, \lambda]^T$ , thereby simplifying the numerator and denominator of  $f(\mathbf{x})$  as appearing in Eq. (3.72), namely,

$$f(\beta, \gamma, \lambda) = \kappa_F^2(\mathbf{K}) = \frac{N}{D} \to \min_{\mathbf{x}}$$
 (3.76)

where

$$N = 144 \left(\beta^2 + 12\gamma^2\right) \left(5\beta^2 + 96\gamma^2\right) \lambda^2 + 24(\beta + 1)^2 \left(5\beta^4 + 99\beta^2\gamma^2 + 360\gamma^4\right) \lambda$$
$$+ (\beta + 1)^4 \left(5\beta^4 + 42\beta^2\gamma^2 + 72\gamma^4\right)$$
$$D = 216\beta^2 (1+\beta)^2 (\beta^2 + 12\gamma^2) \lambda = 144 \times \frac{3}{2}\beta^2 (1+\beta)^2 (\beta^2 + 12\gamma^2) \lambda$$
 (3.77)

Next, we solve the optimization problem by differentiating  $f(\mathbf{x})$  with respect to  $\beta, \gamma$  and  $\lambda$ . By zeroing the partial derivative of f w.r.t.  $\lambda$ , we obtain  $\lambda$  as a function of  $\beta$  and  $\gamma$ , i.e.,

$$\lambda = \frac{1}{12} \sqrt{\frac{(\beta + 1)^4 (5\beta^4 + 42\beta^2 \gamma^2 + 72\gamma^4)}{5\beta^4 + 156\beta^2 \gamma^2 + 1152\gamma^4}}$$
(3.78)

Substitution of Eq. (3.78) into Eq. (3.76) leads to a bivariate function, which only involves the design parameters  $\beta$  and  $\gamma$ . Next we plot<sup>15</sup>  $\kappa_F^{-1}(\mathbf{K})$  as  $1/\sqrt{f}$  vs.  $\beta$  and  $\gamma$ , as shown in Fig. 3.12.

It is observed that the minimum condition number is achieved when  $\gamma = 0$  and  $\beta \neq 0$ , the said minimum being

$$\kappa_F(\mathbf{K})_{min} = \frac{\sqrt{10}}{3} \tag{3.79}$$

i.e.,  $\kappa_F(\mathbf{K})_{min} = 1.0541$ , to four decimal places, or pretty close to unity.

Next, we calculate the characteristic length for a given architecture, i.e., for a given  $\beta$ . It is observed that the minimum condition number is achieved when  $\gamma = 0$ . Then we can

 $<sup>^{15}</sup>$ As  $\kappa_F(\mathbf{K})$  is unbounded from above, but bounded from below by unity, it is more meaningful to plot  $1/\kappa_F(\mathbf{K})$ .

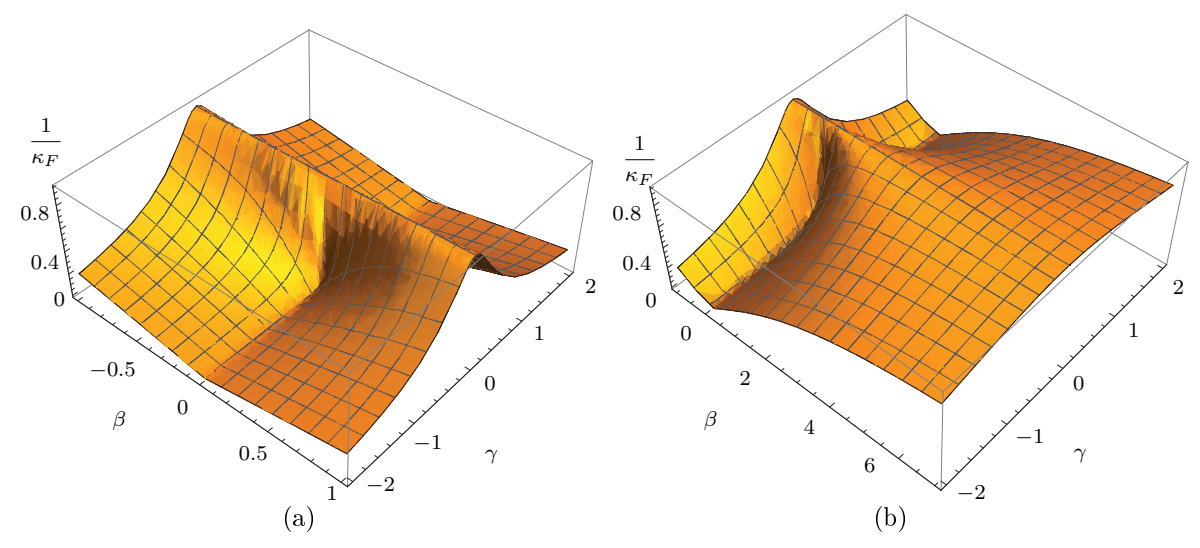


Figure 3.12: Inverse condition number of the robot vs.  $\beta$  and  $\gamma$ , (a)  $\beta \in (-1,1), \gamma \in (-2,2)$  (b)  $\beta \in (-1,7), \gamma \in (-2,2)$ 

obtain L as

$$L = b\rho = b\sqrt{\lambda}|_{\gamma=0} = \sqrt{\frac{1}{12}} \left( \frac{(\beta+1)^4 \cdot 5\beta^4}{5\beta^4} \right)^{\frac{1}{4}} b = \frac{1}{\sqrt{3}} |\alpha| b = \frac{\sqrt{3}}{3} a$$
 (3.80)

That is, the characteristic length is the distance from any spherical-joint centre to the operation point, which is meaningful.

#### 3.6.2.4 Some Remarks

It can be concluded from Fig. 3.12 that

- The graph is symmetric w.r.t.  $\beta = 0$  and  $\gamma = 0$ . Moreover, The dexterity is higher when the MP plane is near the BP plane.
- For the choice of a, it is found that the farther a is from b/2, the lower the condition number. A reasonable range for  $\alpha$  may be given around  $(0, 0.4] \cup [0.6, 4]$  or, equivalently,  $\beta \in (-1, -0.2] \cup [0.2, 7]$ .
- If we want the MP to operate near the BP, we should choose a such that a < b/2; under these conditions, the smaller the MP, the higher the dexterity. It is, however, noteworthy that when a is relatively large, for example, when a = 2b ( $\beta = 3$ ), it can be seen that even if we change the value of  $\gamma$ , the condition number remains below 10.0, which means a good

dexterity, as shown in Fig. 3.13, although the MP cannot cross the BP in this case. It is noteworthy that this figure only shows the information for a set of symmetric MP poses, rather than arbitrary poses.

• The characteristic length for a given architecture, i.e., for given  $\alpha$  and b, is given in Eq. (3.80). It is noted from Eq. (3.78), however, that the value of  $\lambda$  varies as  $\gamma$  changes. This means that the characteristic length for a given architecture can minimize the condition number of the robot at the optimum pose, but does not necessarily minimize the condition number elsewhere. Considering this fact, we re-plot the condition number using the characteristic length given in Eq. (3.80), as shown in Fig. 3.13, where the range of  $\beta$  is set as  $\beta \in [0.2, 7]$  in order to avoid the singularity when  $\beta = 0$ . It is shown that the difference is relatively small when the MP is at the reference orientation.

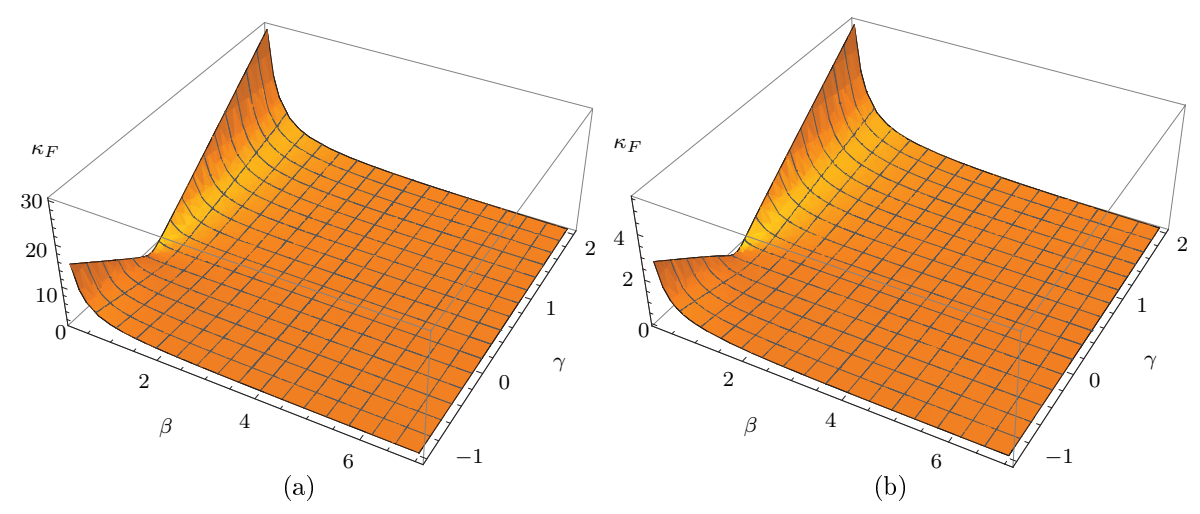


**Figure 3.13:** (a) Condition number of the SDelta Robot vs.  $\beta$  and  $\gamma$ , using the unique characteristic length for the architecture (b) the difference between (a) and previous calculation shown in Fig. 3.12

## 3.6.3 Discussion of the Optimization Results

From the above optimization exercise, we can conclude that the dexterity is generally higher when the distance from the centroid of the MP to the BP plane (i.e.,  $c_z^{16}$ ) is smaller. It is shown that the SDelta can always achieve a minimum condition number close to unity when the centroids of the MP and the BP coincide and the former finds itself at the reference orientation, regardless of the ratio a/b; this leaves us a big margin to optimize other

<sup>&</sup>lt;sup>16</sup>The Z- component of the position vector  $\mathbf{c}$  of the operation point.



Figure 3.14: An example of the SDelta indicating its large orientation capacity when the centroid of the MP is close to the BP plane

performance indices. Moreover, from tests in CAD software, the MP can almost flip w.r.t. some axes in the BP plane when  $c_z$  is small, the angle of rotation being around  $\pm 80^{\circ}$  about these axes. An example is shown in Fig. 3.14 with  $\alpha = 0.32$ . Hence, this architecture has a good potential to extend the orientation workspace, which is useful, e.g., for increasing the operation range of machine tools and motion simulators. However, this layout requires a small-size MP w.r.t. that of the BP, and a small range of the stroke of the intermediate P joint of each limb. These physical constraints limit the positioning workspace. Fortunately, the analyses and optimization reveal that when the distance from the centroid of the MP to the BP plane is bigger, the condition number is also reasonably low, and the positioning workspace becomes larger. This means that, upon proper choice of a, b and  $\gamma$ , we can obtain relatively large operation zones with high dexterity within the workspace.

The above statements indicate that there is a compromise in the choice of  $c_z$  between the requirements of high dexterity and large positioning workspace in the current design of the SDelta, although the dexterity is generally acceptable. This compromise is mostly introduced by the physical constraints of the limb kinematic chains. The idea of exploring different layouts of the three C-drives, proposed at the end of Section 3.5, is brought up again here, which, in our opinion, have the potential to yield a larger singularity-free workspace together with a good dexterity. For example, it can be readily shown that the layout with three vertical axes yields a larger workspace volume, while the highest dexterity (with the same optimal value of the current design) can be obtained along a continuous vertical axes, though this layout is more suitable for small-size workpieces. Hence, other layouts of the three C-drives may be explored, such as those with three vertical axes, three intersecting

orthogonal axes or three skew orthogonal axes. These alternatives have the potential to provide a larger singularity-free workspace and a good dexterity. This work is recommended for future research.

So far we have completed the forward-displacement, singularity and workspace analyses of the SDelta, which are essential for robot evaluation, simulation and control. Moreover, its optimization, based on a dexterity index, is provided. These analyses and optimization give us the whole picture of the performance of the robot at the kinematics level.

During the analyses for the SDelta, we found an expression for the inverse of its forward Jacobian matrix in symbolic form, which applies to a large class of PKMs. This expression is quite useful in many applications, e.g., in singularity analysis, design for isotropy and optimization. In Chapter 4 we will elaborate on its application in the optimum design of this large class of PKMs.

## Chapter 4

## THE DESIGN FOR ISOTROPY OF A CLASS OF SIX-DOF PKMS

The design for isotropy of a large class of six-dof parallel-kinematics machines is investigated in this chapter, for the plausible case in which the axes of the six actuated wrenches intersect pairwise. As stated previously, two Jacobian matrices occur in the basic kinematic model of a PKM, relating the moving-platform twist with the array of motor rates. The one multiplying the former is termed the forward Jacobian [68], denoted  $\mathbf{K}$ , that multiplying the latter, the inverse Jacobian, denoted  $\mathbf{D}$  in this chapter<sup>1</sup>. A low condition number of  $\mathbf{K}$ , say, within O(2), is needed to avoid large roundoff-error amplification when solving for the MP twist in terms of the array of joint rates. This is needed in forward kinematics, for example, to estimate the MP positioning error, to be fed back into the motors for error-compensation. A similarly well-conditioned inverse Jacobian is needed to compute the actuated-joint rates in real time, to be fed back into the motor controllers.

Several isotropic six-limb, six-dof PKMs have been proposed [68–70]. Moreover, design for isotropy has been investigated in a fairly general framework via the geometric relations of the six lines (representing the axes of the six actuated wrenches) and one point (the operation point), based on which Tsai et al. [87] proposed the concept of "isotropy generator". With this approach, several designs of six-limb isotropic robots have been reported; however, in the foregoing paper, the authors assume that the two  $3 \times 3$  blocks of the Jacobian associated with the six unit vectors of the actuated wrenches are orthogonal matrices, which is not a necessary condition for isotropy, the condition thereby leading to a limited class of isotropic

<sup>&</sup>lt;sup>1</sup>For the general PKM investigated in this chapter—which is not actuated by the C-drive, the inverse Jacobian is no longer a product two matrices—the *drive Jacobian* and the *actuator Jacobian*, as proposed in this dissertation. Hence, we use **D** itself to represent the inverse Jacobian for the general PKM investigated in this chapter.

designs. In a follow-up paper, Tsai et al. [88] proposed a numerical method capable of using the parameters of a n-dof redundant isotropic PKM as the initial guess to obtain a (n-1)-dof isotropic PKM, and eventually, obtain six-dof isotropic PKMs. This method does not impose requirements either on the shape of the MP or on the distances from the wrench lines to the operation point; however, the design thus obtained depends heavily on the choice of the initial guess of the design parameters.

In this chapter, firstly, the kinematics relations, the expressions for the underlying forward Jacobian matrix [68] and its inverse in symbolic form, derived in Chapter 3, are briefly recalled. Next, based on this symbolic expression, a novel approach is proposed for the DfI of this class of PKMs. Several numerical examples are given. Expressions are provided for the design parameters that yield isotropy. It is noteworthy that this method does not require any initial guess and is capable of giving all the possible solutions leading to isotropy, and hence, completes the DfI of this class of PKMs. Moreover, we propose the concept of quasi-isotropy, which guarantees a small condition number with six orthogonal wrench axes, yielding high dexterity, accuracy, and homogeneity of the motion of the MP, within a finite region of the workspace. This greatly enriches the list of candidates for the MP shape and the location of the operation point, required, e.g., when a gripper or another tool is attached to the MP triangle.

## 4.1 The Kinematics Jacobian Matrix and Its Symbolic Inverse

#### 4.1.1 The Kinematics Relations

A large class of six-dof PKMs with six actuated-wrench axes intersecting pairwise have been reported<sup>2</sup> [39], an example being the SDelta, whose architecture and actuated wrenches are reproduced in Figs. 4.1 and 4.2 for quick reference<sup>3</sup>. Next, we use this example to derive

<sup>&</sup>lt;sup>2</sup>Numerous examples of such PKMs can be found in the literature [41, 44].

<sup>&</sup>lt;sup>3</sup>Slight differences between these two figures and the corresponding figures in previous chapters are to be highlighted: notation items not needed in Chapter 4 are removed; the joint variables for a general PKM of this class are denoted with alternative symbols to make a distinction with those of the specific instance of the SDelta.

the kinematics relations, the Jacobian matrix and its symbolic inverse for this class of PKMs.

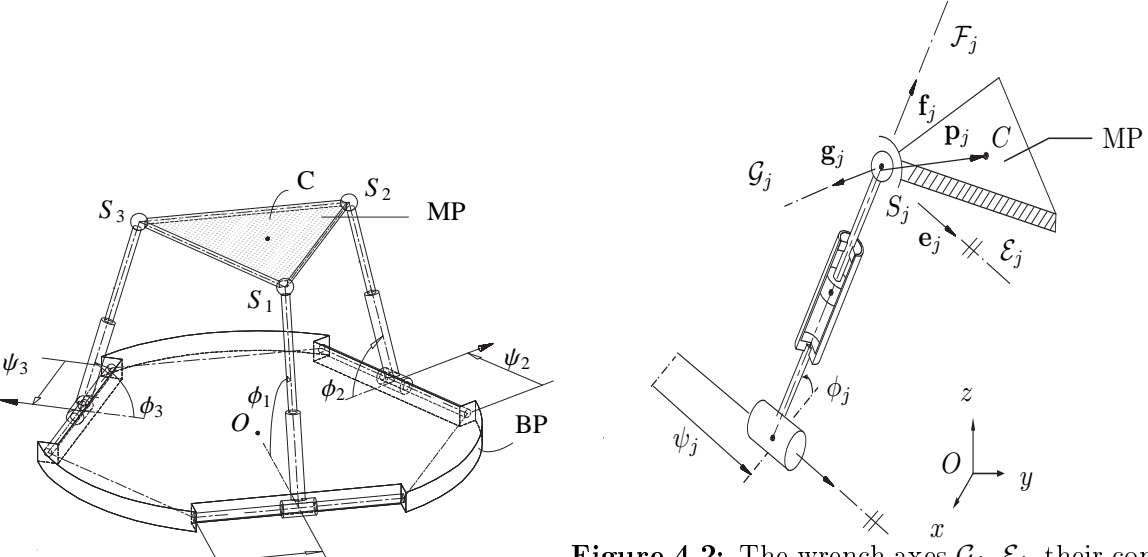


Figure 4.1: Architecture of the SDelta Robot

**Figure 4.2:** The wrench axes  $\mathcal{G}_j$ ,  $\mathcal{E}_j$ , their common perpendicular  $\mathcal{F}_j$ , and vector  $\mathbf{p}_j$  of the jth limb of the SDelta Robot

We start by introducing the pertinent notation:  $\mathbf{e}_j$  and  $\mathbf{g}_j$  are again defined as the unit vectors parallel to the axes of the jth pair of actuated wrenches of the jth limb, for j = 1, 2, 3, as shown in Fig. 4.2. Moreover, the corresponding axes of the actuated wrenches are denoted  $\mathcal{E}_j$  and  $\mathcal{G}_j$ , respectively, which intersect at  $^4$   $S_j$ , for j = 1, 2, 3. The plane defined by  $\mathcal{E}_j$  and  $\mathcal{G}_j$  is labeled  $\Pi_j$ , for j = 1, 2, 3, the plane of the moving platform triangle  $S_1S_2S_3$  being  $\Pi_4$ .

Next, the *operation point* on the MP is C, of position vector  $\mathbf{c}$ ;  $\mathbf{p}_j$  is defined as vector  $\overrightarrow{S_jC}$ . Lastly, the twist of the MP, already defined, is recalled:  $\mathbf{t} = [\boldsymbol{\omega}^T, \ \dot{\mathbf{c}}^T]^T$ .

It is noteworthy that, due to the special layout of the SDelta, we have  $\mathbf{e}_j \perp \mathbf{g}_j$ , for j = 1, 2, 3. Moreover, depending on the type of actuated joints (if we regard the six-dimensional C-drive array as the input of the SDelta, then the actuated joints are one  $\underline{\mathbf{R}}$  and one  $\underline{\mathbf{P}}$  joint for each limb), the six diagonal entries of the inverse Jacobian—as per Eq. (3.6)—bear different units, three of them being constant. However, for an arbitrary six-dof PKM whose actuated-wrench axes intersect pairwise, none of these special features necessarily holds. In

<sup>&</sup>lt;sup>4</sup>For the case of a three-limb PKM with one spherical joint in each limb,  $S_j$  refers to the centre of the spherical joint of the jth limb.

order to keep the derivation general, we define the input array as

$$\dot{\boldsymbol{\phi}} = [\dot{\phi}_1, \, \dot{\psi}_1, \, \dot{\phi}_2, \, \dot{\psi}_2, \, \dot{\phi}_3, \, \dot{\psi}_3]^T \tag{4.1}$$

with  $\dot{\phi}_j$ ,  $\dot{\psi}_j$  representing the joint rates corresponding to the wrenches of axes  $\mathcal{G}_j$  and  $\mathcal{E}_j$ , respectively, for j = 1, 2, 3, as shown in Fig. 4.2. It is noteworthy that  $\{\phi_j\}_1^3$  or  $\{\psi_j\}_1^3$  can represent either translation or rotation for a general PKM of this class.

According to screw theory [77, 78], it can be readily shown that the kinematics relation of this class of robots bears the form [75]

$$\mathbf{Kt} = \mathbf{D}\dot{\boldsymbol{\phi}} \tag{4.2}$$

with

$$\mathbf{K} = \begin{bmatrix} (\mathbf{g}_1 \times \mathbf{p}_1)^T & \mathbf{g}_1^T \\ (\mathbf{e}_1 \times \mathbf{p}_1)^T & \mathbf{e}_1^T \\ (\mathbf{g}_2 \times \mathbf{p}_2)^T & \mathbf{g}_2^T \\ (\mathbf{e}_2 \times \mathbf{p}_2)^T & \mathbf{e}_2^T \\ (\mathbf{g}_3 \times \mathbf{p}_3)^T & \mathbf{g}_3^T \\ (\mathbf{e}_3 \times \mathbf{p}_3)^T & \mathbf{e}_3^T \end{bmatrix}, \quad \mathbf{D} = \operatorname{diag}(l_1, m_1, l_2, m_2, l_3, m_3)$$
(4.3)

Moreover,  $l_j$  and  $m_j$  represent the reciprocal products [89] of  $\mathcal{G}_j$  and  $\mathcal{E}_j$  with their corresponding axes of actuated joints, which can either carry units of length or being dimensionless, depending on the type of the corresponding actuated joint ( $\underline{R}$  or  $\underline{P}$ ).

## 4.1.2 The Symbolic Inverse of the Forward Jacobian

Due to the special layout of the six actuated wrenches, the Jacobian matrix  $\mathbf{K}$  of the said large class of robots always bears the form in Eq. (4.3), i.e., the six rows of  $\mathbf{K}$  represent the Plücker coordinates of six lines that intersect pairwise. Furthermore,  $\mathbf{K}^{-1}$ , denoted  $\overline{\mathbf{K}}$  and derived in Chapter 3, is reproduced here for quick reference

$$\overline{\mathbf{K}} = \frac{1}{t} \begin{bmatrix} \mathbf{u}_1 & -\mathbf{u}_2 & \mathbf{u}_3 & -\mathbf{u}_4 & \mathbf{u}_5 & -\mathbf{u}_6 \\ \mathbf{m}_1 & -\mathbf{m}_2 & \mathbf{m}_3 & -\mathbf{m}_4 & \mathbf{m}_5 & -\mathbf{m}_6 \end{bmatrix}$$
(4.4)

with

$$t = 2s_{\Delta}(\mathbf{f}_1 \times \mathbf{r}_1) \cdot \mathbf{n} \tag{4.5}$$

and its first two columns given by

$$\mathbf{u}_{1} = -(\mathbf{r}_{1}^{T}\mathbf{e}_{1})(\mathbf{p}_{2} - \mathbf{p}_{3}) + 2s_{\Delta}(\mathbf{n}^{T}\mathbf{e}_{1})(\mathbf{f}_{2} \times \mathbf{f}_{3})$$

$$\mathbf{m}_{1} = 2s_{\Delta}(\mathbf{n}^{T}\mathbf{e}_{1})\mathbf{h}_{1} - (\mathbf{r}_{1}^{T}\mathbf{e}_{1})\mathbf{p}_{2} \times \mathbf{p}_{3}$$

$$(4.6)$$

and

$$\mathbf{u}_{2} = -(\mathbf{r}_{1}^{T}\mathbf{g}_{1})(\mathbf{p}_{2} - \mathbf{p}_{3}) + 2s_{\Delta}(\mathbf{n}^{T}\mathbf{g}_{1})(\mathbf{f}_{2} \times \mathbf{f}_{3})$$

$$\mathbf{m}_{2} = 2s_{\Delta}(\mathbf{n}^{T}\mathbf{g}_{1})\mathbf{h}_{1} - (\mathbf{r}_{1}^{T}\mathbf{g}_{1})\mathbf{p}_{2} \times \mathbf{p}_{3}$$

$$(4.7)$$

with  $\mathbf{r}_1$  and  $\mathbf{h}_1$  defined as

$$\mathbf{r}_1 = [(\mathbf{p}_1 - \mathbf{p}_3)^T \mathbf{f}_3] \mathbf{f}_2 - [(\mathbf{p}_1 - \mathbf{p}_2)^T \mathbf{f}_2] \mathbf{f}_3$$

$$\mathbf{h}_1 = (\mathbf{f}_2^T \mathbf{p}_2) \mathbf{f}_3 - (\mathbf{f}_3^T \mathbf{p}_3) \mathbf{f}_2$$

$$(4.8)$$

Moreover,  $\mathbf{f}_j \equiv \mathbf{g}_j \times \mathbf{e}_j$ , for j = 1, 2, 3,  $s_{\Delta}$  denoting the area of the triangle  $S_1 S_2 S_3$ , and  $\mathbf{n}$  representing the unit vector normal to the MP triangle, namely,  $\mathbf{n} \equiv \overrightarrow{S_2 S_1} \times \overrightarrow{S_3 S_2} / \|\overrightarrow{S_2 S_1} \times \overrightarrow{S_3 S_2} \|_2$ .

Furthermore, the third and fifth columns of  $\overline{\mathbf{K}}$  can be found upon exchanging subscripts 1, 2, 3 with 2, 3, 1 or 3, 1, 2 in the RHS of Eqs. (4.6), respectively; its fourth and sixth columns can be obtained upon exchanging subscripts 1, 2, 3 with 2, 3, 1 or, correspondingly, with 3, 1, 2 in the RHS of Eqs. (4.7)<sup>5</sup>. It is noteworthy that the expression for  $\mathbf{K}^{-1}$  does not impose any constraint on the location of the operation point C. As a matter of fact, C need not even lie in the plane of  $S_1S_2S_3$ . Hence, we have more flexibility in choosing the location of the operation point, which may ease the design when, e.g., a gripper or another tool is to be attached to the MP triangle.

<sup>&</sup>lt;sup>5</sup>The corresponding subscripts of  $\mathbf{r}_j$ ,  $\mathbf{h}_j$  and all the terms within  $\mathbf{r}_j$  and  $\mathbf{h}_j$  have to be exchanged as well.

## 4.2 The Isotropic Design

As noted previously, dexterity characterizes the kinematic accuracy and the homogeneity of the motion of the MP along different directions in the motion space, which is crucial for an acceptable robot performance. The conditions for isotropy, i.e., for maximum dexterity, can be stated as

$$\mathbf{K}_h \mathbf{K}_h^T = \sigma_K^2 \mathbf{1}_{6 \times 6}, \quad \mathbf{D}_h \mathbf{D}_h^T = \sigma_D^2 \mathbf{1}_{6 \times 6}$$

$$\tag{4.9}$$

with  $\mathbf{K}_h$  and  $\mathbf{D}_h$  denoting the two Jacobian matrices in their homogeneous form, to be introduced presently; in this case, all the singular values of  $\mathbf{K}_h$  are identical, and the same goes for  $\mathbf{D}_h$ , with  $\sigma_K$  and  $\sigma_D$  representing, correspondingly, their sextuple singular values.

The maximum dexterity is generally obtained via a mathematical-programming problem (MPP). However, when the problem at hand admits an isotropic solution, as in this case, the isotropy condition in Eqs. (4.9) obviates the MPP. In this section, we derive the isotropy condition for three-limb, six-dof PKMs whose actuated wrench axes intersect pairwise, with an arbitrarily chosen location of the operation point.

Firstly, we study the isotropy condition of  $\mathbf{K}$ . Since its entries bear different units, we again produce the homogeneous form  $\mathbf{K}_h$  of  $\mathbf{K}$  upon introducing the characteristic length L [68],  $\mathbf{K}$  and  $\overline{\mathbf{K}}$  then taking the homogeneous forms

$$\mathbf{K}_{h} = \begin{bmatrix} (\mathbf{g}_{1} \times \mathbf{p}_{1})^{T} & L\mathbf{g}_{1}^{T} \\ (\mathbf{e}_{1} \times \mathbf{p}_{1})^{T} & L\mathbf{e}_{1}^{T} \\ (\mathbf{g}_{2} \times \mathbf{p}_{2})^{T} & L\mathbf{g}_{2}^{T} \\ (\mathbf{e}_{2} \times \mathbf{p}_{2})^{T} & L\mathbf{e}_{2}^{T} \\ (\mathbf{g}_{3} \times \mathbf{p}_{3})^{T} & L\mathbf{g}_{3}^{T} \\ (\mathbf{e}_{3} \times \mathbf{p}_{3})^{T} & L\mathbf{e}_{3}^{T} \end{bmatrix}$$

$$(4.10)$$

and

$$\overline{\mathbf{K}}_h = \frac{1}{t} \begin{bmatrix} \mathbf{u}_1 & -\mathbf{u}_2 & \mathbf{u}_3 & -\mathbf{u}_4 & \mathbf{u}_5 & -\mathbf{u}_6 \\ \mathbf{m}_1/L & -\mathbf{m}_2/L & \mathbf{m}_3/L & -\mathbf{m}_4/L & \mathbf{m}_5/L & -\mathbf{m}_6/L \end{bmatrix}$$
(4.11)

It is noteworthy that some authors use other approaches to cope with this inconsistency

of units; for example, Tsai et al. [88] proposed an index based on the three criteria for isotropy proposed by Klein [90]. However, it can be readily verified that the method using the characteristic length to make **K** into a dimensionally homogeneous matrix is a necessary and sufficient condition for the three Klein criteria [90], and hence, equivalent to the measure of isotropy used by Tsai et al. [88]. Since using the characteristic length yields a much simpler formulation, we adopt here the approach based on this length.

From the isotropy condition (4.9), we have

$$\mathbf{K}_h^T = \sigma_K^2 \mathbf{K}_h^{-1} = \sigma_K^2 \overline{\mathbf{K}}_h \tag{4.12}$$

Now we look at the first two columns of the matrix equation (4.12). Since  $\sigma_K$  and L are undetermined at this stage, we define  $\sigma_u = \sigma_K^2/t$ ,  $\sigma_m = \sigma_K^2/(tL^2)$ , with t given in Eq. (4.5). Then the first two columns of Eq. (4.12) yield the conditions:

$$\mathbf{u}_{1} = -\mathbf{r}_{1}^{T} \mathbf{e}_{1} \mathbf{s}_{23} + 2s_{\Delta} \mathbf{n}^{T} \mathbf{e}_{1} (\mathbf{f}_{2} \times \mathbf{f}_{3}) = \mathbf{g}_{1} \times \mathbf{p}_{1} / \sigma_{u}$$

$$\mathbf{u}_{2} = -\mathbf{r}_{1}^{T} \mathbf{g}_{1} \mathbf{s}_{23} + 2s_{\Delta} \mathbf{n}^{T} \mathbf{g}_{1} (\mathbf{f}_{2} \times \mathbf{f}_{3}) = -\mathbf{e}_{1} \times \mathbf{p}_{1} / \sigma_{u}$$

$$(4.13)$$

and

$$\mathbf{m}_{1} = 2s_{\Delta}(\mathbf{n}^{T}\mathbf{e}_{1})\mathbf{h}_{1} - (\mathbf{r}_{1}^{T}\mathbf{e}_{1})\mathbf{p}_{2} \times \mathbf{p}_{3} = \mathbf{g}_{1}/\sigma_{m}$$

$$\mathbf{m}_{2} = 2s_{\Delta}(\mathbf{n}^{T}\mathbf{g}_{1})\mathbf{h}_{1} - (\mathbf{r}_{1}^{T}\mathbf{g}_{1})\mathbf{p}_{2} \times \mathbf{p}_{3} = -\mathbf{e}_{1}/\sigma_{m}$$

$$(4.14)$$

where  $\mathbf{s}_{ij} \equiv \mathbf{p}_i - \mathbf{p}_j$  denotes vector  $\overrightarrow{S_iS_j}$ . Next, we conduct the geometric analysis in the MP frame, as  $\mathbf{p}_j$  is a known constant vector in this frame, for j = 1, 2, 3. It is apparent that  $\mathbf{u}_1$  and  $\mathbf{u}_2$  are both linear combinations of  $\mathbf{s}_{23}$  and  $\mathbf{f}_2 \times \mathbf{f}_3$ . Hence,  $\mathbf{s}_{23}$  and  $\mathbf{f}_2 \times \mathbf{f}_3$  define a plane whose normal is parallel to  $(\mathbf{g}_1 \times \mathbf{p}_1) \times (\mathbf{e}_1 \times \mathbf{p}_1) = [(\mathbf{g}_1 \times \mathbf{e}_1)^T \mathbf{p}_1] \mathbf{p}_1 = (\mathbf{f}_1^T \mathbf{p}_1) \mathbf{p}_1$ . Thus, the normal to the foregoing plane is parallel to  $\mathbf{p}_1$ , i.e.,

$$\mathbf{s}_{23}^T \mathbf{p}_1 = 0, \quad (\mathbf{f}_2 \times \mathbf{f}_3)^T \mathbf{p}_1 = 0 \tag{4.15}$$

However, it is noteworthy that the above derivation is based on the assumption that  $\mathbf{s}_{23}$  and  $\mathbf{f}_2 \times \mathbf{f}_3$  are linearly independent. Let us analyze the case when they are linearly dependent. This involves two possibilities:

- $\mathbf{f}_2 \times \mathbf{f}_3 = \mathbf{0}$ , namely,  $\mathbf{f}_2 \parallel \mathbf{f}_3$ . Then,  $\mathbf{u}_1 \parallel \mathbf{u}_2 \parallel \mathbf{s}_{23} \parallel (\mathbf{g}_1 \times \mathbf{p}_1) \parallel (\mathbf{e}_1 \times \mathbf{p}_1)$ , yielding  $(\mathbf{g}_1 \times \mathbf{p}_1) \times (\mathbf{e}_1 \times \mathbf{p}_1) = (\mathbf{f}_1^T \mathbf{p}_1) \mathbf{p}_1 = \mathbf{0}$ , and hence,  $\mathbf{f}_1 \perp \mathbf{p}_1$ . Moreover, since  $\mathbf{f}_j$  is normal to the  $\Pi_j$  plane, for j = 1, 2, 3, we can conclude that  $\mathbf{p}_1$  lies in the plane  $\Pi_1$ . Furthermore, since  $\mathbf{e}_1$  and  $\mathbf{g}_1$  lie in  $\Pi_1$ , we can conclude that  $(\mathbf{g}_1 \times \mathbf{p}_1) \parallel (\mathbf{e}_1 \times \mathbf{p}_1) \parallel \mathbf{f}_1 \parallel \mathbf{s}_{23}$ . This means that  $\mathbf{s}_{23}$  is normal to  $\Pi_1$ , while  $\mathbf{p}_1$  lies in  $\Pi_1$ . It is apparent that Eqs. (4.15) still hold in this case, and need not be discussed further.
- the scalar coefficients in Eqs. (4.13) obey the relation

$$(-\mathbf{r}_1^T \mathbf{e}_1)/(2s_{\Delta} \mathbf{n}^T \mathbf{e}_1) = (-\mathbf{r}_1^T \mathbf{g}_1)/(2s_{\Delta} \mathbf{n}^T \mathbf{g}_1)$$
(4.16)

which, upon simplification, yields

$$-(\mathbf{r}_1^T \mathbf{e}_1)(\mathbf{n}^T \mathbf{g}_1) + (\mathbf{n}^T \mathbf{e}_1)(\mathbf{r}_1^T \mathbf{g}_1) = [(\mathbf{g}_1 \times \mathbf{e}_1) \times \mathbf{r}_1]^T \mathbf{n} = (\mathbf{f}_1 \times \mathbf{r}_1)^T \mathbf{n} = t/(2s_\Delta) = 0 \quad (4.17)$$

thereby leading to a singularity, and hence, this condition cannot yield isotropy.

In summary,  $\mathbf{s}_{23}$  and  $\mathbf{f}_2 \times \mathbf{f}_3$  must be linearly independent and Eqs. (4.15) must hold, in order to reach isotropy. Considering this condition for the three pairs of intersecting wrenches, we can conclude that the operation point C (or its projection on  $\Pi_4$ ) must be chosen as the orthocentre of the triangle  $S_1S_2S_3$ .

Next, we look at Eqs. (4.14). A similar analysis leads to two possibilities:

- $\mathbf{h}_1 \perp \mathbf{f}_1$  and  $\mathbf{p}_2 \times \mathbf{p}_3 \perp \mathbf{f}_1$ , or
- $\mathbf{h}_1 = \mathbf{0}$ ; then,  $\mathbf{g}_1 \parallel \mathbf{e}_1$ , which leads to a singularity.

In summary, the geometric conditions below must be satisfied for isotropy:

$$\mathbf{s}_{23}^T \mathbf{p}_1 = 0 \tag{4.18a}$$

$$(\mathbf{f}_2 \times \mathbf{f}_3)^T \mathbf{p}_1 = 0 \tag{4.18b}$$

$$\mathbf{h}_1^T \mathbf{f}_1 = 0 \tag{4.18c}$$

$$(\mathbf{p}_2 \times \mathbf{p}_3)^T \mathbf{f}_1 = 0 \tag{4.18d}$$

which still hold when we exchange subscripts 1, 2, 3 with 2, 3, 1 or 3, 1, 2, respectively. Next, we derive the remaining isotropy conditions.

### 4.2.1 The Operation Point Lying in the MP Triangle

Firstly, we study the case when the operation point C lies in  $\Pi_4$ . According to Eq. (4.18a), C must coincide with the ortho-centre of triangle  $S_1S_2S_3$ . Moreover, it is apparent that  $\mathbf{p}_2 \times \mathbf{p}_3 \parallel \mathbf{n}$  in this case; according to Eq. (4.18d), we conclude that  $\mathbf{f}_1$  has to lie in  $\Pi_4$ , as shown in Fig 4.3. Similarly,  $\mathbf{f}_2$  and  $\mathbf{f}_3$  must lie in  $\Pi_4$ . Under these conditions, Eq. (4.18b) naturally holds. Since  $\mathbf{f}_j$  is in fact normal to the plane  $\Pi_j$ , for j = 1, 2, 3, these three planes must be normal to  $\Pi_4$ .

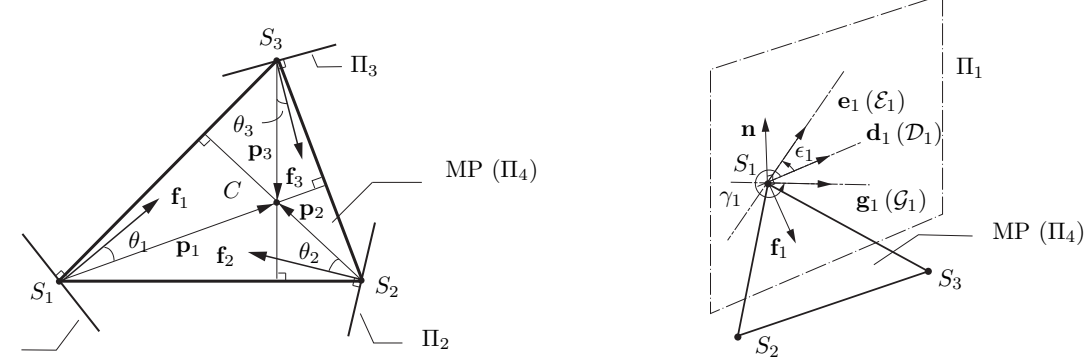


Figure 4.3: The layout of  $\mathbf{f}_j$  in the MP plane Figure 4.4: The definition of  $\epsilon_j$  and  $\gamma_j$ , in plane  $(\Pi_4)$  and the definition of  $\theta_j$  (top view)  $\Pi_j$ 

It is apparent that  $\mathbf{s}_{23} \perp \mathbf{n}$  and  $\mathbf{h}_1 \perp \mathbf{n}$  in this case. Moreover,  $\mathbf{f}_2 \times \mathbf{f}_3 \parallel \mathbf{n}$ ; more specifically,

$$\mathbf{f}_2 \times \mathbf{f}_3 = (\mathbf{g}_2 \times \mathbf{e}_2) \times (\mathbf{g}_3 \times \mathbf{e}_3) = \sin \alpha_2 \sin \alpha_3 \sin \phi_{ij} \mathbf{n}$$
(4.19)

where  $\alpha_j$  is defined as the angle between  $\mathbf{g}_j$  and  $\mathbf{e}_j$ , and  $\phi_{ij}$  denotes that between  $\mathbf{f}_i$  and  $\mathbf{f}_j$ . Then, we rewrite  $\mathbf{u}_j$  and  $\mathbf{m}_j$ , for j = 1, 2, as per Eqs. (4.13) and (4.14), as

$$\mathbf{u}_{1} = -s_{23}\mathbf{r}_{1}^{T}\mathbf{e}_{1}\mathbf{s}_{n23} + 2\sin\alpha_{2}\sin\alpha_{3}\sin\phi_{ij}s_{\Delta}\mathbf{n}^{T}\mathbf{e}_{1}\mathbf{n} = (p_{1}/\sigma_{u})\mathbf{g}_{1} \times \mathbf{p}_{n1}$$

$$\mathbf{u}_{2} = -s_{23}\mathbf{r}_{1}^{T}\mathbf{g}_{1}\mathbf{s}_{n23} + 2\sin\alpha_{2}\sin\alpha_{3}\sin\phi_{ij}s_{\Delta}\mathbf{n}^{T}\mathbf{g}_{1}\mathbf{n} = -(p_{1}/\sigma_{u})\mathbf{e}_{1} \times \mathbf{p}_{n1}$$

$$(4.20)$$

and

$$\mathbf{m}_{1} = 2s_{\Delta}(\mathbf{n}^{T}\mathbf{e}_{1})\mathbf{h}_{1} - 2s_{\Delta 23}(\mathbf{r}_{1}^{T}\mathbf{e}_{1})\mathbf{n} = \mathbf{g}_{1}/\sigma_{m}$$

$$\mathbf{m}_{2} = 2s_{\Delta}(\mathbf{n}^{T}\mathbf{g}_{1})\mathbf{h}_{1} - 2s_{\Delta 23}(\mathbf{r}_{1}^{T}\mathbf{g}_{1})\mathbf{n} = -\mathbf{e}_{1}/\sigma_{m}$$

$$(4.21)$$

with  $s_{ij}$  and  $\mathbf{s}_{nij}$  defined as the magnitude of  $\overrightarrow{S_iS_j}$  and the unit vector parallel to  $\overrightarrow{S_iS_j}$ ,  $p_{nj}$  and  $\mathbf{p}_{nj}$  defined likewise, as the magnitude of vector  $\mathbf{p}_j$  and the unit vector parallel to the same. Furthermore, the area of the triangle  $CS_iS_j$  is denoted as  $s_{\Delta ij}$ .

Next, we decompose  $\mathbf{u}_1$  and  $\mathbf{m}_1$  according to the corresponding orthogonal directions, namely,

$$-s_{23}\mathbf{r}_{1}^{T}\mathbf{e}_{1} = p_{1}/\sigma_{u}(\mathbf{p}_{n1} \times \mathbf{s}_{n23})^{T}\mathbf{g}_{1} = (p_{1}/\sigma_{u})\mathbf{n}^{T}\mathbf{g}_{1}$$

$$-s_{23}\mathbf{r}_{1}^{T}\mathbf{g}_{1} = -p_{1}/\sigma_{u}(\mathbf{p}_{n1} \times \mathbf{s}_{n23})^{T}\mathbf{e}_{1} = -(p_{1}/\sigma_{u})\mathbf{n}^{T}\mathbf{e}_{1}$$

$$2\sin\alpha_{2}\sin\alpha_{3}\sin\phi_{ij}s_{\Delta}\mathbf{n}^{T}\mathbf{e}_{1} = -(p_{1}/\sigma_{u})\mathbf{s}_{n23}^{T}\mathbf{g}_{1}$$

$$2\sin\alpha_{2}\sin\alpha_{3}\sin\phi_{ij}s_{\Delta}\mathbf{n}^{T}\mathbf{g}_{1} = (p_{1}/\sigma_{u})\mathbf{s}_{n23}^{T}\mathbf{e}_{1}$$

$$(4.22)$$

and

$$-2s_{\Delta 23}(\mathbf{r}_{1}^{T}\mathbf{e}_{1}) = \mathbf{n}^{T}\mathbf{g}_{1}/\sigma_{m}$$

$$-2s_{\Delta 23}(\mathbf{r}_{1}^{T}\mathbf{g}_{1}) = -\mathbf{n}^{T}\mathbf{e}_{1}/\sigma_{m}$$

$$2s_{\Delta}(\mathbf{n}^{T}\mathbf{e}_{1})\mathbf{h}_{1}^{T}\mathbf{h}_{1} = \mathbf{h}_{1}^{T}\mathbf{g}_{1}/\sigma_{m}$$

$$2s_{\Delta}(\mathbf{n}^{T}\mathbf{g}_{1})\mathbf{h}_{1}^{T}\mathbf{h}_{1} = -\mathbf{h}_{1}^{T}\mathbf{e}_{1}/\sigma_{m}$$

$$(4.23)$$

When the robot finds itself at an isotropic posture, Eqs. (4.22) and (4.23) must all hold. From the first of Eqs. (4.22) and that of (4.23), we can find the characteristic length as

$$L = \sqrt{\sigma_u/\sigma_m} = \sqrt{\frac{2s_{\Delta 23}p_1}{s_{23}}} = \sqrt{p_1 p_1'}$$
 (4.24)

where  $p'_1$  is defined as the distance from C to  $S_2S_3$ . Since C is the orthocentre of triangle  $S_1S_2S_3$ , this product is the same for the other two pairs of columns, namely,

$$\sqrt{p_1 p_1'} = \sqrt{p_2 p_2'} = \sqrt{p_3 p_3'} \tag{4.25}$$

In this way, we can represent  $\sigma_u$  as  $L^2\sigma_m$ . Now we rearrange the set of equations (4.22) and

(4.23) to obtain the geometric constraint on the distribution of the wrench axes that lead to isotropy. Firstly, we let the angle between  $\mathbf{p}_j$  and  $\mathbf{f}_j$  be  $\theta_j$ , as shown in Fig. 4.3. Furthermore,  $\mathcal{D}_j$  is defined as the intersection line of  $\Pi_j$  with  $\Pi_4$ , for j=1,2,3, with the unit vector  $\mathbf{d}_j$ . Since  $\Pi_j \perp \Pi_4$ , for j=1,2,3,  $\mathbf{d}_j$  can be found as  $\mathbf{d}_j \equiv \mathbf{n} \times \mathbf{f}_j$ . Then,  $\mathbf{f}_j$ ,  $\mathbf{d}_j$  and  $\mathbf{n}$  form a right-handed triad. In this way,  $\mathbf{e}_j$  and  $\mathbf{g}_j$  can be obtained upon rotating  $\mathbf{d}_j$  about  $\mathbf{f}_j$  through an angle  $\epsilon_j$  and  $\gamma_j$ , respectively, with  $\epsilon_j$  and  $\gamma_j$  as yet to be determined. Then<sup>6</sup>,  $\alpha_j = \epsilon_j - \gamma_j$ .

Moreover, since  $\mathbf{h}_1 \in \Pi_4$ , we have, according to the three-cosine theorem<sup>7</sup>,

$$\mathbf{h}_1^T \mathbf{g}_1 = (\mathbf{d}_1^T \mathbf{h}_1) \cos \gamma_1, \quad \mathbf{h}_1^T \mathbf{e}_1 = (\mathbf{d}_1^T \mathbf{h}_1) \cos \epsilon_1 \tag{4.26}$$

If we cross-multiply the two sides of the last two of Eqs. (4.23), we obtain

$$(\mathbf{h}_1^T \mathbf{d}_1)(\cos \epsilon_1 \sin \epsilon_1 + \cos \gamma_1 \sin \gamma_1) = (\mathbf{h}_1^T \mathbf{d}_1) \sin(\epsilon_1 + \gamma_1) = 0 \tag{4.27}$$

It is noteworthy that  $\mathbf{h}_1 \neq \mathbf{0}$ ; otherwise, according to Eq. (4.21), we have  $\mathbf{g}_1 \parallel \mathbf{m}_1 \parallel \mathbf{n} \parallel \mathbf{m}_2 \parallel \mathbf{e}_1$ , which leads to singularity. Hence, Eq. (4.27) holds under two possible cases:

- $\mathbf{h}_1 \perp \mathbf{d}_1$  or, equivalently,  $\mathbf{h}_1 \parallel \mathbf{f}_1$ . It can be readily shown that the condition  $\mathbf{h}_1^T \mathbf{f}_1 = 0$  does not hold in this case. Hence, this layout is not feasible.
- $\sin(\epsilon_1 + \gamma_1) = 0$ , then,  $\epsilon_1 + \gamma_1 = 2k\pi$  or  $\epsilon_1 + \gamma_1 = \pi + 2k\pi$ ,  $k \in \mathbb{Z}$ . This means that,  $\mathcal{E}_1$  and  $\mathcal{G}_1$  must be symmetric w.r.t.  $\mathcal{D}_1$ , as shown in Fig. 4.4 or, equivalently,  $\mathcal{D}_1$  is a bisector of the angle made by  $\mathcal{E}_1$  and  $\mathcal{G}_1$ .

It can be readily verified that, if one changes the sign of  $\mathbf{e}_j$  and (or) of  $\mathbf{g}_j$  in  $\mathbf{K}_h$ , the product  $\mathbf{K}_h\mathbf{K}_h^T$  does not change; as a result, the choice of the sign of these unit vectors becomes immaterial. Hence, we only look at one of the two previous conditions, e.g.,  $\gamma_1 = -\epsilon_1 + 2k\pi$ .

Now we summarize the conditions required by the isotropic postures: a) the normals  $\mathbf{f}_j$  of  $\Pi_j$  must lie in  $\Pi_4$ , for j = 1, 2, 3; b) the two wrench axes  $\mathcal{E}_j$  and  $\mathcal{G}_j$  must be symmetric w.r.t.  $\Pi_4$ ; c) the characteristic length must satisfy Eq. (4.24). Now, we insert these relations into the original expression (4.9): according to the geometric conditions summarized above, we

<sup>&</sup>lt;sup>6</sup>The sign is chosen to make  $\mathbf{g}_j$ ,  $\mathbf{e}_j$  and  $\mathbf{f}_j$  a right-handed triad.

<sup>&</sup>lt;sup>7</sup>Included in the Appendix, for quick reference.

can use six (redundant) parameters to characterize an isotropic posture, namely,  $\{\epsilon_j\}_{1}^{3}$  and  $\{\theta_j\}_{1}^{3}$ . Furthermore, without loss of generality, we assume the location of the centres of the three S joints to be

$$\mathbf{s}_1 = m \left[ -1/2, 0, 0 \right]^T, \quad \mathbf{s}_2 = m \left[ 1/2, 0, 0 \right]^T, \quad \mathbf{s}_3 = m \left[ x_0, y_0, 0 \right]^T$$
 (4.28)

where m represents the norm of  $\overrightarrow{S_1S_2}$ . Then,  $\mathbf{K}_h\mathbf{K}_h^T$  in Eq (4.9) has only six distinct offdiagonal entries and three distinct diagonal entries, which, upon some manipulations, yield nine equations in nine unknowns:  $\{\theta_i\}_1^3$ ,  $\{\epsilon_i\}_1^3$ ,  $\{\sigma_i\}_1^3$ . These equations are

$$\left(-\sin\theta_{1} + 4x_{0}^{2}\sin\theta_{1} + 4y_{0}^{2}\sin\theta_{1} + 4y_{0}\cos\theta_{1}\right) \left(-\sin\theta_{2} + 4x_{0}^{2}\sin\theta_{2} + 4y_{0}^{2}\sin\theta_{2} - 4y_{0}\cos\theta_{2}\right) = 0$$

$$\left(-\sin\theta_{1} + 2x_{0}\sin\theta_{1} + 2y_{0}\cos\theta_{1}\right) \left(-\sin\theta_{3} + 2x_{0}\sin\theta_{3} - 2y_{0}\cos\theta_{3}\right) = 0$$

$$\left(\sin\theta_{2} + 2x_{0}\sin\theta_{2} + 2y_{0}\cos\theta_{2}\right) \left(\sin\theta_{3} + 2x_{0}\sin\theta_{3} - 2y_{0}\cos\theta_{3}\right) = 0$$

$$-8y_{0}^{2}\sin^{2}\epsilon_{1} - \cos^{2}\epsilon_{1} \left(\sin^{2}\theta_{1} + 8x_{0}^{3}\sin^{2}\theta_{1} - 4x_{0}^{2}\sin^{2}\theta_{1} + 2x_{0}\left(4y_{0}^{2} - 1\right)\sin^{2}\theta_{1} - 2y_{0}^{2}\left(\cos\left(2\theta_{1}\right) + 3\right)\right) = 0$$

$$-8y_{0}^{2}\sin^{2}\epsilon_{2} - \cos^{2}\epsilon_{2} \left(-\sin^{2}\theta_{2} + 8x_{0}^{3}\sin^{2}\theta_{1} - 4x_{0}^{2}\sin^{2}\theta_{2} + 2x_{0}\left(4y_{0}^{2} - 1\right)\sin^{2}\theta_{1} - 2y_{0}^{2}\left(\cos\left(2\theta_{1}\right) + 3\right)\right) = 0$$

$$-4y_{0}^{2}\sin^{2}\epsilon_{2} - \cos^{2}\epsilon_{3} \left(\sin^{2}\theta_{2} + 4x_{0}^{2}\sin^{2}\theta_{2} + 2x_{0}\left(4y_{0}^{2} - 1\right)\sin^{2}\theta_{2} + 2y_{0}^{2}\left(\cos\left(2\theta_{2}\right) + 3\right)\right) = 0$$

$$-4y_{0}^{2}\sin^{2}\epsilon_{3} + \cos^{2}\epsilon_{3} \left(\sin^{2}\theta_{3} - 4x_{0}^{2}\sin^{2}\theta_{3} + 4y_{0}^{2}\cos^{2}\theta_{3}\right) = 0$$

$$m^{2}\left(2x_{0} + 1\right)\sin^{2}\epsilon_{1} = \sigma_{1}$$

$$m^{2}\left(1 - 2x_{0}\right)\sin^{2}\epsilon_{2} = \sigma_{2}$$

$$\frac{1}{2}m^{2}\left(4x_{0}^{2} + 4y_{0}^{2} - 1\right)\sin^{2}\epsilon_{3} = \sigma_{3}$$

$$(4.29)$$

which lead to isotropy when  $\sigma_1 = \sigma_2 = \sigma_3 = \sigma_K^2$ . It is noteworthy that we have shown that it is sufficient to assume  $\epsilon_j \in [-\pi/2, \pi/2]$  and  $\theta_j \in [-\pi/2, \pi/2]$  in the calculation, because  $\theta_j$  and  $\theta_j + \pi$  characterize the same plane  $\Pi_j$ , while  $\epsilon_j$  and  $\epsilon_j + \pi$  represent the same line  $\mathcal{E}_j$ ; moreover, each of the first three equations involves two decoupled terms, from which we can obtain two sets of  $\{\theta_j\}_1^3$  values, namely,

$$\theta_1 = \arctan \frac{4y_0}{-4x_0^2 - 4y_0^2 + 1}, \quad \theta_2 = -\arctan \frac{2y_0}{2x_0 + 1}, \quad \theta_3 = \arctan \frac{2y_0}{2x_0 - 1}$$
 (4.30)

or

$$\theta_1 = \arctan \frac{2y_0}{1 - 2x_0}, \quad \theta_2 = \arctan \frac{4y_0}{4x_0^2 + 4y_0^2 - 1}, \quad \theta_3 = \arctan \frac{2y_0}{2x_0 + 1}$$
 (4.31)

after which  $\mathbf{f}_i$  follows. It can be verified that the above condition yields the relation

$$\mathbf{f}_1 \perp \overline{S_1 S_3}, \quad \mathbf{f}_2 \perp \overline{S_2 S_1}, \quad \mathbf{f}_3 \perp \overline{S_3 S_2},$$
 (4.32)

or

$$\mathbf{f}_1 \perp \overline{S_1 S_2}, \quad \mathbf{f}_2 \perp \overline{S_2 S_3}, \quad \mathbf{f}_3 \perp \overline{S_3 S_1},$$
 (4.33)

meaning that the three planes  $\{\Pi_j\}_1^3$  must coincide with the three planes passing through the three edges of  $S_1S_2S_3$  and normal to the MP plane  $\Pi_4$ , i.e.,  $\overline{S_1S_3} \in \Pi_1$ ,  $\overline{S_1S_2} \in \Pi_2$ ,  $\overline{S_2S_3} \in \Pi_3$ , or  $\overline{S_1S_2} \in \Pi_1$ ,  $\overline{S_2S_3} \in \Pi_2$ ,  $\overline{S_3S_1} \in \Pi_3$ , as shown in Fig. 4.5. Hence, we do not really need to calculate  $\theta_j$  via Eqs. (4.30) or (4.31); the directions of  $\mathbf{f}_j$  can be determined directly from these geometric relations.

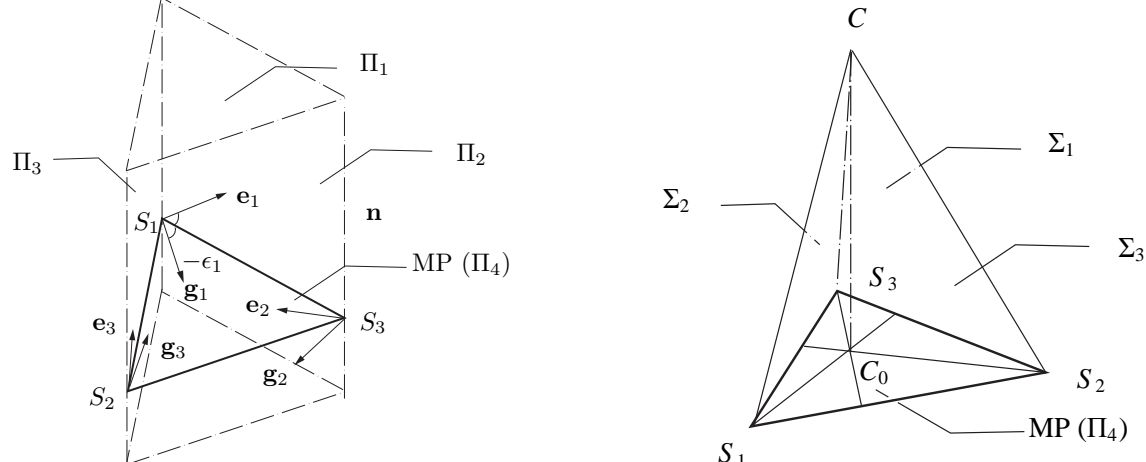


Figure 4.5: One of the two layouts of  $\Pi_j$ , Figure 4.6: The directions of  $\mathbf{f}_j$  coinciding with the  $\mathbf{e}_j$  and  $\mathbf{g}_j$  that may render isotropy three edges of the the tetrahedron

Next, we insert the values of  $\{\theta_j\}_1^3$  into the fourth to sixth of equations (4.29) to obtain the corresponding  $\{\epsilon_j\}_1^3$ , namely,

$$\epsilon_{1} = \pm \frac{1}{2} \arccos \left( \frac{2x_{0} + 1}{4x_{0}^{2} + 2x_{0} + 4y_{0}^{2}} \right), \ \epsilon_{2} = \pm \frac{1}{2} \arccos \left( \frac{1 - 2x_{0}}{2x_{0} + 3} \right), \ \epsilon_{3} = \pm \frac{1}{2} \arccos \left( \frac{4x_{0}^{2} + 4y_{0}^{2} - 1}{4x_{0}^{2} - 8x_{0} + 4y_{0}^{2} + 3} \right)$$

$$(4.34)$$

or

$$\epsilon_1 = \pm \frac{1}{2} \arccos\left(\frac{2x_0 + 1}{3 - 2x_0}\right), \ \epsilon_2 = \pm \frac{1}{2} \arccos\frac{1 - 2x_0}{4x_0^2 - 2x_0 + 4y_0^2}, \ \epsilon_3 = \pm \frac{1}{2} \arccos\frac{4x_0^2 + 4y_0^2 - 1}{4x_0^2 + 8x_0 + 4y_0^2 + 3}$$
(4.35)

Finally, we insert the values of  $\{\epsilon_j\}_1^3$  into the last three equations, to verify whether they are

compatible. These three equations yield

$$\sigma_{1} = \frac{m^{2} (2x_{0} + 1) (4x_{0}^{2} + 4y_{0}^{2} - 1)}{4 (2x_{0}^{2} + x_{0} + 2y_{0}^{2})}, \quad \sigma_{2} = \frac{m^{2} (1 - 4x_{0}^{2})}{2x_{0} + 3}, \quad \sigma_{3} = -\frac{m^{2} (2x_{0} - 1) (4x_{0}^{2} + 4y_{0}^{2} - 1)}{4x_{0}^{2} - 8x_{0} + 4y_{0}^{2} + 3}$$

$$(4.36)$$

or

$$\sigma_{1} = \frac{m^{2} (4x_{0}^{2} - 1)}{2x_{0} - 3}, \quad \sigma_{2} = \frac{m^{2} (2x_{0} - 1) (4x_{0}^{2} + 4y_{0}^{2} - 1)}{-8x_{0}^{2} + 4x_{0} - 8y_{0}^{2}}, \quad \sigma_{3} = \frac{m^{2} (2x_{0} + 1) (4x_{0}^{2} + 4y_{0}^{2} - 1)}{4x_{0}^{2} + 8x_{0} + 4y_{0}^{2} + 3}$$

$$(4.37)$$

After inserting the values of  $\{\theta_j\}_1^3$  and  $\{\epsilon_j\}_1^3$ ,  $\mathbf{K}_h\mathbf{K}_h^T$  becomes

$$\mathbf{K}_h \mathbf{K}_h^T = \operatorname{diag}(\sigma_1, \sigma_1, \sigma_2, \sigma_2, \sigma_3, \sigma_3) \tag{4.38}$$

It is found that  $\sigma_1 = \sigma_2 = \sigma_3$  if and only if the MP bears the shape of an equilateral triangle, i.e.,  $\mathbf{s}_3 = m [0, \sqrt{3}/2, 0]^T$ , the corresponding parameters being

$$\theta_2 = \theta_3 = \theta_1 = \pm 60^\circ$$
,  $\epsilon_1 = \pm \epsilon_2 = \pm \epsilon_3 = \pm \arctan(\sqrt{2}/2) \text{rad} = \pm 0.6155 \text{rad} = \pm 35.2644^\circ$ 
(4.39)

which represent two different postures, under which  $\Pi_i$  passes through the edge  $S_iS_j$  or  $S_iS_k$ , for distinct i, j, k, as stated above. Moreover, each pair of lines of the actuated wrenches must make an angle of 35.2644° w.r.t. plane  $\Pi_4$  of the MP triangle. A possible isotropic design is depicted in Fig. 4.7, using the Stewart-Gough platform as an example<sup>8</sup>, where we chose the case for which  $\Pi_1$  passes through  $S_1S_2$ .  $\sigma_K^2$  being  $m^2/3$  in this case.

On the other hand, when the shape of the MP triangle is not equilateral, and the operation point is chosen in the MP plane, it is shown that isotropy is not possible. However, the above analysis indicates that under some postures, the product  $\mathbf{K}_h \mathbf{K}_h^T$  can be diagonal, with only three distinct values, and its condition number can be well bounded with proper choice of the MP shape. For example, if we choose

$$\mathbf{s}_3 = m[1/4, 1, 0]^T \tag{4.40}$$

<sup>&</sup>lt;sup>8</sup>We choose the Stewart-Gough platform as an example because its actuated-wrench axes are parallel to its six limbs, making it illustrative for the demonstration of the isotropic designs. Other three-limb PKMs can also be designed once the layout of the actuated wrenches is known, e.g., with the method proposed by Tsai and Lee [71].



centroid of the MP triangle

Figure 4.7: An example of an isotropic Stewart- Figure 4.8: An example of an isotropic Stewart-Gough platform with the operation point at the Gough platform with the operation point lying outside of the plane of the MP triangle

then we have either

$$\sigma_1 = \frac{39m^2}{76}, \ \sigma_2 = \frac{3m^2}{14}, \ \sigma_3 = \frac{13m^2}{42},$$
 (4.41)

or

$$\sigma_1 = \frac{3m^2}{10}, \ \sigma_2 = \frac{13m^2}{60}, \ \sigma_3 = \frac{39m^2}{74},$$
 (4.42)

thereby yielding a condition number  $\kappa_F$  of either 1.065 or 1.069, which is small enough to guarantee accuracy and the homogeneity of the motion capacity of the MP along different directions. A mapping represented by a given  $n \times n$  matrix **A** carries the unit ball in the domain space into a n-axis ellipsoid in the image space. The mapping, and hence its matrix representation, is said to be isotropic when the unit ball remains a ball. We can now define an index of distortion  $\iota$  as

$$\iota = \log_{10}(\kappa) \in (0, \infty) \tag{4.43}$$

which vanishes when the Jacobian matrix is isotropic, and becomes unbounded when the matrix is singular. To this end, we call a posture "quasi-isotropic" when all the rows of  $\mathbf{K}_h$ are orthogonal to each other, while the distortion of  $\mathbf{K}_h$  is sufficiently small, e.g., between 0 and 1.0, thereby guaranteeing accuracy and the homogeneity of the motion capacity of the MP along different directions.

It is noteworthy that the MP triangle must be an acute triangle; otherwise, the characteristic length, as per Eq. (4.24), becomes a complex number, meaning the set of equations (4.22) and (4.23) cannot be satisfied simultaneously. Moreover, it appears that the closer the shape of the MP is to an equilateral triangle, the smaller the condition number it can achieve. However, it is noteworthy that even for an acute MP triangle, we did not show that the condition number is minimum under quasi isotropy. Hence, strictly speaking, the characteristic length in Eq. (4.24) is not necessarily the one that minimizes the condition number globally. However, the condition number under quasi isotropy is quite close to unity, using the quasi isotropy and the corresponding characteristic length should be sufficient in most situations: When  $\mathbf{K}_h \mathbf{K}_h^T$  becomes diagonal, the different rows of  $\mathbf{K}_h$  are orthogonal to each other; moreover, a small condition number means that the Euclidean norms of the rows of  $\mathbf{K}_h$  are "close" to each other, which brings the PKM close to an isotropic posture, thus guaranteeing the accuracy and homogeneity of the motion of the MP.

### 4.2.2 The Operation Point Lying Outside of the MP Triangle

Next, we address the case when the operation point lies outside the MP triangle, which is needed, e.g., when a tool is attached to the MP triangle. Let  $C_0$  denote the ortho-centre of the MP triangle, and C the operation point. According to Eq. (4.18a),  $\overline{C_0C}$  must be normal to the MP plane in order to yield isotropy, as shown in Fig. 4.6. Moreover, we label the plane composed of  $\overline{S_2C}$  and  $\overline{S_3C}$   $\Sigma_1$ , that composed of  $\overline{S_3C}$  and  $\overline{S_1C}$   $\Sigma_2$ , and that of  $\overline{S_1C}$  and  $\overline{S_2C}$   $\Sigma_3$ . Furthermore, the relation  $\mathbf{p}_2 \times \mathbf{p}_3 \perp \mathbf{f}_1$  indicates that  $\mathbf{f}_1$  must be coplanar with  $\mathbf{p}_2$  and  $\mathbf{p}_3$ ; hence,  $\mathbf{f}_1$  is a vector parallel to the  $\Sigma_1$  plane. Similarly,  $\mathbf{f}_2 \parallel \Sigma_2$  and  $\mathbf{f}_3 \parallel \Sigma_3$ . Moreover, the condition  $(\mathbf{f}_2 \times \mathbf{f}_3) \cdot \mathbf{p}_1 = 0$  indicates that the three vector factors are coplanar. This is possible only when  $\mathbf{f}_2$  or  $\mathbf{f}_3$  coincides with  $\mathbf{p}_1$ . A similar analysis for the last four columns of  $\mathbf{K}_h \mathbf{K}_h^T$  indicates that

$$\mathbf{f}_1 \parallel \mathbf{p}_3, \ \mathbf{f}_2 \parallel \mathbf{p}_1, \ \mathbf{f}_3 \parallel \mathbf{p}_2 \quad \text{or} \quad \mathbf{f}_1 \parallel \mathbf{p}_2, \ \mathbf{f}_2 \parallel \mathbf{p}_3, \ \mathbf{f}_3 \parallel \mathbf{p}_1$$
 (4.44)

It can be verified that the condition  $\mathbf{h}_j \perp \mathbf{f}_j$  naturally holds, given the previous directions of  $\mathbf{f}_j$ .

Once their normals  $\{\mathbf{f}_j\}_1^3$  are available, the planes  $\{\Pi_j\}_1^3$  are defined, together with the unit vector parallel to the intersection line of  $\Pi_j$  with  $\Pi_4$ , denoted  $\mathbf{d}_j$ , where  $\mathbf{d}_j \parallel \mathbf{n} \times \mathbf{f}_j$ . Then, the unit vectors  $\mathbf{e}_j$  and  $\mathbf{g}_j$  can, again, be obtained upon rotating  $\mathbf{d}_j$  about  $\mathbf{f}_j$  through an angle  $\epsilon_j$  and  $\gamma_j$ , respectively. It is noteworthy that the expression for the characteristic length, in Eq. (4.24) no longer holds; we thus have seven unknown parameters,  $\{\epsilon_j\}_1^3$ ,  $\{\gamma_j\}_1^3$  and L. After inserting them into the expression of  $\mathbf{K}_h\mathbf{K}_h^T$ , we obtain six distinct diagonal entries and fifteen distinct off-diagonal entries, among which 12 of the off-diagonal entries bear a common factor that is a linear combination of  $m^2$  and  $L^2$ . Hence, that term should be zero in order to make all the 12 entries vanish. In this way, we obtain the characteristic length, which, is shown to be

$$L = \sqrt{L_0^2 - h^2} \tag{4.45}$$

where  $L_0$  is the characteristic length when the OP is selected as the ortho-centre  $C_0$  of the MP, as per Eq. (4.24), and h is the distance from the operation point C to the MP plane<sup>9</sup>.

Upon recalling the expression for the characteristic length, we are left with three non-zero off-diagonal entries and six distinct diagonal entries, that should equal the same constant  $\sigma_K^2$  under isotropy, thereby ending up with nine equations and seven unknowns. Since these equations are extremely lengthy if we leave  $\mathbf{s}_3$  as unknown, they are not included here. However, when  $\mathbf{s}_3$  is specified, the display becomes manageable. For example, if we use the

<sup>&</sup>lt;sup>9</sup>In order to make  $L_c$  a real number, the distance from the operation point C to the MP plane must be smaller than L.

same  $\mathbf{s}_3$  as shown in Eq. (4.40), the nine equations<sup>10</sup>, after simplification, yield

$$-384\nu\sqrt{256\nu^{2} + 169}\sin\left(\gamma_{1} + \epsilon_{1}\right) + \left(2535 - 256\nu^{2}\right)\cos\left(\gamma_{1} - \epsilon_{1}\right) + \left(1792\nu^{2} - 1521\right)\cos\left(\gamma_{1} + \epsilon_{1}\right) = 0$$

$$-256\nu\sqrt{256\nu^{2} + 153}\sin\left(\gamma_{2} + \epsilon_{2}\right) + \left(2295 - 4352\nu^{2}\right)\cos\left(\gamma_{2} - \epsilon_{2}\right) + 6\left(1280\nu^{2} - 51\right)\cos\left(\gamma_{2} + \epsilon_{2}\right) = 0$$

$$-6656\nu\sqrt{256\nu^{2} + 25}\sin\left(\gamma_{3} + \epsilon_{3}\right) + 25\left(2304\nu^{2} + 481\right)\cos\left(\gamma_{3} - \epsilon_{3}\right) + \left(22272\nu^{2} - 4225\right)\cos\left(\gamma_{3} + \epsilon_{3}\right) = 0$$

$$\frac{-384\sqrt{256\nu^{2} + 169}\nu\sin\left(2\epsilon_{1}\right) + \left(1792\nu^{2} - 1521\right)\cos\left(2\epsilon_{1}\right) - 256\nu^{2} + 2535}{8192\nu^{2} + 5408}m^{2} = \sigma_{11}$$

$$\frac{-384\sqrt{256\nu^{2} + 169}\nu\sin\left(2\gamma_{1}\right) + \left(1792\nu^{2} - 1521\right)\cos\left(2\gamma_{1}\right) - 256\nu^{2} + 2535}{8192\nu^{2} + 5408}m^{2} = \sigma_{12}$$

$$\frac{-256\sqrt{256\nu^{2} + 153}\nu\sin\left(2\epsilon_{2}\right) + 6\left(1280\nu^{2} - 51\right)\cos\left(2\epsilon_{2}\right) - 4352\nu^{2} + 2295}{68\left(256\nu^{2} + 153\right)}m^{2} = \sigma_{21}$$

$$\frac{-256\sqrt{256\nu^{2} + 153}\nu\sin\left(2\gamma_{2}\right) + 6\left(1280\nu^{2} - 51\right)\cos\left(2\gamma_{2}\right) - 4352\nu^{2} + 2295}{68\left(256\nu^{2} + 153\right)}m^{2} = \sigma_{22}$$

$$\frac{-6656\sqrt{256\nu^{2} + 25}\nu\sin\left(2\epsilon_{3}\right) + \left(22272\nu^{2} - 4225\right)\cos\left(2\epsilon_{3}\right) + 57600\nu^{2} + 12025}{800\left(256\nu^{2} + 25\right)}m^{2} = \sigma_{31}$$

$$\frac{-6656\sqrt{256\nu^{2} + 25}\nu\sin\left(2\gamma_{3}\right) + \left(22272\nu^{2} - 4225\right)\cos\left(2\gamma_{3}\right) + 57600\nu^{2} + 12025}{800\left(256\nu^{2} + 25\right)}m^{2} = \sigma_{32}$$

$$\frac{-6656\sqrt{256\nu^{2} + 25}\nu\sin\left(2\gamma_{3}\right) + \left(22272\nu^{2} - 4225\right)\cos\left(2\gamma_{3}\right) + 57600\nu^{2} + 12025}{800\left(256\nu^{2} + 25\right)}m^{2} = \sigma_{32}$$

$$\frac{-6656\sqrt{256\nu^{2} + 25}\nu\sin\left(2\gamma_{3}\right) + \left(22272\nu^{2} - 4225\right)\cos\left(2\gamma_{3}\right) + 57600\nu^{2} + 12025}{800\left(256\nu^{2} + 25\right)}m^{2} = \sigma_{32}$$

where  $\nu \equiv h/m$ , which yields isotropy when  $\sigma_{11} = \sigma_{12} = \sigma_{21} = \sigma_{22} = \sigma_{31} = \sigma_{32}$ . Since we have nine equations and only six unknowns, this system does not admit a compatible solution, and hence, we cannot make all six  $\sigma_{ij}$  identical—as required by isotropy. However, considering the symmetries among the last three pairs of Eqs. (4.46), we can make these values equal by pairs, i.e.,  $\sigma_{11} = \sigma_{12}$ ,  $\sigma_{21} = \sigma_{22}$ ,  $\sigma_{31} = \sigma_{32}$ . To this end, we define  $\tau_j$  such that  $\tan \tau_j = r_j/s_j$ , where  $r_j$  and  $s_j$  represent the coefficients of  $\cos(2\epsilon_j)$  and  $\sin(2\epsilon_j)$  of the fourth, sixth and eighth equations, which leads to

$$2\epsilon_j + 2\gamma_j + 2\tau_j = \pi + 2k\pi, k \in \mathbb{Z}$$
(4.47)

Moreover, after inserting this expression into the first three of equations (4.46), we can find their difference, and eventually, obtain their values. For example, for the given  $s_3$ , we obtain

<sup>&</sup>lt;sup>10</sup>As stated above, two choices for the directions of  $\{\mathbf{f}_j\}_1^3$  are possible; we choose  $\mathbf{f}_1 \parallel \mathbf{p}_3$ ,  $\mathbf{f}_2 \parallel \mathbf{p}_1$ ,  $\mathbf{f}_3 \parallel \mathbf{p}_2$  for demonstration, the other case being handled likewise.

$$\epsilon_{1} = \frac{1}{2} \left( -\arccos\left(\frac{-6400\nu^{2} - 1521}{256\nu^{2} - 2535}\right) + \arctan\left(\frac{1792\nu^{2} - 1521}{384\nu\sqrt{256\nu^{2} + 169}}\right) + \frac{\pi}{2} \right)$$

$$\epsilon_{2} = \frac{1}{2} \left( -\arccos\left(-\frac{2\left(256\nu^{2} + 9\right)}{256\nu^{2} - 135}\right) + \arctan\left(\frac{3\left(1280\nu^{2} - 51\right)}{128\nu\sqrt{256\nu^{2} + 153}}\right) + \frac{\pi}{2} \right)$$

$$\epsilon_{3} = \frac{1}{2} \left( -\arccos\left(\frac{4352\nu^{2} + 169}{2304\nu^{2} + 481}\right) + \arctan\left(\frac{22272\nu^{2} - 4225}{6656\nu\sqrt{256\nu^{2} + 25}}\right) + \frac{\pi}{2} \right)$$

$$\gamma_{1} = \frac{1}{2} \left( \arccos\left(\frac{-6400\nu^{2} - 1521}{256\nu^{2} - 2535}\right) + \arctan\left(\frac{1792\nu^{2} - 1521}{384\nu\sqrt{256\nu^{2} + 169}}\right) + \frac{\pi}{2} \right)$$

$$\gamma_{2} = \frac{1}{2} \left( \arccos\left(-\frac{2\left(256\nu^{2} + 9\right)}{256\nu^{2} - 135}\right) + \arctan\left(\frac{3\left(1280\nu^{2} - 51\right)}{128\nu\sqrt{256\nu^{2} + 153}}\right) + \frac{\pi}{2} \right)$$

$$\gamma_{3} = \frac{1}{2} \left( \arccos\left(\frac{4352\nu^{2} + 169}{2304\nu^{2} + 481}\right) + \arctan\left(\frac{22272\nu^{2} - 4225}{6656\nu\sqrt{256\nu^{2} + 25}}\right) + \frac{\pi}{2} \right)$$

and

$$\mathbf{KK}^T = m^2 \operatorname{diag} \left( \frac{48672}{256\nu^2 - 2535} + \frac{39}{2}, \frac{48672}{256\nu^2 - 2535} + \frac{39}{2}, \frac{72}{256\nu^2 - 135} + \frac{3}{4}, \frac{72}{256\nu^2 - 135} + \frac{3}{4}, \frac{507 - 3328\nu^2}{4608\nu^2 + 962}, \frac{507 - 3328\nu^2}{4608\nu^2 + 962}, \frac{1000}{4608\nu^2 + 9$$

With these relations<sup>11</sup>, we guarantee that  $\mathbf{K}_h \mathbf{K}_h^T$  bears the form of a diagonal matrix with three distinct entries; this type of posture, although not isotropic, yields a small condition number under a proper choice of the design parameters. For example, when  $\nu = 0.1$ ,  $\kappa_F = 1.05848$ .

If we further impose  $\sigma_{11} = \sigma_{21} = \sigma_{31} = \sigma_K^2$ , required for isotropy, it will be found that this happens only when the MP bears the shape of an equilateral triangle, the solutions then becoming

$$\epsilon_{1} = \epsilon_{2} = \epsilon_{3} = \frac{1}{2} \left( -\arccos\left(\frac{1}{3} \left(12\nu^{2} + 1\right)\right) + \arctan\left(\frac{6\nu^{2} - 1}{6\nu\sqrt{3\nu^{2} + 1}}\right) + \frac{\pi}{2} \right)$$

$$\gamma_{1} = \gamma_{2} = \gamma_{3} = \frac{1}{2} \left(\arccos\left(\frac{1}{3} \left(12\nu^{2} + 1\right)\right) + \arctan\left(\frac{6\nu^{2} - 1}{6\nu\sqrt{3\nu^{2} + 1}}\right) + \frac{\pi}{2} \right)$$

$$\sigma_{K}^{2} = \left(\frac{1}{3} - 2\nu^{2}\right) m^{2}$$
(4.50)

<sup>&</sup>lt;sup>11</sup>The values of  $\epsilon_j$  and  $\gamma_j$  are obtained upon assuming  $\epsilon_j = -\gamma_j - \tau_j + \pi/2$ ; it can be readily shown that if we assume  $\epsilon_j = -\gamma_j - \tau_j - \pi/2$ , then the corresponding result can be obtained simply upon exchanging  $\epsilon_j$  and  $\gamma_j$ ; moreover, if we substitute  $\epsilon_j$  and (or)  $\gamma_j$  with  $\epsilon_j + \pi$  and (or)  $\gamma_j + \pi$ , then the condition number does not change. In summary, the foregoing results determine two lines in  $\{\Pi_j\}_{1}^3$ ; as long as  $\mathbf{e}_j$  and  $\mathbf{g}_j$  are parallel to these two lines simultaneously, the corresponding condition number remains constant.

when  $\mathbf{f}_1 \parallel \mathbf{p}_3$ ,  $\mathbf{f}_2 \parallel \mathbf{p}_1$ ,  $\mathbf{f}_3 \parallel \mathbf{p}_2$ , or

$$\epsilon_{1} = \epsilon_{2} = \epsilon_{3} = \frac{1}{2} \left( -\arccos\left(\frac{1}{3} \left(-12\nu^{2} - 1\right)\right) - \arctan\left(\frac{6\nu^{2} - 1}{6\nu\sqrt{3\nu^{2} + 1}}\right) + \frac{\pi}{2} \right)$$

$$\gamma_{1} = \gamma_{2} = \gamma_{3} = \frac{1}{2} \left(\arccos\left(\frac{1}{3} \left(-12\nu^{2} - 1\right)\right) - \arctan\left(\frac{6\nu^{2} - 1}{6\nu\sqrt{3\nu^{2} + 1}}\right) + \frac{\pi}{2} \right)$$

$$\sigma_{K}^{2} = \left(\frac{1}{3} - 2\nu^{2}\right) m^{2}$$

$$(4.51)$$

when  $\mathbf{f}_1 \parallel \mathbf{p}_2$ ,  $\mathbf{f}_2 \parallel \mathbf{p}_3$ ,  $\mathbf{f}_3 \parallel \mathbf{p}_1$ . It is apparent that for an equilateral MP, when the distance from the operation point to the MP plane is smaller than  $L_0$ , with  $L_0$  calculated as per Eq. (4.45), there always exist postures that yield isotropy.

The isotropic design is displayed in Fig. 4.8 for the case of an equilateral MP with  $\nu = 0.3$ , as described by Eq. (4.50) for illustration. The display of the quasi-isotropic design, as described by Eqs. (4.46) and (4.48), is similar to that of Fig. 4.8; it is hence omitted for brevity. Interestingly, in order to render isotropy,  $\Pi_j$  must also pass through one of the edges of the triangle  $S_1S_2S_3$  when the operation point is outside the MP plane, just as the case when the OP is in the MP plane. For example, for the first case described by Eqs. (4.44), we have  $\mathbf{f}_1 \parallel \mathbf{p}_3 \perp S_1S_2$ ; then,  $S_1S_2$  passes through a point  $(S_1)$  on  $\Pi_1$  and perpendicular to its normal; hence,  $\Pi_1$  passes through  $S_1S_2$ .

Finally, isotropy can be achieved only when the MP triangle is equilateral, and the OP is chosen to be on the line normal to the MP plane and passing through its ortho-centre; when the MP is not an equilateral triangle, it is possible to find some postures that we call quasi isotropic, that bear a small condition number. Formulas for the corresponding parameters were provided.

# 4.2.3 The Isotropy of the Inverse Jacobian Matrix

Next, we briefly discuss the isotropy of the inverse Jacobian matrix, denoted  $\mathbf{D}_h$ . Since  $\mathbf{D}_h$  is a diagonal matrix, its isotropy is obtained when all its six diagonal entries have identical absolute values; moreover, its *i*th diagonal entry is equal to the *reciprocal product* [89] of the two axes associated with the *i*th pair of actuated twist and actuated wrench, for  $i = 1, \ldots, 6$ . It has been shown in the previous derivation in Section 4.2 that the axes of the six actuated wrenches are already determined by the isotropy of  $\mathbf{K}_h$ ; however, one can still change the

location and directions of the axes of the actuated twists to make  $\mathbf{D}_h$  isotropic.

Let us take an arbitrary three-limb, six-dof PKM—whose MP is connected to the three limbs via three passive spherical joints—as an example. We assume that the axes of the actuated wrenches of the jth limb are given by  $\mathcal{E}_j$  and  $\mathcal{G}_j$ , for j=1,2,3, while the realizations of the first three joints of each limb are not yet known. Then, the passive joint can be found such that its axis  $\mathcal{P}_j$  is reciprocal to both  $\mathcal{E}_j$  and  $\mathcal{G}_j$ , meaning  $\mathcal{P}_j$  is either a line at infinity whose direction is normal to both  $\mathbf{e}_j$  and  $\mathbf{g}_j$ , or a finite line that lies in the plane defined by  $\mathcal{E}_j$  and  $\mathcal{G}_j$ , but does not pass through  $S_j$ . As for the choice of the location of the two actuated twists, we simply need to guarantee that they are reciprocal to only one of  $\mathcal{E}_j$  or  $\mathcal{G}_j$ . Thus, there are infinitely many choices for these actuated twists, which yields a large margin of manoeuvre to change the values of the entries of  $\mathbf{D}_h$ . Hence, it is a simple matter to make  $\mathbf{D}_h$  isotropic. It is noteworthy that, when the actuated joints bear different units, e.g., when the two actuated joints in each limb are a P joint and a R joint, the entries of  $\mathbf{D}$  bear different units; thus, a pertinent characteristic length is needed for the  $\mathbf{D}$  matrix, as well.

Since the design for isotropy of  $\mathbf{D}_h$  is straightforward, it is omitted for conciseness.

## 4.3 Discussion

In this Chapter we discussed the DfI of a large class of six-dof PKMs whose actuated-wrench axes intersect pairwise. Based on the symbolic form of the inverse of the forward Jacobian matrix, the isotropic design is investigated here, which indicates that isotropy is feasible only when the MP bears the shape of an equilateral triangle and the operation point lies on the line normal to the MP plane and passes through the orthocentre of the MP. Moreover, for a general shape of the MP triangle, there exist some postures that we call quasi isotropic, under which the product  $\mathbf{K}_h \mathbf{K}_h^T$  becomes diagonal, with three distinct entries, whose condition number is small, say, below 10.0. The expressions for the corresponding parameters are provided, not only offering a quick way to find such layouts, but also providing a better insight of how these parameters affect the condition number. While the design for maximum dexterity, in general, leads to an optimization problem, requiring a mathematical-

programming solution, the problem studied here allows for isotropic solutions, that can be found by equation-solving. Furthermore, we showed that the solution can be expressed by means of formulas and provided fairly general design guidelines. This is more advantageous compared with iterative methods targeting design for isotropy, used, e.g., by Tsai et al., since the latter require an initial guess and can only provide one solution at a time. This work covers the isotropic design of a large class of PKMs, whose six wrench axes intersect pairwise. These include all the three-limb parallel robots whose limbs, each, bears one passive spherical joint at one end, and Stewart-Gough platforms with three attachment points at the MP.

So far we have provided the analyses and optimization of the SDelta robot, and the design for isotropy of a large class of three-limb PKMs whose limbs, each, bears one passive spherical joint at one end, based on the results (the expression of  $\mathbf{K}^{-1}$  in symbolic form) found during the optimization of the SDelta. Next, we investigate the last topic of this dissertation, i.e., the analyses and optimization of an alternative architecture—the 3- $\underline{\mathbf{C}}$ CC PKM. Compared with the SDelta, this architecture bears different yet interesting features, making it not only a good candidate for high-speed and shaking operations, but also in many other possible applications, such as machine tools, medical devices and motion simulators, among others.

# THE 3-CCC PARALLEL-KINEMATICS MACHINE

An alternative architecture, i.e., the 3-CCC PKM is investigated in this chapter. Given that there are infinitely many different layouts of the C joints involved here, this in fact represents a large class of PKMs. Firstly, the design for isotropy of this class is investigated, based on which we find the conditions on the design parameters yielding a continuous set of isotropic postures [91]. This feature is quite advantageous and rare, probably unique, for six-dof PKMs. The conditions yielding this feature are investigated in detail. Next, the forward-displacement, singularity and workspace analyses of this class of PKMs are conducted, which reveal many interesting features. For example, their forward-displacement analysis allows for a simple formulation, which can be solved in closed form; the rotation and translation motions of the MP are decoupled, singularity being determined solely by the MP orientation, and occurring only under very large rotations. These PKMs bear a large workspace volume, among other properties. These features make this class of PKMs promising in many possible applications.

The concept of the 3-CCC PKM was first proposed by Daniali et al. as the six-dof version of a more general class of PKMs, i.e., the double-triangular mechanisms, whose BP and MP are, each, a planar or a spherical triangle [92–94]. The forward-displacement analysis, singularity analysis and optimum design of this class of robots were the subjects of the foregoing references. However, the main subject of these references is the disclosure of a novel concept, the six-dof version of the double-triangular PKMs as a generalization of their three-dof counterparts, along with their kinematic relations. In fact, the kinematic relations derived therein were not in their simplest form, which hides the kinematic meaning of the relevant quantities involved, and leads to unnecessary constraints on their isotropic design. As a result, many interesting features of the 3-CCC PKM were not revealed in those papers.

We have re-derived the kinematic relations of the 3-CCC PKM in a more systematic way, namely, using screw theory, which yields simpler kinematic relations. From these relations, we found several new, interesting features of this class of robots. It is noteworthy that the kinematics analysis included here is more general than those in the previous works, since we do not require any two of the three C-joint axes to intersect or be perpendicular to each other. Moreover, based on our kinematic analysis, we found a rich set of possible isotropic architectures, as some conditions imposed in the previous references turned out to be unnecessary to attain isotropy. Finally, our analysis reveals the existence of a line of isotropy, namely a locus of isotropic designs, out of which a few are instantiated.

More recently, some researchers have conducted the analysis and optimum design of 3-CCC PKMs [95,96], in which the middle cylindrical joints are actuated. This class of PKMs suffers in that a) their actuation is quite challenging to implement, and b) at least one motor in each limb is floating, thereby increasing significantly the inertia load on the system. This feature invariably affects the load-carrying capacity and dynamic response of the robot.

## 5.1 Kinematics

#### 5.1.1 The Derivation of the Jacobian Matrix

The general architecture of a 3-<u>C</u>CC PKM is displayed in Fig. 2.5. Let us consider the ith limb, for i = 1, 2, 3. First, we define the unit vectors parallel to the axes of the three cylindrical joints in the ith limb as  $\mathbf{a}_i$ ,  $\mathbf{r}_i$  and  $\mathbf{b}_i$ —see Fig. 2.5. Moreover,  $\mathbf{p}_{ai}$ ,  $\mathbf{p}_{ri}$  and  $\mathbf{p}_{bi}$  are the vectors pointing from an arbitrary point on each of the three corresponding axes to the operation point C, fixed to the MP. Next, we array the joint variables of the ith limb into vector  $\boldsymbol{\theta}_i = [\theta_{ia}, r_{ia}, \theta_{ir}, r_{ir}, \theta_{ib}, r_{ib}]^T$ , with  $\theta_{iJ}$  and  $r_{iJ}$  representing the angle of rotation and the translation of the cylindrical joint J of the ith limb, for J = a, r, b; this leads to the relation

$$\mathbf{J}_i \dot{\boldsymbol{\theta}}_i = \mathbf{t}, \quad i = 1, 2, 3 \tag{5.1}$$

where  $\dot{\boldsymbol{\theta}}_i = [\dot{\theta}_{ia}, \dot{r}_{ia}, \dot{\theta}_{ir}, \dot{r}_{ir}, \dot{\theta}_{ib}, \dot{r}_{ib}]^T$ , and

$$\mathbf{J}_{i} = \begin{bmatrix} \mathbf{a}_{i} & \mathbf{0} & \mathbf{r}_{i} & \mathbf{0} & \mathbf{b}_{i} & \mathbf{0} \\ \mathbf{a}_{i} \times \mathbf{p}_{ai} & \mathbf{a}_{i} & \mathbf{r}_{i} \times \mathbf{p}_{ri} & \mathbf{r}_{i} & \mathbf{b}_{i} \times \mathbf{p}_{bi} & \mathbf{b}_{i} \end{bmatrix}, \ \mathbf{t} = \begin{bmatrix} \boldsymbol{\omega} \\ \dot{\mathbf{c}} \end{bmatrix}$$
(5.2)

again, for i = 1, 2, 3, with **t** denoting the six-dimensional array of the twist of the moving platform and **0** the three-dimensional zero vector. Moreover, we assume that the cylindrical joint whose axis is parallel to  $\mathbf{a}_i$  is actuated.

Now we seek the kinematic relation of the 3-CCC PKM, which bears the form

$$\mathbf{Kt} = \mathbf{D}\dot{\boldsymbol{\phi}} \tag{5.3}$$

where

$$\dot{\phi} = [\dot{\theta}_{1a}, \dot{\theta}_{2a}, \dot{\theta}_{3a}, \dot{r}_{1a}, \dot{r}_{2a}, \dot{r}_{3a}]^T \tag{5.4}$$

is the six-dimensional array of C-drive rates,  $\mathbf{D}$  is the *drive Jacobian*, and  $\mathbf{K}$  the *forward Jacobian*. Now we find the rows of  $\mathbf{K}$  independently. First, we define  $\mathbf{K}$  as

$$\mathbf{K} = [\mathbf{k}_{rt1}, \mathbf{k}_{rt2}, \mathbf{k}_{rt3}, \mathbf{k}_{tr1}, \mathbf{k}_{tr2}, \mathbf{k}_{tr3}]^{T}$$
(5.5)

where  $\mathbf{k}_{rti}$  and  $\mathbf{k}_{tri}$  represent six-dimensional arrays, for i = 1, 2, 3; next, we regard the foregoing vector arrays as screws with their upper and lower three-dimensional blocks in axis coordinates<sup>1</sup>, that are reciprocal [97] to all but the first or, correspondingly, to the second columns of  $\mathbf{J}_i$ , for i = 1, 2, 3. It can be readily seen that arrays  $\mathbf{k}_{rti}$  are, in fact, screws with infinite pitch, their blocks, represented in axis-coordinates, as

$$\mathbf{k}_{rti} = [(\mathbf{b}_i \times \mathbf{r}_i)^T, \mathbf{0}^T]^T, \quad i = 1, 2, 3$$
(5.6)

It can be verified that the inner product of  $\mathbf{k}_{rti}$  with the last five columns of  $\mathbf{J}_i$ —the reciprocal product of the corresponding screws—indeed vanishes. As for  $\mathbf{k}_{tri}$ , let us assume that it bears the general form of a screw:

$$\mathbf{k}_{tri} = [(\mathbf{s}_i \times \mathbf{p}_{si} + k_i \mathbf{s}_i)^T, \mathbf{s}_i^T]^T, \quad i = 1, 2, 3$$

$$(5.7)$$

<sup>&</sup>lt;sup>1</sup>A screw is represented in axis coordinates when the direction vector of the axis of the screw is in the lower block of the screw [97].

with  $\mathbf{s}_i$  representing the unit vector parallel to the axis of the screw, as yet to be determined. The inner product of  $\mathbf{k}_{tri}$  with the 4th and 6th column of  $\mathbf{J}_i$ , i.e., the reciprocal product of the two screws, must vanish:

$$\mathbf{s}_i^T \mathbf{r}_i = 0, \quad \mathbf{s}_i^T \mathbf{b}_i = 0 \tag{5.8}$$

Hence, we can assign  $\mathbf{s}_i$  as

$$\mathbf{s}_i = \mathbf{b}_i \times \mathbf{r}_i \tag{5.9}$$

Next, the inner product of  $\mathbf{k}_{tri}$  with the first column of  $\mathbf{J}_i$  must vanish as well, i.e.,

$$(\mathbf{s}_i \times \mathbf{p}_{si} + k_i \mathbf{s}_i)^T \mathbf{a}_i + \mathbf{s}_i^T (\mathbf{a}_i \times \mathbf{p}_{ai}) = 0$$
 (5.10)

which, after simplification, yields

$$(\mathbf{a}_i \times \mathbf{s}_i)^T \mathbf{p}_{si} + \mathbf{a}_i \cdot \mathbf{s}_i k_i = (\mathbf{a}_i \times \mathbf{s}_i)^T \mathbf{p}_{ai}$$
 (5.11a)

Similarly, we can derive the inner product of  $\mathbf{k}_{tri}$  with the third and fifth columns of  $\mathbf{J}_i$ , namely,

$$(\mathbf{r}_i \times \mathbf{s}_i)^T \mathbf{p}_{si} + \mathbf{r}_i \cdot \mathbf{s}_i k_i = (\mathbf{r}_i \times \mathbf{s}_i)^T \mathbf{p}_{ri}$$
 (5.11b)

$$(\mathbf{b}_i \times \mathbf{s}_i)^T \mathbf{p}_{si} + \mathbf{b}_i \cdot \mathbf{s}_i k_i = (\mathbf{b}_i \times \mathbf{s}_i)^T \mathbf{p}_{bi}$$
 (5.11c)

Now we have three linear equations, (5.11a-c), with four unknowns (the three components of  $\mathbf{p}_{si}$  and  $k_i$ ), and hence, we need one fourth equation. Since the component of  $\mathbf{p}_{si}$  along  $\mathbf{s}_i$  does not affect the cross product  $\mathbf{s}_i \times \mathbf{p}_{si}$ ,  $\mathbf{p}_{si}$  is indeterminate; we can thus define  $\mathbf{p}_{si}$  as normal to  $\mathbf{s}_i$ , to make it of *minimum norm*. We thus obtain four equations in four unknowns, i.e.,

$$\begin{bmatrix} (\mathbf{a}_{i} \times \mathbf{s}_{i})^{T} & \mathbf{a}_{i} \cdot \mathbf{s}_{i} \\ (\mathbf{r}_{i} \times \mathbf{s}_{i})^{T} & \mathbf{r}_{i} \cdot \mathbf{s}_{i} \\ (\mathbf{b}_{i} \times \mathbf{s}_{i})^{T} & \mathbf{b}_{i} \cdot \mathbf{s}_{i} \\ \mathbf{s}_{i}^{T} & 0 \end{bmatrix} \begin{bmatrix} \mathbf{p}_{si} \\ k_{i} \end{bmatrix} = \begin{bmatrix} (\mathbf{a}_{i} \times \mathbf{s}_{i})^{T} \mathbf{p}_{ai} \\ (\mathbf{r}_{i} \times \mathbf{s}_{i})^{T} \mathbf{p}_{ri} \\ (\mathbf{b}_{i} \times \mathbf{s}_{i})^{T} \mathbf{p}_{bi} \\ 0 \end{bmatrix}$$

$$(5.12)$$

Moreover, we notice that  $\mathbf{s}_i$  is normal to  $\mathbf{r}_i$  and  $\mathbf{b}_i$ ; after rearranging the four equations given

above, and casting them in block form, we obtain

$$\begin{bmatrix} \mathbf{E}_i & \mathbf{0} \\ \mathbf{g}_i^T & h_i \end{bmatrix} \begin{bmatrix} \mathbf{p}_{si} \\ k_i \end{bmatrix} = \begin{bmatrix} \mathbf{z}_i \\ z_{0i} \end{bmatrix}$$
 (5.13)

where

$$\mathbf{E}_{i} \equiv \begin{bmatrix} (\mathbf{b}_{i} \times \mathbf{s}_{i})^{T} \\ (\mathbf{r}_{i} \times \mathbf{s}_{i})^{T} \\ \mathbf{s}_{i}^{T} \end{bmatrix} \in \mathbb{R}^{3 \times 3}, \ \mathbf{g}_{i} \equiv \mathbf{a}_{i} \times \mathbf{s}_{i} \in \mathbb{R}^{3}, \ h_{i} \equiv \mathbf{a}_{i} \cdot \mathbf{s}_{i} \in \mathbb{R}$$

$$\begin{bmatrix} \mathbf{p}_{si} \\ k_{i} \end{bmatrix} \in \mathbb{R}^{4}, \ \mathbf{z}_{i} \equiv \begin{bmatrix} (\mathbf{b}_{i} \times \mathbf{s}_{i})^{T} \mathbf{p}_{bi} \\ (\mathbf{r}_{i} \times \mathbf{s}_{i})^{T} \mathbf{p}_{ri} \\ 0 \end{bmatrix} \in \mathbb{R}^{3}, \ z_{0i} \equiv (\mathbf{a}_{i} \times \mathbf{s}_{i})^{T} \mathbf{p}_{ai} \in \mathbb{R}$$

$$(5.14)$$

Next, we solve for  $[\mathbf{p}_{si}^T, k_i]^T$  from Eq. (5.13), using the formula for the inverse of a block matrix:

$$\begin{bmatrix} \mathbf{p}_{si} \\ k_i \end{bmatrix} = \begin{bmatrix} \mathbf{E}_i^{-1} \mathbf{z}_i \\ -h_i^{-1} \mathbf{g}_i^T \mathbf{E}_i^{-1} \mathbf{z}_i + h_i^{-1} z_{0i} \end{bmatrix}$$
 (5.15)

Hence, by resorting to reciprocal bases [98] to derive  $\mathbf{E}_{i}^{-1}$ ,  $\mathbf{p}_{si}$  can be found, upon simplification, as

$$\mathbf{p}_{si} = \frac{\|\mathbf{s}_i\|^2}{\Delta_{E_i}} [-\mathbf{r}_i \ \mathbf{b}_i] \begin{bmatrix} (\mathbf{b}_i \times \mathbf{s}_i)^T \mathbf{p}_{bi} \\ (\mathbf{r}_i \times \mathbf{s}_i)^T \mathbf{p}_{ri} \end{bmatrix}$$
(5.16)

where  $\Delta_{Ei}$  denotes  $\det(\mathbf{E}_i)$ , which can be readily obtained by means of the double mixed product of its three row vectors. After simplification,

$$\Delta_{E_i} = \|\mathbf{s}_i\|^2 \tag{5.17}$$

Therefore,

$$\mathbf{p}_{si} = \begin{bmatrix} -\mathbf{r}_i & \mathbf{b}_i \end{bmatrix} \begin{bmatrix} (\mathbf{b}_i \times \mathbf{s}_i)^T \mathbf{p}_{bi} \\ (\mathbf{r}_i \times \mathbf{s}_i)^T \mathbf{p}_{ri} \end{bmatrix}$$
(5.18)

 $k_i$  then following from Eq. (5.15). Now we have a general expression for the K matrix of

Eq. (5.3), associated with a 3- $\underline{C}$ CC PKM, regardless of which C joint is actuated; the angles and the distances between any neighboring pair of those axes ( $\mathcal{A}_i$ ,  $\mathcal{R}_i$ ,  $\mathcal{B}_i$ ) are arbitrary. Hence, these relations are fairly general.

Next, we limit ourselves to the case whereby the axis of the ith-limb cylindrical joint is the common perpendicular of the first and third cylindrical axes, as Daniali et al. did [92–94], which greatly simplifies the pertinent relations. This class of robot is shown to entail many simplifications in the design and analysis, and hence, we will henceforth focus on this class.

Let the intersecting points of  $\mathcal{R}_i$  with  $\mathcal{A}_i$  and  $\mathcal{B}_i$  be  $L_i$  and  $U_i$ , respectively, as shown in Fig. 2.5; it is found, that due to the relation  $\mathbf{b}_i \perp \mathbf{r}_i$ , vectors  $\mathbf{b}_i$ ,  $\mathbf{r}_i$  and  $\mathbf{s}_i$  form an orthonormal triad, and hence, an orthonormal basis, matrix  $\mathbf{E}_i$  then simplifying to

$$\mathbf{E}_{i} = \begin{bmatrix} (\mathbf{b}_{i} \times \mathbf{s}_{i})^{T} \\ (\mathbf{r}_{i} \times \mathbf{s}_{i})^{T} \\ \mathbf{s}_{i}^{T} \end{bmatrix} = \begin{bmatrix} -\mathbf{r}_{i}^{T} \\ \mathbf{b}_{i}^{T} \\ \mathbf{s}_{i}^{T} \end{bmatrix}$$
(5.19)

which is, in fact, proper orthogonal. Indeed,  $\mathbf{s}_i$  is of unit norm in this case, the axis of the second and third axes,  $\mathcal{R}_i$  and  $\mathcal{B}_i$ , intersecting at point  $U_i$ . We can thus choose this point to represent the Plücker coordinates of the foregoing axes. If we denote vector  $\overrightarrow{U_iC}$  as  $\mathbf{p}_i$ , then the derivation of  $\mathbf{p}_{si}$  simplifies to

$$\mathbf{p}_{si} = (\mathbf{r}_i \cdot \mathbf{p}_i)\mathbf{r}_i + (\mathbf{b}_i \cdot \mathbf{p}_i)\mathbf{b}_i = \mathbf{p}_i - (\mathbf{p}_i \cdot \mathbf{s}_i)\mathbf{s}_i$$
 (5.20)

which is nothing but the projection of  $\mathbf{p}_i$  onto the plane defined by the intersecting axes of the two passive cylindrical joints. Moreover, even though we assume  $\mathbf{p}_{si}$  to be normal to  $\mathbf{s}_i$  to obtain a unique solution, this is not necessary because a component along the  $\mathbf{s}_i$  direction does not affect the inner product of  $\mathbf{p}_{si}$  and  $\mathbf{s}_i$ . As a result, we can simply assign  $\mathbf{p}_{si}$  as

$$\mathbf{p}_{si} = \mathbf{p}_i \tag{5.21}$$

which is a vector pointing from the intersection of the axes of the two passive C-joints,  $U_i$ ,

to the operation point C. Moreover,  $\mathbf{r}_i \perp \mathbf{a}_i$  leads to

$$-h_i^{-1} \mathbf{g}_i^T \mathbf{E}_i^{-1} = -\frac{1}{\mathbf{a}_i \cdot \mathbf{s}_i} (\mathbf{a}_i \times \mathbf{s}_i)^T [-\mathbf{r}_i, \mathbf{b}_i, \mathbf{s}_i]$$

$$= -\frac{1}{\mathbf{a}_i \cdot \mathbf{s}_i} [-(\mathbf{s}_i \times \mathbf{r}_i)^T \mathbf{a}_i, (\mathbf{s}_i \times \mathbf{b}_i)^T \mathbf{a}_i, 0]$$

$$= -\frac{1}{\mathbf{a}_i \cdot \mathbf{s}_i} [\mathbf{b}_i^T \mathbf{a}_i, 0, 0]$$
(5.22)

 $k_i$  now being calculated accordingly; after straightforward simplifications, we obtain

$$k_i = \frac{1}{\mathbf{a}_i \cdot \mathbf{s}_i} \{ [\mathbf{a}_i \times (\mathbf{b}_i \times \mathbf{r}_i)] \cdot (\mathbf{p}_i + r_i \mathbf{r}_i) + \mathbf{b}_i \cdot \mathbf{a}_i (\mathbf{r}_i \cdot \mathbf{p}_i) \}$$
(5.23)

with  $r_i$  denoting the distance between  $\mathcal{A}_i$  and  $\mathcal{B}_i$ , namely, the variable length of the middle link. Furthermore,

$$\mathbf{a}_i \times \mathbf{s}_i = \mathbf{a}_i \times (\mathbf{b}_i \times \mathbf{r}_i) = (\mathbf{a}_i \cdot \mathbf{r}_i)\mathbf{b}_i - (\mathbf{a}_i \cdot \mathbf{b}_i)\mathbf{r}_i = -(\mathbf{a}_i \cdot \mathbf{b}_i)\mathbf{r}_i$$
 (5.24)

Then,  $k_i$  simplifies to

$$k_i = \frac{1}{\mathbf{a}_i \cdot \mathbf{s}_i} [-(\mathbf{a}_i \cdot \mathbf{b}_i)\mathbf{r}_i \cdot (\mathbf{p}_i + r_i\mathbf{r}_i) + \mathbf{b}_i \cdot \mathbf{a}_i(\mathbf{r}_i \cdot \mathbf{p}_i)] = -\frac{\mathbf{a}_i \cdot \mathbf{b}_i}{\mathbf{a}_i \cdot \mathbf{s}_i} r_i$$
(5.25)

Consequently, K bears the form

$$\mathbf{K} = \begin{bmatrix} \mathbf{s}_{1}^{T} & \mathbf{0}^{T} \\ \mathbf{s}_{2}^{T} & \mathbf{0}^{T} \\ \mathbf{s}_{3}^{T} & \mathbf{0}^{T} \\ (\mathbf{s}_{1} \times \mathbf{p}_{1} + k_{1}\mathbf{s}_{1})^{T} & \mathbf{s}_{1}^{T} \\ (\mathbf{s}_{2} \times \mathbf{p}_{2} + k_{2}\mathbf{s}_{2})^{T} & \mathbf{s}_{1}^{T} \\ (\mathbf{s}_{3} \times \mathbf{p}_{3} + k_{3}\mathbf{s}_{3})^{T} & \mathbf{s}_{3}^{T} \end{bmatrix}$$

$$(5.26)$$

where

$$\mathbf{s}_i = \mathbf{b}_i \times \mathbf{r}_i, \quad k_i = -\frac{\mathbf{a}_i \cdot \mathbf{b}_i}{\mathbf{a}_i \cdot \mathbf{s}_i} r_i$$
 (5.27)

Next, **D**, which appears in Eq. (5.3), is obtained as a diagonal matrix, namely,

$$\mathbf{D} = \operatorname{diag}(d_{rt1}, d_{rt2}, d_{rt3}, d_{tr1}, d_{tr2}, d_{tr3}) \tag{5.28}$$

whose entries can be expressed as

$$d_{rti} = [\mathbf{s}_i^T, \mathbf{0}^T] \begin{bmatrix} \mathbf{a}_i \\ \mathbf{a}_i \times \mathbf{p}_{ai} \end{bmatrix} = \mathbf{s}_i \cdot \mathbf{a}_i, \quad i = 1, 2, 3$$
 (5.29)

and

$$d_{tri} = \left[ (\mathbf{s}_i \times \mathbf{p}_1 + k_1 \mathbf{s}_2)^T, \mathbf{s}_i^T \right] \begin{bmatrix} \mathbf{0} \\ \mathbf{a}_i \end{bmatrix} = \mathbf{s}_i \cdot \mathbf{a}_i, \quad i = 1, 2, 3$$
 (5.30)

As a result,

$$\mathbf{D} = \operatorname{diag}(\mathbf{s}_1 \cdot \mathbf{a}_1, \mathbf{s}_2 \cdot \mathbf{a}_2, \mathbf{s}_3 \cdot \mathbf{a}_3, \mathbf{s}_1 \cdot \mathbf{a}_1, \mathbf{s}_2 \cdot \mathbf{a}_2, \mathbf{s}_3 \cdot \mathbf{a}_3)$$
 (5.31)

Moreover, if we define the angle between the axes of the actuated and the distal C-joints, namely, the angle between  $\mathbf{a}_i$  and  $\mathbf{b}_i$ , as  $\alpha_i$ , then<sup>2</sup>

$$\mathbf{s}_i \cdot \mathbf{a}_i = (\mathbf{b}_i \times \mathbf{r}_i) \cdot \mathbf{a}_i = (\mathbf{a}_i \times \mathbf{b}_i) \cdot \mathbf{r}_i = \sin \alpha_i$$
 (5.32)

and hence,

$$\mathbf{D} = \operatorname{diag}(\sin \alpha_1, \sin \alpha_2, \sin \alpha_3, \sin \alpha_1, \sin \alpha_2, \sin \alpha_3) \tag{5.33}$$

Moreover,  $k_i$  also simplifies to

$$k_i = -(\cot \alpha_i)r_i \tag{5.34}$$

It can be readily verified that the inner product of  $\mathbf{k}_{tri}$  with the first and the last four columns of  $\mathbf{J}_i$  indeed vanishes; the proof being straightforward is thus omitted.

Next, we verify the decoupled property of this type of PKM and offer a brief singularity analysis to show that singularity depends only on the orientation of the MP. If we represent

This angle, appearing in both **K** and **D**, is a function of  $[\mathbf{a}_i]_B$ ,  $[\mathbf{b}_i]_M$ , and the orientation of the MP. It is noteworthy that we assume that the set  $\{\mathbf{a}_i, \mathbf{b}_i, \mathbf{r}_i\}_1^3$  forms a right-handed system, i.e., its double product, in the given order, is positive.

 $\mathbf{K}$ ,  $\mathbf{D}$  and  $\boldsymbol{\phi}$  in block form, namely,

$$\mathbf{K} = \begin{bmatrix} \mathbf{S} & \mathbf{O} \\ \mathbf{T} & \mathbf{S} \end{bmatrix}, \quad \mathbf{D} = \operatorname{diag}(\mathbf{D}_0, \mathbf{D}_0), \quad \boldsymbol{\phi} = \begin{bmatrix} \boldsymbol{\theta}_a \\ \mathbf{r}_a \end{bmatrix}$$
(5.35)

with

$$\mathbf{S} = \begin{bmatrix} \mathbf{s}_{1}^{T} \\ \mathbf{s}_{2}^{T} \\ \mathbf{s}_{3}^{T} \end{bmatrix}, \quad \mathbf{T} = \begin{bmatrix} (\mathbf{s}_{1} \times \mathbf{p}_{1} + k_{1}\mathbf{s}_{1})^{T} \\ (\mathbf{s}_{2} \times \mathbf{p}_{2} + k_{2}\mathbf{s}_{2})^{T} \\ (\mathbf{s}_{3} \times \mathbf{p}_{3} + k_{3}\mathbf{s}_{3})^{T} \end{bmatrix}$$

$$\mathbf{D}_{0} = \operatorname{diag}(\sin \alpha_{1}, \sin \alpha_{2}, \sin \alpha_{3}), \qquad (5.36)$$

$$\boldsymbol{\theta}_{a} = \begin{bmatrix} \boldsymbol{\theta}_{1a} \\ \boldsymbol{\theta}_{2a} \\ \boldsymbol{\theta}_{3a} \end{bmatrix}, \quad \mathbf{r}_{a} = \begin{bmatrix} r_{1a} \\ r_{2a} \\ r_{3a} \end{bmatrix}$$

then, the kinematics relations in Eq. (5.3) can be rewritten as

$$\mathbf{S}\boldsymbol{\omega} = \mathbf{D}_0 \dot{\boldsymbol{\theta}}_a, \quad \mathbf{T}\boldsymbol{\omega} + \mathbf{S}\dot{\mathbf{c}} = \mathbf{D}_0 \dot{\mathbf{r}}_a$$
 (5.37)

from which it is apparent that the angular velocity is only dependent on the angular rates of the three actuated cylindrical joints, which means that the rotation is decoupled from the translation at the velocity level. However, the velocity  $\dot{\mathbf{c}}$  of the operation point is linearly related to the angular velocity of the MP. Next, we conduct a brief singularity analysis for this robot. Firstly, the singularity locus can be obtained upon setting the determinant of  $\mathbf{K}$  (or of  $\mathbf{D}$ ) to zero<sup>3</sup>; since  $\mathbf{K}$  is a block-lower-triangular matrix, its determinant  $\Delta_{\mathbf{K}}$  reduces to

$$\Delta_{\mathbf{K}} = (\Delta_{\mathbf{S}})^2 \tag{5.38}$$

where  $\Delta_{\mathbf{S}}$  denotes  $\det(\mathbf{S})$ . As a result, the singularity of **K** is defined by the condition

$$\Delta_{\mathbf{S}} \equiv (\mathbf{s}_1 \times \mathbf{s}_2) \cdot \mathbf{s}_3 = 0 \tag{5.39}$$

<sup>&</sup>lt;sup>3</sup>There is another type of singularity involved in PKMs, which is the limb singularity. It can be readily shown that the limb singularity occurs iff  $\mathbf{D}$  becomes singular for the 3- $\underline{\mathbf{CCC}}$  PKM.

where

$$\mathbf{s}_i = \mathbf{b}_i \times \mathbf{r}_i \parallel \mathbf{b}_i \times (\mathbf{a}_i \times \mathbf{b}_i) = \mathbf{a}_i - \mathbf{b}_i \cos \alpha_i \tag{5.40}$$

which is also affected only by the orientation of the MP. As for  $\mathbf{D}$ , it becomes singular when  $\mathbf{a}_i \parallel \mathbf{b}_i$  for some i, i = 1, 2, 3, which is obviously only affected by the orientation of the MP. To summarize, the singularity is totally determined by the orientation of the MP. Moreover, even though the above analysis is conducted at the velocity level, the rotation of the MP of the proposed robot is in fact decoupled from its translation at the displacement level as well, which can be verified from the forward displacement analysis in Section 5.3.

As stated at the beginning of this chapter, the kinematics of this class of PKMs was, in fact, investigated by Daniali et al. [92–94], but their derivation yields cumbersome forms of **K** and **D**; for example, our **D** is diagonal, which dramatically simplifies the analysis and brings about novel results. Moreover, the six rows of **K** in the same references do not represent the screws associated with the corresponding joints. As a result, the evaluation of these matrices is cumbersome. Furthermore, it will be shown that the derivation therein imposes unnecessary constraints on the isotropic design, to be discussed in Section 5.2.

In summary, the proposed robot entails simple kinematics, by virtue of the rotation of the MP being decoupled from its translation. This not only simplifies significantly the control and analysis of the robot, but also makes the singularity analysis dependent only on the orientation of the MP, thereby making singularity avoidance dramatically simpler. These features are rarely seen in six-dof PKMs.

#### 5.1.2 The Inverse Jacobian and Actuator Jacobian

In Subsection 5.1.1 we obtained the kinematic relation of the 3- $\underline{\text{CCC}}$  PKM between the MP twist  $\mathbf{t}$  and the six-dimensional array of C-drive rates  $\dot{\boldsymbol{\phi}}$ . Based on this result, we derive the kinematic relation between the MP twist and the six-dimensional motor-rate array as

$$\mathbf{Kt} = \mathbf{J}\dot{\boldsymbol{\psi}} \tag{5.41}$$

where  $\dot{\boldsymbol{\psi}} = [\dot{\psi}_{L1}, \, \dot{\psi}_{R1}, \, \dot{\psi}_{L2}, \, \dot{\psi}_{R2}, \, \dot{\psi}_{L3}, \, \dot{\psi}_{R3}]^T$  represents the array of the six motor rates, and

$$\mathbf{J} = \mathbf{DJ}_m \tag{5.42}$$

with  $\mathbf{J}$  and  $\mathbf{J}_m$  representing the *inverse Jacobian* and the *actuator Jacobian*, respectively. Furthermore,  $\mathbf{J}_m$  takes the form

$$\mathbf{J}_{m} = \frac{1}{2} \begin{bmatrix} 1 & 1 & 0 & 0 & 0 & 0 \\ 0 & 0 & 1 & 1 & 0 & 0 \\ 0 & 0 & 0 & 0 & 1 & 1 \\ p_{n} - p_{n} & 0 & 0 & 0 & 0 \\ 0 & 0 & p_{n} - p_{n} & 0 & 0 \\ 0 & 0 & 0 & 0 & p_{n} - p_{n} \end{bmatrix}$$

$$(5.43)$$

where if p represents the pitch of the  $\underline{C}$ -joints,  $p_n = p/(2\pi)$  represents the normalized pitch, meaning the pitch measured in mm/rad, to express it in SI units. It is noteworthy that the above  $\mathbf{J}_m$  is different from that of the SDelta, displayed in Eq. (3.9), which is solely due to the different ordering of the six components of the C-drive array, as per Eqs. (3.2) and (5.4).

## 5.1.3 Introducing the Characteristic Length

Before we conduct the optimization based on the condition number of the Jacobian matrices, we need to render them dimensionally homogeneous. It is apparent that the four  $3 \times 3$  blocks of both  $\mathbf{K}$  and  $\mathbf{J}_m$  bear different units. Next, we make them dimensionally homogeneous with the aid of the characteristic length L and some manipulations of the matrices. Firstly,  $\mathbf{J}_m$  is rewritten as

$$\mathbf{J}_m = \frac{\sqrt{2}}{2} \mathbf{PW} \tag{5.44}$$

where

$$\mathbf{P} = \operatorname{diag}(1, 1, 1, p_n, p_n, p_n), \quad \mathbf{W} = \frac{\sqrt{2}}{2} \begin{bmatrix} 1 & 1 & 0 & 0 & 0 & 0 \\ 0 & 0 & 1 & 1 & 0 & 0 \\ 0 & 0 & 0 & 0 & 1 & 1 \\ 1 & -1 & 0 & 0 & 0 & 0 \\ 0 & 0 & 1 & -1 & 0 & 0 \\ 0 & 0 & 0 & 0 & 1 & -1 \end{bmatrix}$$
(5.45)

the latter being orthogonal. As a result, Eq. (5.41) takes the form

$$\mathbf{Kt} = \mathbf{D}\dot{\boldsymbol{\phi}} = \mathbf{DJ}_{m}\dot{\boldsymbol{\psi}} = \frac{\sqrt{2}}{2}\mathbf{DPW}\dot{\boldsymbol{\psi}} = \frac{\sqrt{2}}{2}\mathbf{PDW}\dot{\boldsymbol{\psi}}$$
 (5.46)

the last equality holding because both  $\mathbf{P}$  and  $\mathbf{D}$  are diagonal, and hence, commute. Since  $\mathbf{D}$  and  $\mathbf{W}$  are dimensionless, while  $\mathbf{K}$  and  $\mathbf{P}$  are not, we multiply both sides of the foregoing equation by  $\mathbf{P}^{-1}$  and redefine the two Jacobian matrices as

$$\mathbf{K}' = \mathbf{P}^{-1}\mathbf{K} = \begin{bmatrix} \mathbf{s}_{1}^{T} & \mathbf{0}^{T} \\ \mathbf{s}_{2}^{T} & \mathbf{0}^{T} \\ \mathbf{s}_{3}^{T} & \mathbf{0}^{T} \\ (\mathbf{s}_{1} \times \mathbf{p}_{1} + k_{1}\mathbf{s}_{1})^{T}/p_{n} & \mathbf{s}_{1}^{T}/p_{n} \\ (\mathbf{s}_{2} \times \mathbf{p}_{2} + k_{2}\mathbf{s}_{2})^{T}/p_{n} & \mathbf{s}_{1}^{T}/p_{n} \\ (\mathbf{s}_{3} \times \mathbf{p}_{3} + k_{3}\mathbf{s}_{3})^{T}/p_{n} & \mathbf{s}_{3}^{T}/p_{n} \end{bmatrix}$$

$$(5.47)$$

and

$$\mathbf{D}' = \frac{\sqrt{2}}{2} \mathbf{DW} \tag{5.48}$$

which leads to the mapping between  ${\bf t}$  and  $\hat{{\boldsymbol \psi}}$ :

$$\mathbf{K}'\mathbf{t} = \mathbf{D}'\dot{\boldsymbol{\psi}} \tag{5.49}$$

Now, if we want to make  $\mathbf{K}'$  dimensionally homogeneous, we recall the characteristic length L, as yet to be determined, and redefine the MP twist and  $\mathbf{K}_h$  as

$$\mathbf{t}_{h} = \begin{bmatrix} \dot{\boldsymbol{\omega}} \\ \dot{\mathbf{c}}^{T}/L \end{bmatrix}, \quad \mathbf{K}_{h} = \begin{bmatrix} \mathbf{s}_{1}^{T} & \mathbf{0}^{T} \\ \mathbf{s}_{2}^{T} & \mathbf{0}^{T} \\ \mathbf{s}_{3}^{T} & \mathbf{0}^{T} \\ (\mathbf{s}_{1} \times \mathbf{p}_{1} + k_{1}\mathbf{s}_{1})^{T}/p_{n} & \mathbf{s}_{1}^{T}L/p_{n} \\ (\mathbf{s}_{2} \times \mathbf{p}_{2} + k_{2}\mathbf{s}_{2})^{T}/p_{n} & \mathbf{s}_{1}^{T}L/p_{n} \\ (\mathbf{s}_{3} \times \mathbf{p}_{3} + k_{3}\mathbf{s}_{3})^{T}/p_{n} & \mathbf{s}_{3}^{T}L/p_{n} \end{bmatrix}$$

$$(5.50)$$

In summary, when taking the six motor rates as the input joint rates, the kinematic relation of interest can be written as

$$\mathbf{K}_h \mathbf{t}_h = \mathbf{D}_h \dot{\boldsymbol{\psi}} \tag{5.51}$$

with  $\mathbf{D}_h$  defined as

$$\mathbf{D}_h = \frac{\sqrt{2}}{2} \mathbf{DW} \tag{5.52}$$

It is apparent that both  $\mathbf{K}_h$  and  $\mathbf{D}_h$  are dimensionally homogeneous, in fact, dimensionless.

## 5.2 The Isotropic Design

# 5.2.1 Geometric Conditions for Isotropy

As discussed in Chapter 4, isotropy is achieved when its two Jacobian matrices bear the condition number of unity, under which the six rows (columns) of the Jacobian matrices are orthogonal, yielding high positioning accuracy and homogeneity of the MP motion along all six directions of the Cartesian space [62,63,65]. Due to the simple form of the kinematic relations for the 3-CCC PKM, this robot class admits an isotropic design, as shown below. The isotropy requirement leads to two conditions, one for each Jacobian, namely,

$$\mathbf{D}_h \mathbf{D}_h^T = \sigma_D^2 \mathbf{1}_{6 \times 6}, \quad \mathbf{K}_h \mathbf{K}_h^T = \sigma_K^2 \mathbf{1}_{6 \times 6} \tag{5.53}$$

with  $\mathbf{K}_h$  and  $\mathbf{D}_h$  defined in Eqs.(5.50) and (5.52), respectively,  $\sigma_D$  and  $\sigma_K$  as yet to be found. First, we look at the  $\mathbf{K}_h$  matrix in block form, namely,

$$\mathbf{K}_{h} = \begin{bmatrix} \mathbf{S} & \mathbf{O}_{3\times3} \\ (1/p_{n})\mathbf{T} & (L/p_{n})\mathbf{S} \end{bmatrix}$$
 (5.54)

Hence,

$$\mathbf{K}_{h}\mathbf{K}_{h}^{T} = \begin{bmatrix} \mathbf{S}\mathbf{S}^{T} & (1/p_{n})\mathbf{S}\mathbf{T}^{T} \\ (1/p_{n})\mathbf{T}\mathbf{S}^{T} & (1/p_{n}^{2})\mathbf{T}\mathbf{T}^{T} + (L^{2}/p_{n}^{2})\mathbf{S}\mathbf{S}^{T} \end{bmatrix}$$
(5.55)

When  $\mathbf{K}_h$  is isotropic,  $\mathbf{S}\mathbf{S}^T$  is proportional to the  $3 \times 3$  identity matrix. Moreover, from knowledge that the rows of  $\mathbf{S}$  are all of unit Euclidean norm, we conclude that  $\mathbf{S}$ , in fact, has to be an orthogonal matrix. Moreover,  $(1/p_n)\mathbf{T}\mathbf{S}^T$  has to vanish, and hence, by virtue of the orthogonality of  $\mathbf{S}$ ,  $\mathbf{T}$  must vanish, i.e.,

$$\mathbf{T} = p_n \mathbf{O}_{3 \times 3} \mathbf{S} = \mathbf{O}_{3 \times 3} \tag{5.56}$$

Now  $\mathbf{K}_h \mathbf{K}_h^T$  becomes

$$\mathbf{K}_{h}\mathbf{K}_{h}^{T} = \begin{bmatrix} \mathbf{1} & \mathbf{O} \\ \mathbf{O} & (L^{2}/p_{n}^{2})\mathbf{1} \end{bmatrix}$$
 (5.57)

with 1 representing the  $3 \times 3$  identity matrix.

Moreover, L is defined as the value that maximizes the dexterity, which is achieved when the condition number equals unity, or equivalently, when the robot is under an isotropic configuration. It is obvious that, in order to render  $\mathbf{K}_h$  isotropic,  $L^2/p_n^2$  has to equal to unity; hence, the characteristic length is nothing but  $L = p_n$ , i.e., the normalized pitch for the proposed class of isotropic PKMs.

Finally, in order to render  $\mathbf{K}_h$  isotropic, we need the set  $\{\mathbf{s}_i\}_1^3$  to be orthonormal, while  $\mathbf{T}$  must vanish. Now, given that each row of  $\mathbf{T}$  is composed of two orthogonal components, as per Eq. (5.36),  $\mathbf{s}_i \times \mathbf{p}_i$  and  $k_i \mathbf{s}_i$ , this means that these two components have to both vanish, namely,  $\mathbf{s}_i \parallel \mathbf{p}_i$  and  $k_i = -r_i \cot \alpha_i = 0$ . The last condition yields  $\mathbf{a}_i \perp \mathbf{b}_i$ ; moreover,  $\mathbf{r}_i$  is the common perpendicular to  $\mathbf{a}_i$  and  $\mathbf{b}_i$ , and hence,  $\mathbf{a}_i$ ,  $\mathbf{r}_i$  and  $\mathbf{b}_i$  form an orthonormal triad under

an isotropic posture, for i = 1, 2, 3. Since each axis has two possible directions, we choose  $\mathbf{r}_i$  to be in the same direction as  $\mathbf{a}_i \times \mathbf{b}_i$ . Under these conditions,  $\mathbf{s}_i = \mathbf{b}_i \times \mathbf{r}_i = \mathbf{a}_i$ . Then, the condition for  $\{\mathbf{s}_i\}_1^3$  to be orthogonal is equivalent to requiring  $\{\mathbf{a}_i\}_1^3$  to be orthonormal. Moreover, the condition  $\mathbf{p}_i \parallel \mathbf{s}_i$  is equivalent to  $\mathbf{p}_i \parallel \mathbf{a}_i$ .

In summary, the isotropy conditions for  $\mathbf{K}_h$  follow:

- 1. the set  $\{\mathbf{a}_i\}_1^3$  is orthogonal
- 2.  $\mathbf{a}_i \perp \mathbf{b}_i$ , for i = 1, 2, 3
- 3.  $\mathbf{s}_i \parallel \mathbf{p}_i$  or, equivalently,  $\mathbf{a}_i \parallel \mathbf{p}_i$

It can be readily verified that these conditions also lead to  $\mathbf{D}_h$  isotropic, and hence, the robot can attain an isotropic posture. This set of constraints is different from that obtained by Daniali et al. for isotropy [92–94]. In fact, different from the conditions reported in the foregoing papers, the conditions derived here allow for a *continuum* of isotropic architectures, as shown below.

### 5.2.2 Realization of the Isotropic Design

#### 5.2.2.1 The Design of the Base Platform

Based on the conditions derived above, we can set up the geometric conditions under which the robot is isotropic. The design procedure is described below.

We denote the coordinate axes of the BP frame as  $X_1, Y_1$  and  $Z_1$ , respectively, as shown in Fig. 5.1. Since  $\{\mathbf{a}_i\}_1^3$  is orthonormal, we define these vectors as parallel to the coordinate axes of the base frame without loss of generality, namely,  $\mathbf{a}_1 = [1, 0, 0]^T$ ,  $\mathbf{a}_2 = [0, 1, 0]^T$  and  $\mathbf{a}_3 = [0, 0, 1]^T$ . The three axes  $\mathcal{A}_i$  do not necessarily intersect each other; hence, there may be an offset between each pair of these. Without loss of generality, we define the BP frame such that the  $X_1$  axis coincides with  $\mathcal{A}_1$ , and the  $Z_1$  axis coincides with the common perpendicular of  $\mathcal{A}_1$  and  $\mathcal{A}_2$ , as shown in Fig. 5.1. In this way, we define the offset vectors  $\{\mathbf{d}_i\}_1^3$ , with  $\mathbf{d}_i$  directed from the *i*th coordinate axis of the base frame to  $\mathcal{A}_i$ , i.e.,  $\mathbf{d}_1 = \mathbf{0}$ ,  $\mathbf{d}_2 = d_2\mathbf{a}_3$  and  $\mathbf{d}_3 = d_{31}\mathbf{a}_1 + d_{32}\mathbf{a}_2$ , with obvious definitions for  $d_{3i}$ , for i = 1, 2. Then, the layout of the

three C-joint axes on the BP is uniquely defined by  $\{\mathbf{a}_i\}_{1}^{3}$ ,  $d_2$ ,  $d_{31}$  and  $d_{32}$ . When the last three parameters are prescribed, all the possible layouts of the BP can be obtained; hence,  $d_2$ ,  $d_{31}$  and  $d_{32}$  are three design parameters, which fully characterize the layout of the BP.

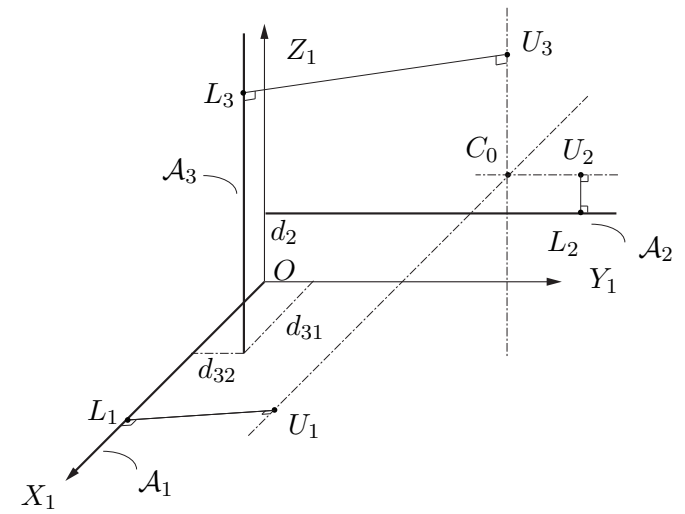


Figure 5.1: The determination of the BP and MP using  $\mathbf{d}_i$ ,  $\mathbf{c}_0$  and  $\mathbf{p}_i$ 

#### 5.2.2.2 Design of the Moving Platform

According with the isotropy conditions, we can now design the MP: First, we choose an arbitrary point  $C_0$  in the BP frame, with the position vector  $\mathbf{c}_0 = [c_{01}, c_{02}, c_{03}]^T$ , in BP-frame coordinates, which is the position vector of the operation point C at the reference posture, as illustrated in Fig. 2.5.  $C_0$  is termed the characteristic point, as this point characterizes the robot isotropic posture. Next, we define three lines  $\{\mathcal{A}'_i\}_1^3$  that pass through  $C_0$ , with  $\mathcal{A}'_i$  parallel to  $\mathcal{A}_i$ , for i = 1, 2, 3 or, equivalently, to the three BP frame axes. Moreover, we choose three arbitrary points  $U_i$  on  $\{\mathcal{A}'_i\}_1^3$ , as shown in Fig. 5.1, where  $U_i$ , introduced earlier, represents the intersection of  $\mathcal{R}_i$  with  $\mathcal{B}_i$ , as shown in Fig. 2.5. Then,  $\mathcal{R}_i$  can be found as the perpendicular from  $U_i$  to  $\mathcal{A}_i$ , namely,  $L_iU_i$ ; moreover,  $\{\mathbf{a}_i, \mathbf{r}_i, \mathbf{b}_i\}_1^3$  form three orthonormal sets under an isotropic configuration; hence, we can find  $\mathbf{b}_i$  as  $^4$   $\mathbf{r}_i \times \mathbf{a}_i$ , and  $\mathcal{B}_i$  as the line passing through  $U_i$ , and parallel to  $\mathbf{b}_i$ .

Since  $\mathbf{p}_i = \overrightarrow{U_iC}$  is parallel to the *i*th axis of the BP frame, the position vector  $\mathbf{u}_i$  of  $U_i$ As there are two possible directions of  $\mathbf{b}_i$ , we assume that  $\{\mathbf{a}_i, \mathbf{r}_i, \mathbf{b}_i\}_1^3$  is a right-handed triad.

can be obtained as

$$\mathbf{u}_{1} = \begin{bmatrix} c_{01} + o_{1} \\ c_{02} \\ c_{03} \end{bmatrix}, \ \mathbf{u}_{2} = \begin{bmatrix} c_{01} \\ c_{02} + o_{2} \\ c_{03} \end{bmatrix}, \ \mathbf{u}_{3} = \begin{bmatrix} c_{01} \\ c_{02} \\ c_{03} + o_{3} \end{bmatrix}$$
(5.58)

in BP-frame coordinates, where  $\{o_i\}_1^3$  represents the offset from  $U_i$  to  $C_0$ . Moreover, as  $L_i$  is the intersection of  $\mathcal{A}_i$  with  $\mathcal{R}_i$ ,

$$\overrightarrow{L_1U_1} = \begin{bmatrix} 0 \\ c_{02} \\ c_{03} \end{bmatrix}, \ \overrightarrow{L_2U_2} = \begin{bmatrix} c_{01} \\ 0 \\ c_{03} - d_2 \end{bmatrix}, \ \overrightarrow{L_3U_3} = \begin{bmatrix} c_{01} - d_{31} \\ c_{02} - d_{32} \\ 0 \end{bmatrix}$$
(5.59)

in BP-frame coordinates. Furthermore,  $\overrightarrow{L_iU_i} = r_i\mathbf{r}_i$ ; as a result,  $\mathbf{r}_i$  can be obtained upon normalizing  $\overrightarrow{L_iU_i}$ . Moreover, it is apparent that  $\mathbf{r}_i$  only involves  $\mathbf{c}_0$  and the prescribed offset  $\{\mathcal{A}_i\}_1^3$ ; once  $\mathbf{r}_i$  is determined, the direction of  $\mathbf{b}_i$  can also be determined as  $\mathbf{r}_i \times \mathbf{a}_i$ . As a result, all the directions involved in the isotropic posture are determined uniquely by the choice of the characteristic point  $\mathbf{c}_0$ , besides the three design parameters  $d_2$ ,  $d_{31}$  and  $d_{32}$ . As for the distances  $o_i$  (the magnitude of  $\overrightarrow{U_iC}$ ), they determine the distance between the three axes  $\mathcal{B}_i$ . Hence,  $\mathbf{c}_0$  and  $d_i$  suffice to define the MP. Moreover, the values for  $d_2$ ,  $d_{31}$ ,  $d_{32}$ ,  $\mathbf{c}_0$  and  $\{o_i\}_1^3$  can be given arbitrarily; as a result, there are infinitely many possibilities to render the robot isotropic.

#### 5.2.2.3 The Feasible Set of Characteristic Points

For most robots, their isotropic postures, if any, are found in finite and discrete sets. For the robots under investigation, however, due to their simple Jacobian matrices, we found that, under proper dimensioning, it is possible to achieve designs within whose workspace a continuous set of isotropic postures exists. This feature guarantees that the accuracy of those properly designed robots attains its maximum within a large region of the workspace, as opposed to isolated points, which is quite advantageous. To the author's knowledge, this feature has not been reported in the literature. Now we seek the conditions under which this can happen.

We assume that we have a 3-<u>C</u>CC robot at a given isotropic posture, and hence,  $\mathbf{a}_i \perp \mathbf{b}_i$ . Moreover, we have to keep this relation at any isotropic posture; now, upon rotating the MP by a rotation matrix  $\mathbf{Q}$  without violating  $\mathbf{a}_i \perp \mathbf{b}_i$ , we have to satisfy the conditions below:

$$\mathbf{a}_{i}^{T}\mathbf{b}_{i} = 0, \ \mathbf{a}_{i}^{T}(\mathbf{Q}\mathbf{b}_{i}) = 0, \ \|\mathbf{b}_{i}\|^{2} = 1$$

$$\mathbf{b}_{i}^{T}\mathbf{b}_{j} = \cos\beta_{ij}, \quad i = 1, 2, 3, \ j \neq i$$

$$(5.60)$$

where  $\beta_{ij}$  is a constant, representing the angle between the unit vectors  $\mathbf{b}_i$  and  $\mathbf{b}_j$ . Since the rotation matrix can be characterized by three independent variables—the three components of the vector in the Euler Rodrigues parameters [64], for example—the above conditions form a system of 12 equations with 12 unknowns (nine from  $\{\mathbf{b}_i\}_{1}^{3}$  and three from  $\mathbf{Q}$ ). The above system is bound to have a discrete set of solutions. This means that we cannot find a continuous rotation maintaining the above condition. As a result, for the set of isotropic postures, if one exists, the MP has to keep a constant orientation under which  $\mathbf{a}_i \perp \mathbf{b}_i$  for i = 1, 2, 3, i.e., the MP can only undergo a pure translation if the isotropic posture is to be preserved. Then, the first two conditions for isotropy, introduced in Section 5.2, are satisfied.

Next, we consider the last condition, i.e.,  $\mathbf{p}_i \parallel \mathbf{a}_i$ , for i=1,2,3: Let us look at vectors  $\mathbf{p}_i = \overrightarrow{U_iC}$ , where  $U_i$  is the intersection of  $\mathcal{R}_i$  with  $\mathcal{B}_i$ . Since we have to keep  $\overrightarrow{U_iC}$  parallel to  $\mathcal{A}_i$  as the MP translates within the set of isotropic postures, the direction of  $\overrightarrow{U_iC}$  must be constant. Moreover, the operation point C is fixed to the MP; hence, point  $U_i$  must be fixed to the MP as well, when the MP undergoes the pure translation required by the first two isotropy conditions. This means that  $U_i$  must be fixed to  $\mathcal{B}_i$ , i.e., there is no translation between the MP and the upper link of the ith limb. Equivalently, the MP has to either undergo a translation as a linear combination of  $\mathbf{a}_i$  and  $\mathbf{r}_i$ , for i=1,2,3, or the translation of the MP must be in the direction normal to the three vectors  $\mathbf{b}_i$ , for i=1,2,3. This is feasible if and only if the set  $\{\mathbf{b}_i\}_1^3$  is coplanar. Let us assume that this is the case and denote their common unit normal as  $\mathbf{n}$ . Once this condition is satisfied, when the MP undergoes a pure translation parallel to  $\mathbf{n}$  (starting from an isotropic posture), there is no translation between the MP and the upper links of the limbs. Hence, all vectors  $\mathbf{a}_i$ ,  $\mathbf{r}_i$ ,  $\mathbf{b}_i$ ,  $\mathbf{p}_i$  remain constant, thereby preserving all three isotropy conditions mentioned at the end of Section 5.2, i.e., the robot still finds itself at an isotropic posture.

Further, we find the isotropy condition under which the set  $\{\mathbf{b}_i\}_1^3$  is coplanar. Since we already have the directions of  $\mathbf{r}_i$  parallel to  $\overrightarrow{L_iU_i}$ , as per Eq. (5.59), finding the vectors  $\{\mathbf{b}_i'\}_1^3$  parallel to the directions of  $\{\mathbf{b}_i\}_1^3$  is straightforward:

$$\mathbf{b}_i' = \overrightarrow{L_i U_i} \times \mathbf{a}_i, \quad i = 1, 2, 3 \tag{5.61}$$

or

$$\mathbf{b}_{1}' = \begin{bmatrix} 0 \\ c_{03} \\ -c_{02} \end{bmatrix}, \ \mathbf{b}_{2}' = \begin{bmatrix} d_{2} - c_{03} \\ 0 \\ c_{01} \end{bmatrix}, \ \mathbf{b}_{3}' = \begin{bmatrix} c_{02} - d_{32} \\ d_{31} - c_{01} \\ 0 \end{bmatrix}$$
 (5.62)

The condition that  $\{\mathbf{b}_i\}_1^3$  be coplanar yields  $(\mathbf{b}_1' \times \mathbf{b}_2') \cdot \mathbf{b}_3' = 0$ ; after simplification, this condition becomes

$$d_2c_{01}c_{02} + d_{31}c_{02}c_{03} - d_{32}c_{01}c_{03} - d_2d_{31}c_{02} = 0 (5.63)$$

which is quadratic in  $\mathbf{c}_0$ . This means that, as long as the chosen point of isotropy (at the design stage) satisfies condition (5.63),  $\{\mathbf{b}_i\}_1^3$  will be coplanar. Then, the proposed robot will be able to achieve a set of continuous isotropic postures along the line passing through  $C_0$  and parallel to  $\mathbf{n}$ , the common normal of  $\{\mathbf{b}_i\}_1^3$ , which can be found as the unit vector parallel to  $\mathbf{b}_i' \times \mathbf{b}_j'$ ,  $i \neq j$ , e.g.<sup>5</sup>,

$$\mathbf{n} \parallel \mathbf{b}_{1}' \times \mathbf{b}_{2}' = \begin{bmatrix} c_{01}c_{03} \\ c_{02}(c_{03} - d_{2}) \\ c_{03}(c_{03} - d_{2}) \end{bmatrix}$$
 (5.64)

#### 5.2.2.4 Several Typical Layouts of the Proposed PKM

We have thus found the condition under which the robot can achieve a set of isotropic postures. Since we have infinitely many choices, we make some further assumptions on the BP frame to determine several typical layouts:

 $<sup>^{5}\</sup>mathbf{b}_{1}^{\prime} \times \mathbf{b}_{2}^{\prime}$  is chosen because it has the simplest form.

- Case I: If we assume that the three axes  $\{A_i\}_1^3$  intersect at one common point, i.e.,  $d_2 = d_{31} = d_{32} = 0$ , then the condition in Eq. (5.63) naturally holds. This means that, when the three orthogonal axes of the C-joints at the base platform intersect at one common point, we can always find a set of motions of the MP along a line, that keeps the robot posture isotropic. The said line passes through the arbitrarily chosen  $C_0$ , its direction being found as that of  $\mathbf{b}'_1 \times \mathbf{b}'_2$ , which turns out to be that of  $\mathbf{c}_0$ . This means that, when the MP moves along the line connecting the origin and the chosen  $C_0$  (with the proper orientation), the robot remains at an isotropic posture.
- Case II: We assume that two of the axes intersect, e.g.  $A_1$  and  $A_2$ , i.e.,  $d_2 = 0$ ; then, the above condition simplifies to

$$(d_{32}c_{01} - d_{31}c_{02})c_{03} = 0 (5.65)$$

which leads to one of two conditions, namely,

$$d_{32}c_{01} - d_{31}c_{02} = 0 \quad \text{or} \quad c_{03} = 0 \tag{5.66}$$

That is, the chosen point of isotropy must lie in the plane of  $\mathcal{A}_1$  and  $\mathcal{A}_2$ , or the plane of the origin and  $\mathcal{A}_3$ , in order to obtain a set of isotropic postures of the given robot. It can be readily verified from Eq. (5.64) that the said line is, again, the line connecting the origin with  $C_0$ .

N.B.: if we choose the axes  $\mathcal{A}_i$  as the edges of a cube of edge length  $\ell$ , then this item covers two special cases:  $\mathcal{A}_1$  and  $\mathcal{A}_2$  coincide with the  $X_1$ - and  $Y_1$ - axes, respectively, while  $\mathcal{A}_3$  can be the line parallel to the  $Z_1$ - axis, but passing through either  $[\ell, 0, 0]^T$  or  $[\ell, \ell, 0]^T$ .

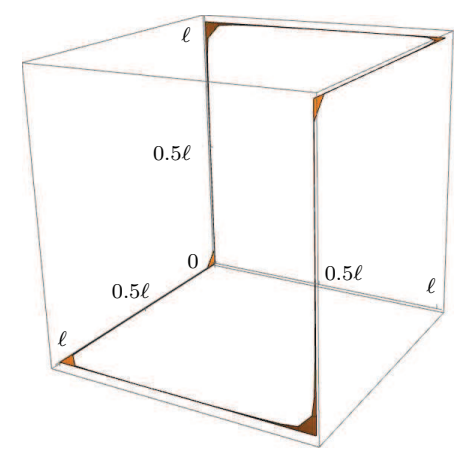
• Case III: Lastly, we assume that the lines are skew, namely, none of  $d_2$ ,  $d_{31}$ ,  $d_{32}$  vanishes. To simplify matters, and to make the robot more "symmetric", we assume that  $d_2 = d_{31} = d_{32} = \ell$ . This covers the case in which we choose three skew edges of the cube. In this case, Eq. (5.63) simplifies to

$$(c_{02}\ell - c_{01}c_{02} - c_{02}c_{03} + c_{01}c_{03})\ell = 0 (5.67)$$

but, since  $\ell \neq 0$ , from the vanishing of the coefficient of  $\ell$  in Eq. (5.67),

$$c_{03} = \frac{c_{02}(c_{01} - \ell)}{c_{01} - c_{02}} \tag{5.68}$$

The surfaces composed of those points that can be used as points of isotropy are plotted in Figs. 5.2 and 5.3, within the range of a cube with an edge length equal to  $\ell$  and to  $1.5\ell$ , respectively.



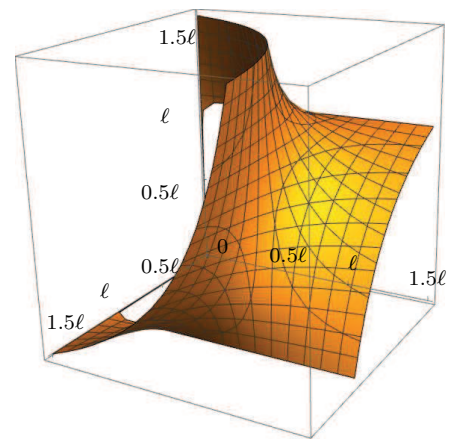


Figure 5.2: The surface of feasible points of Figure 5.3: The surface of feasible points of isotropy within a cube of edge length  $\ell$  isotropy within a cube of edge length  $1.5\ell$ 

Furthermore, we know that the set of characteristic points must pass through point  $C_0$ , of position vector  $\mathbf{c}_0$ . Considering the direction of the line given in Eq. (5.64), we can find the line, and further conclude that the line intersects the  $X_1$  axis at point H, of position vector  $\mathbf{h}$ , namely,

$$[\mathbf{h}]_{\mathcal{B}} = \begin{bmatrix} -c_{01}d_2/(c_{03} - d_2) \\ 0 \\ 0 \end{bmatrix}$$
 (5.69)

when viewed in the base frame (as indicated by the subscript). We can use this point to locate the line of isotropy in the desired region, thus choosing from an infinity of possibilities.

From the above analysis, it is apparent that we still have a large margin of maneuver to choose the layout of the robot while guaranteeing a set of isotropy postures. Hence, we have a continuous set of design variables that yield infinitely many different robot designs; within the workspace of any of these robots, a continuous set of isotropic postures is feasible.

#### 5.2.2.5 Enumeration of Several Representative Designs

Symmetry in robot design, or design at large, for that matter, is advantageous. We introduce below some further assumptions on symmetry, to come up with some representative layouts.

As for the MP, we make the assumption that the angles between each pair of axes  $\{\mathcal{B}_i\}_1^3$  are equal, if this is at all possible. Notice that the three lines  $\{\mathcal{B}_i\}_1^3$  are not necessarily coplanar, but their direction vectors  $\{\mathbf{b}_i\}_1^3$  have to be so in order to guarantee the existence of a line of isotropic postures. This requires that the angles between  $\mathbf{b}_i$  and  $\mathbf{b}_j$  be  $2\pi/3$ , namely,  $\mathbf{b}_i \cdot \mathbf{b}_j = -1/2$ , for  $i, j = 1, 2, 3, i \neq j$ . In fact, this layout defines an equilateral spatial triangle. The foregoing inner products can be obtained as

$$\mathbf{b}_i \cdot \mathbf{b}_j = \frac{\mathbf{b}_i' \cdot \mathbf{b}_j'}{\|\mathbf{b}_i'\|_2 \|\mathbf{b}_j'\|_2}$$

$$(5.70)$$

Then, the set of conditions

$$\mathbf{b}_1 \cdot \mathbf{b}_2 = -\frac{1}{2}, \quad \mathbf{b}_2 \cdot \mathbf{b}_3 = -\frac{1}{2}, \quad \mathbf{b}_3 \cdot \mathbf{b}_1 = -\frac{1}{2}$$
 (5.71)

constitutes a set of constraints on the choice of the characteristic point  $C_0$ .

Below we elaborate on four layouts:

- Layout I: the base is characterized by  $d_2 = d_{31} = d_{32} = 0$ . Then, constraint (5.71) yields the condition  $c_{01} = c_{02} = c_{03}$  (due to symmetry, we keep only the solution in the first quadrant in this case, without loss of generality). As a result, we choose  $C_0$  as any point on the line passing through the origin and one point with the position vector  $[1, 1, 1]^T$ . For example, we choose the centroid of the cube, i.e.,  $\mathbf{c}_0 = [0.5\ell, 0.5\ell, 0.5\ell]^T$ . Moreover, we assume  $o_1 = o_2 = o_3 = o$  to keep the robot "more symmetric", in which case, the three axes  $\{\mathcal{B}_i\}_1^3$  form a planar equilateral triangle. Upon choosing  $o = 0.2\ell$ , we obtain the robot shown in Fig. 5.4, with the small sphere representing the characteristic point.
- Layout II: This case is shown in Fig. 5.5, where we require  $d_2 = d_{32} = 0$ ,  $d_{31} = \ell$ . It is found that the operation point has to lie either in the plane of  $\mathcal{A}_1$  and  $\mathcal{A}_2$  or in the plane of the origin and  $\mathcal{A}_3$ , the latter also being the plane of  $\mathcal{A}_1$  and  $\mathcal{A}_3$  in this case. Without loss

of generality, the characteristic point is chosen to lie in the plane of  $\mathcal{A}_1$  and  $\mathcal{A}_3$ ; moreover, the characteristic point is chosen as the centroid of the face of the cube in the plane of  $\mathcal{A}_1$  and  $\mathcal{A}_3$ , i.e.,  $\mathbf{c}_0 = [0.5\ell, 0, 0.5\ell]^T$ . We again set  $o_1 = o_2 = o_3 = 0.2\ell$ , which gives the isotropic design shown in Fig. 5.5. It is apparent that  $\mathcal{B}_1$  and  $\mathcal{B}_3$  must be both parallel to  $\mathcal{A}_2$  in this case, while normal to  $\mathcal{B}_2$ , which makes it impossible to have the three axes  $\{\mathcal{B}_i\}_1^3$  at equal angles pairwise. The simplest version in this category may be the one with the distances from  $\mathcal{B}_2$  to  $\mathcal{B}_1$  and to  $\mathcal{B}_3$  equal. This requires the relation  $o_3/o_1 = c_{01}/c_{03}$ .

- Layout III: This case is shown in Fig. 5.6, where we require  $d_2 = 0$ ,  $d_{31} = d_{32} = \ell$ . It is found that the operation point has to lie in the plane of  $\mathcal{A}_1$  and  $\mathcal{A}_2$  or the plane of the origin and  $\mathcal{A}_3$ . If we choose the latter, we can choose the operation point as the centroid of the cube i.e.,  $\mathbf{c}_0 = [0.5\ell, 0.5\ell, 0.5\ell]^T$ . We again set  $o_1 = o_2 = o_3 = 0.2\ell$ , which gives the isotropic design shown in Fig. 5.6. As can be seen, this layout is similar to Layout I.
- Layout IV: This case is shown in Fig. 5.7, where we require  $d_2 = d_{31} = d_{32} = \ell$ . From Fig. 5.2, we can choose the operation point on the three axes  $\mathcal{A}_i$  for i = 1, 2, 3, or their three common perpendiculars. The former is not feasible, since it yields the middle link of some limb of zero length; for the latter, an example is shown in Fig. 5.7, with  $\mathbf{c}_0 = [\ell, 0.5\ell, 0]^T$  and  $o_1 = o_2 = o_3 = 0.2\ell$ .

This category of layout is generally complex and difficult to analyze, so we will not elaborate on this category further.

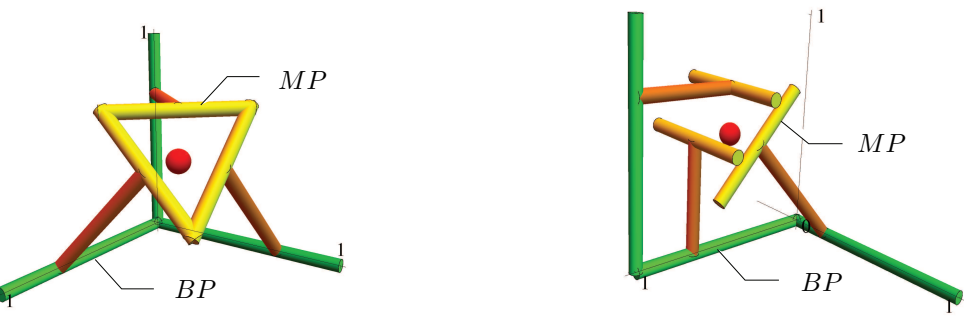
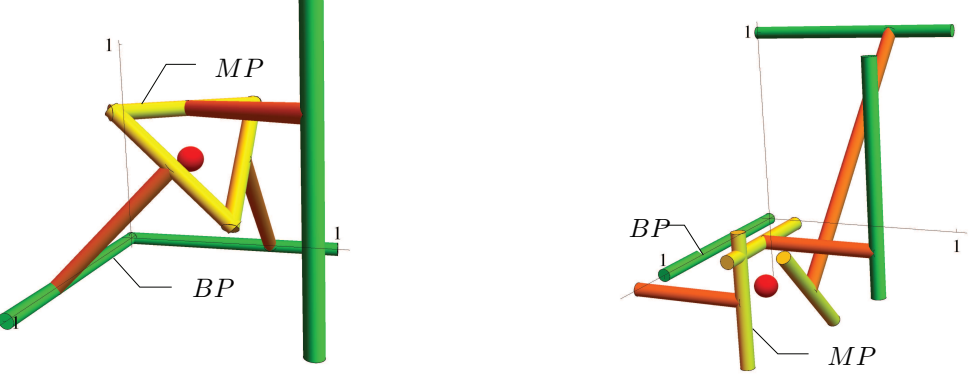


Figure 5.4: An example of an isotropic design for Layout I Figure 5.5: An example of an isotropic design for Layout II



**Figure 5.6:** An example of an isotropic design **Figure 5.7:** An example an the isotropic design for Layout III for Layout IV

#### 5.2.3 Discussion

Based on the Jacobian matrices derived here, it is found that one of the constraints for isotropy imposed in previous works [94] are not necessary, which allows us to find a rich set of isotropic architectures. Moreover, the conditions yielding the existence of a line of isotropy were revealed. We identified a class of PKMs within whose workspace a continuous set of postures of isotropy is feasible, thereby guaranteeing the accuracy and the homogeneity of the PKM motion inside a region of the workspace, rather than at a discrete set of points, as is usually the case. This feature is rare and quite advantageous; moreover, as discussed in this section, there are infinitely many choices of design variables that yield this property. Hence, there is a large margin for us to optimize the performance of the robot in terms of other aspects.

Next, we focus on this subclass of 3-CCC PKM, and conduct its forward-displacement, singularity and workspace analyses, to provide a whole picture of the robot performance. As stated previously, the general 3-CCC PKM was first analyzed by Daniali et al. as the six-

dof version of the double-triangular mechanisms [92–94]. However, the kinematic relations derived therein based on dual quaternions do not yield the simplest formulation: The forward kinematics thus yields eight equations with six unknowns, which is neither decoupled nor minimal; moreover, solving this system is computationally cumbersome, which is thus not suitable for real-time control. Some singular configurations were enumerated, but they did not provide a complete analysis of the singularity loci and their graphic representation. These issues are studied in this dissertation yielding a simpler formulation and pertinent results.

It is also noteworthy that, compared with the 3-CCC PKMs [95,96] mentioned at the beginning of Chapter 5, besides the advantages mentioned therein, the proposed 3-CCC PKM also bears simpler and better kinematics performance. For example, it will be shown that the proposed robot bears a simpler formulation of the forward-displacement problem, which admits eight solutions, as opposed to 64 for the 3-CCC PKM, besides many other interesting and advantageous features of the 3-CCC PKM in terms of singularity and workspace.

# 5.3 The Forward-displacement Analysis

It is apparent that  $\mathbf{J}_m$ —which establishes the mapping between the rates of the cylindrical motion of the three collars of the three actuated C-Drives and the six motor rates—is a constant matrix, which becomes trivial in the forward-displacement and singularity analyses. Hence, we regard  $\boldsymbol{\phi}$  as the input in these analyses for simplicity. Now we derive the forward-displacement analysis of the 3-<u>CCC PKMs</u>, which involves finding the pose coordinates of the MP for a given set of input variables  $\boldsymbol{\phi}$ .

#### 5.3.1 The Orientation Problem

Firstly, we study the orientation subproblem. It is noteworthy that we provide two different formulations for the orientation problem, one for 3- $\underline{CCC}$  PKMs with a) coplanar, and one for b) non-coplanar  $\{\mathbf{b}_i\}_1^3$  triad. It was found [91] that PKMs in case a) are quite advantageous, since they entail a continuous locus of isotropic postures within the robot workspace, guaranteeing the accuracy and homogeneity of the motion of the MP within a large region. Moreover, this class of PKMs allows a simpler formulation for the orientation problem,

compared with PKMs in case b). Hence, we mainly focus on class a), using an approach similar to that of Gosselin et al.'s for a spherical parallel manipulator with a coplanar<sup>6</sup> platform [99]. Thereafter, we briefly discuss the formulation for case b), but will not elaborate on it.

Since the three axes  $\{\mathcal{B}_i\}_1^3$  are rigidly fixed to the MP, it is obvious that the orientation of the MP is totally defined once all the directions of  $\mathbf{b}_i$  are known, for i = 1, 2, 3. When the three unit vectors  $\{\mathbf{b}_i\}_1^3$  are coplanar<sup>7</sup>, they become linearly dependent, in which case there exist three scalars  $\{\delta_i\}_1^3$ , such that

$$\delta_1 \mathbf{b}_1 + \delta_2 \mathbf{b}_2 + \delta_3 \mathbf{b}_3 = \mathbf{0} \tag{5.72}$$

with  $\{\delta_i\}_1^3$  being constant known parameters for a given MP. For example, for an equilateral MP, we have

$$\delta_1 = \delta_2 = \delta_3 = 1, \quad \mathbf{b}_1 + \mathbf{b}_2 + \mathbf{b}_3 = \mathbf{0}$$
 (5.73)

Moreover, as the direction vectors  $\mathbf{a}_i$  are known, while  $\mathbf{r}_i$ —the direction vectors of the common perpendicular of  $\mathcal{A}_i$  and  $\mathcal{B}_i$ —are uniquely determined by  $\theta_{ia}$ , we can express the direction vector  $\mathbf{b}_i$  as

$$\mathbf{b}_{i} = \cos \alpha_{i} \mathbf{a}_{i} + \sin \alpha_{i} \mathbf{r}_{i}(\theta_{ia}) \times \mathbf{a}_{i}, \quad i = 1, 2, 3$$

$$(5.74)$$

with only  $\alpha_i$  as yet to be determined. If we insert Eqs. (5.74) into Eqs. (5.72), the three components of this vector equation lead to three constraint equations with three unknowns, linear in  $\sin \alpha_i$  and  $\cos \alpha_i$ . This system of equations can be transformed into a set of polynomial equations upon introducing  $x_i = \sin \alpha_i$  and  $y_i = \cos \alpha_i$ , namely,

$$\delta_{1}x_{1}\mathbf{r}_{1} \times \mathbf{a}_{1} + \delta_{2}x_{2}\mathbf{r}_{2} \times \mathbf{a}_{2} + \delta_{3}x_{3}\mathbf{r}_{3} \times \mathbf{a}_{3} + \delta_{1}y_{1}\mathbf{a}_{1} + \delta_{2}y_{2}\mathbf{a}_{2} + \delta_{3}y_{3}\mathbf{a}_{3} = \mathbf{0}$$

$$x_{1}^{2} + y_{1}^{2} = 1$$

$$x_{2}^{2} + y_{2}^{2} = 1$$

$$x_{3}^{2} + y_{3}^{2} = 1$$

$$(5.75)$$

<sup>&</sup>lt;sup>6</sup>This means that the axes of the distal R joints of the three limbs are coplanar.

<sup>&</sup>lt;sup>7</sup>It is noteworthy that this does not mean that the three axes  $\{\mathcal{B}_i\}_1^3$  are coplanar since these axes may be offset.

bearing a Bezout number [81] of 8, i.e., it admits up to eight solutions; it will be shown, with the aid of one case study, that the number is minimal. Once  $\{\alpha_i\}_{1}^{3}$  are determined, the orientation of the MP is totally determined. The MP rotation being decoupled from its translation offers several advantages in terms of control, analysis, etc.

Next, we briefly discuss the orientation problem for PKMs of case b). The orientation problem of its forward-displacement will be shown to be equivalent to that of the spherical three-dof PKM investigated by Gosselin et al. [99–101]. Indeed, the translation of the axes  $\{A_i\}_{1}^{3}, \{B_i\}_{1}^{3}$  and  $\{\mathcal{R}_i\}_{1}^{3}$  does not affect the orientation of the MP; hence, we can always establish a spherical PKM upon translating all the foregoing nine axes to intersect at a given common point, whose forward-displacement problem bears the same solution as the 3-CCC PKM. Hence, the derivation and conclusions about the forward-displacement problem therein also apply to the orientation problem of the 3-CCC PKM. The forward-displacement problem of a general spherical PKM was formulated based on a set of Euler angles [100, 101] which yield an octic univariate polynomial. Due to the equivalence described above, this conclusion applies to the orientation problem of PKMs for case b) also. Since we do not focus on this type, we will not elaborate on it.

The above formulation displayed in Eqs. (5.72) and (5.74), and that in Eqs. (5.75), especially the latter, are probably good enough for the real-time calculation of the forward-displacement problem. In fact, this system of equations might be the simplest formulation the author has seen for the forward-displacement problem of six-dof PKMs. However, solving Eqs. (5.75) still requires an iterative algorithm, just as the case of other six-dof PKMs. Such an algorithm, though adequate in most cases when good initial guesses are provided, can converge to solutions of other branches and sometimes even diverge, especially when the robot finds itself near a singular configuration. These issues can lead to large error, high computational cost and even failure to converge. Hence, closed-form solution is quite advantageous in such situations.

As will be seen from Eqs. (5.98) in the case study, when the set  $\{\alpha_i\}_1^3$  satisfies the orientation constraint, as per Eq. (5.72), so does  $\{-\alpha_i\}_1^3$ . This can be readily explained considering that this simply changes the sign of  $\{\mathbf{b}_i\}_1^3$  in Eq. (5.74) into  $\{-\mathbf{b}_i\}_1^3$ , under which

Eq. (5.72) still holds. Hence, the eight solutions can be grouped into four pairs. Based on this finding, we manage to represent the resolvent polynomial into an equivalent polynomial of degree four, which can be solved in closed form, via Ferrari's formula [102]. In this way, all the solutions can be obtained simultaneously while the computation cost is reduced, especially when a large number of iterations is needed. Next, we discuss the procedure for obtaining the quartic resolvent polynomial. This polynomial is derived based on Eq. (5.72). We focus on the case when the set  $\{\mathbf{a}_i\}_{1}^{3}$  is orthonormal, which yields a continuous set of isotropy loci [91]. Without loss of generality, we assume

$$\mathbf{a}_1 = [1, 0, 0]^T, \ \mathbf{a}_2 = [0, 1, 0]^T, \ \mathbf{a}_3 = [0, 0, 1]^T,$$
 (5.76)

Moreover, we let  $\theta_{ip}$  be the angle between  $\mathbf{r}_i$  and the corresponding frame plane (X-O-Y, Y-O-Z, Z-O-X, respectively, for i=1,2,3), as shown in Fig. 5.8, namely,

$$\theta_{ip} = \theta_{i0} + \theta_{ia} \tag{5.77}$$

which is given in the forward-displacement problem, with  $\theta_{i0}$  representing the angle between  $\mathbf{r}_i$  and the corresponding coordinate plane at the reference pose. Then, Eqs. (5.72) take the form

$$\delta_1 \cos \alpha_1 - \delta_2 \cos \theta_{2p} \sin \alpha_2 + \delta_3 \sin \theta_{3p} \sin \alpha_3 = 0$$

$$\delta_1 \sin \theta_{1p} \sin \alpha_1 + \delta_2 \cos \alpha_2 - \delta_3 \cos \theta_{3p} \sin \alpha_3 = 0$$

$$-\delta_1 \cos \theta_{1p} \sin \alpha_1 + \delta_2 \sin \theta_{2p} \sin \alpha_2 + \delta_3 \cos \alpha_3 = 0$$

$$(5.78)$$

Next, we eliminate  $\alpha_3$  from the above equations to obtain two equations with two unknowns. We solve for  $\sin \alpha_3$  from the first two equations, which gives us one equation free of  $\alpha_3$ , namely,

$$\sin \alpha_3 = \csc \theta_{3p} (\delta_{23} \cos \theta_{2p} \sin \alpha_2 - \delta_{13} \cos \alpha_1) = \sec \theta_{3p} (\delta_{23} \cos \alpha_2 + \delta_{13} \sin \theta_{1p} \sin \alpha_1) \quad (5.79)$$

with  $\delta_{ij} \equiv \delta_i/\delta_j$ . This equation is linear in terms of  $\cos \alpha_2$  and  $\sin \alpha_2$ . Moreover, we solve for  $\cos \alpha_3$  from the third of Eqs. (5.78), and insert the values of  $\sin \alpha_3$  and  $\cos \alpha_3$  into

$$\sin^2 \alpha_3 + \cos^2 \alpha_3 = 1 \tag{5.80}$$

thereby obtaining a second equation free of  $\alpha_3$ , namely,

$$E_{s2}\sin^2\alpha_2 + E_{c2}\cos^2\alpha_2 + E_{s1}\sin\alpha_2 + E_{c1}\cos\alpha_2 + E_0 = 0$$
 (5.81)

with

$$E_{s2} = \delta_{23}^2 \sin^2 \theta_{2p} \equiv \epsilon_1, \quad E_{c2} = \delta_{23}^2 \sec^2 \theta_{3p} \equiv \epsilon_2$$

$$E_{s1} = -2\delta_{13}\delta_{23}\cos\theta_{1p}\sin\theta_{2p}\sin\alpha_1 \equiv \epsilon_3\sin\alpha_1$$

$$E_{c1} = 2\delta_{13}\delta_{23}\sin\theta_{1p}\sec^2\theta_{3p}\sin\alpha_1 \equiv \epsilon_4\sin\alpha_1$$

$$E_{0} = -\cos^2\alpha_1 + \left(\delta_{13}^2(\cos^2\theta_{1p} + \sin^2\theta_{1p}\sec^2\theta_{3p}) - 1\right)\sin^2\alpha_1 \equiv \epsilon_5\cos^2\alpha_1 + \epsilon_6\sin^2\alpha_1$$
(5.82)

where the scalars  $\{\epsilon_i\}_1^6$ —and  $\{\varphi_i\}_1^3$ ,  $\{\lambda_i\}_1^5$ ,  $\{\mu_i\}_1^6$ ,  $\{\nu_i\}_0^2$ ,  $\{\sigma_i\}_0^1$ , to be defined presently—are intermediate results introduced for computational purposes. Next, we solve for  $\sin \alpha_2$  from Eq. (5.79), namely,

$$\sin \alpha_2 = F_1 \cos \alpha_2 + F_0 \tag{5.83}$$

with

$$F_{1} = \sec \theta_{2p} \tan \theta_{3p} \equiv \varphi_{1}$$

$$F_{0} = \sec \theta_{2p} \delta_{12} (\cos \alpha_{1} + \sin \theta_{1p} \tan \theta_{3p} \sin \alpha_{1}) \equiv \varphi_{2} \cos \alpha_{1} + \varphi_{3} \sin \alpha_{1}$$

$$(5.84)$$

Moreover, we insert Eq. (5.83) into the Eq. (5.81) and into

$$\sin^2 \alpha_2 + \cos^2 \alpha_2 = 1 \tag{5.85}$$

thereby obtaining two equations in  $\alpha_2$ :

$$G_2 \cos^2 \alpha_2 + G_1 \cos \alpha_2 + G_0 = 0$$

$$H_2 \cos^2 \alpha_2 + H_1 \cos \alpha_2 + H_0 = 0$$
(5.86)

where

$$G_2 = E_{c2} - E_{s2}, \quad G_1 = E_{s1}F_1 + E_{c1}, \quad G_0 = E_{s1}F_0 + E_0 + E_{s2}$$

$$H_2 = F_1^2 + 1, \quad H_1 = 2F_1F_0, \quad H_0 = F_0^2 - 1$$
(5.87)

The above procedure is similar to that used by Gosselin et al. for a special three-dof spherical PKM [99]; next, dialytic elimination [64] was used by the same authors to obtain an octic

univariate polynomial from Eq. (5.86). Here we use a different approach which is simpler to derive and simplify, and end up with a quartic univariate polynomial: We multiply the two equations in Eq. (5.86) by  $H_2$  and  $G_2$ , respectively, and find their difference as

$$\cos \alpha_2 = \frac{G_2 H_0 - G_0 H_2}{G_1 H_2 - G_2 H_1} \equiv \frac{N}{D}$$
 (5.88)

whose RHS only involves  $\alpha_1$ . Once we insert Eq. (5.88) into the second of Eqs. (5.86), a univariate equation in  $\alpha_1$  is obtained, namely,

$$H_2N^2 + H_1ND + H_0D^2 = 0 (5.89)$$

which is found to be a homogeneous quartic equation in  $\sin \alpha_1$  and  $\cos \alpha_1$ . If we divide both sides by  $\sin^4 \alpha_1$ , the LHS will become a quartic equation in  $\rho \equiv \cot \alpha_1$ , which, after simplification, becomes

$$\zeta_4 \rho^4 + \zeta_3 \rho^3 + \zeta_2 \rho^2 + \zeta_1 \rho + \zeta_0 = 0 \tag{5.90}$$

whose coefficients are derived in the Appendix. This equation can be solved in closed form, and hence, all the solutions can be obtained precisely and simultaneously without resorting to an iterative solution, which might converge to other branches of solutions, and even diverge. This feature, rare for six-dof PKMs, is quite advantageous in simulation and control, especially when the the robot operates near a singular configuration, where an iterative approach is likely to fail.

#### 5.3.2 The Positioning Problem

Next, we study the translational displacement of the MP. Once  $\{\alpha_i\}_1^3$  are known from Eqs. (5.72) or (5.75) or Eq. (5.90), the directions  $\{\mathbf{b}_i\}_1^3$  are determined, from which the orientation  $\mathbf{Q}$  of the MP can be readily derived. Below we solve the translation subproblem.

Three translation equations can be obtained from the condition of the intersection of  $\mathcal{B}_i$  and  $\mathcal{R}_i$ , for i = 1, 2, 3. It is known that two lines intersect if and only if the reciprocal product of their Plücker coordinates vanishes [103]. The calculation of the Plücker coordinates of  $\mathcal{R}_i$  and  $\mathcal{B}_i$  calls for the unit vectors associated with their axes  $(\mathbf{r}_i, \mathbf{b}_i)$  and the position vectors of

two arbitrary points on them. We choose  $L_i$  and  $U'_i$  as these two points, where the position vector of  $L_i$  can be readily calculated as  $\mathbf{l}_i = \mathbf{l}_{0i} + r_{ia}\mathbf{a}_i$ —with  $\mathbf{l}_{0i}$  representing the position vector of  $L_i$  at the reference posture, while  $U'_i$  represents the current location of the point on the MP (more precisely, on  $\mathcal{B}_i$ ) that coincides with  $\mathcal{R}_i$  at the reference pose. If we denote the vector stemming from the operation point C to  $U'_i$  as  $\mathbf{q}_i$ , then the position vector  $\mathbf{u}'_i$  of  $U'_i$  can be calculated as

$$\mathbf{u}_i' = \mathbf{c} + \mathbf{q}_i = \mathbf{c} + \mathbf{Q}\mathbf{q}_{i0} \tag{5.91}$$

which is linear in  $\mathbf{c}$ , while  $\mathbf{q}_{i0}$  can be readily calculated under the reference pose. Now the Plücker coordinates of  $\mathcal{R}_i$  and  $\mathcal{B}_i$  can be readily obtained as

$$[\mathbf{r}_i^T, \mathbf{n}_{ri}^T]^T = [\mathbf{r}_i^T, \mathbf{l}_i \times \mathbf{r}_i^T]^T, \quad [\mathbf{b}_i^T, \mathbf{n}_{bi}^T]^T = [\mathbf{b}_i^T, \mathbf{u}_i' \times \mathbf{b}_i^T]^T$$
(5.92)

where the only unknown is  $\mathbf{c}$ , their reciprocal product yielding

$$(\mathbf{b}_i \times \mathbf{r}_i) \cdot (\mathbf{u}_i' - \mathbf{l}_i) \equiv \mathbf{s}_i^T (\mathbf{c} + \mathbf{Q} \mathbf{q}_{i0} - \mathbf{l}_i) = 0$$
(5.93)

or, equivalently,

$$\mathbf{s}_{i}^{T}\mathbf{c} = \mathbf{s}_{i}^{T}(\mathbf{l}_{0i} + r_{ia}\mathbf{a}_{i} - \mathbf{Q}\mathbf{q}_{i0}) \equiv w_{i}, \ i = 1, 2, 3$$

$$(5.94)$$

In this way, the translation problem is formulated upon casting the three foregoing equations in the form

$$\begin{bmatrix} \mathbf{s}_1^T \\ \mathbf{s}_2^T \\ \mathbf{s}_3^T \end{bmatrix} \mathbf{c} = \mathbf{w} \tag{5.95}$$

Finally, the position vector of the intersection of  $\mathcal{R}_i$  and  $\mathcal{B}_i$ , i.e.,  $\mathbf{u}_i$ , may be needed, e.g., in simulation, which can be readily calculated as [104]

$$\mathbf{u}_i = \frac{\mathbf{n}_{ri} \times \mathbf{n}_{bi}}{\mathbf{b}_i \cdot \mathbf{n}_{ri}} \tag{5.96}$$

after which the lengths of the intermediate limbs  $r_i$  can be readily found as  $r_i = \|\overline{L_i U_i}\|_2$ .

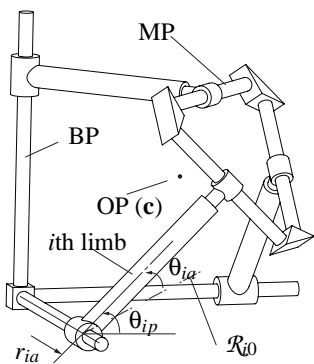


Figure 5.8: The architecture of a 3CCC PKM for case study

## 5.3.3 Case Study

Next, a case study is provided for verification. We will choose a set of design parameters that yield a continuous locus of isotropic postures. The conditions for isotropy are reproduced below for quick reference:

- 1. The set  $\{\mathbf{a}_i\}_1^3$  is orthogonal
- 2.  $\mathbf{a}_i \perp \mathbf{b}_i$ , for i = 1, 2, 3
- 3.  $\mathbf{s}_i \parallel \mathbf{p}_i$  or, equivalently,  $\mathbf{a}_i \parallel \mathbf{p}_i$
- 4. The three direction vectors  $\{\mathbf{b}_i\}_1^3$  are coplanar

Based on these conditions, we choose a *symmetric* layout as shown in Fig. 5.8 for illustration: the length of the sides, of a cube that encloses the BP is denoted  $\ell$ , the reference position of the operation point<sup>8</sup> is specified as  $\mathbf{c}_0 = 1/2[\ell, \ell, \ell]^T$ . Moreover, the distance between  $C_0$  and  $\mathcal{B}_i$  is prescribed  $0.2\ell$ , yielding an equilateral shape of the MP, with a length  $0.4\sqrt{2}\ell$ .

A set of input design parameters is tested:

$$\boldsymbol{\phi} = [\theta_{1a}, \theta_{2a}, \theta_{3a}, r_{1a}, r_{2a}, r_{3a}]^T = [0.1, 0.05, 0.15, 0.1, 0.2, 0.15]$$
(5.97)

It is noteworthy that  $\theta_{ia}$  and  $r_{ia}$  are defined to be 0 at the reference pose. The system of Eqs. (5.75) is adopted in this case study, since a set of polynomials is easier to handle than

<sup>&</sup>lt;sup>8</sup>It is noteworthy that even though the operation point is not located on the plane defined by the three coplanar axes  $\{\mathcal{B}_i\}_{1}^{3}$ , it is fixed to the MP.

those involving trigonometric functions. It is found that the orientation problem admits eight real solutions, arrayed in  $\text{sol}_{roi} = [x_1, y_1, x_2, y_2, x_3, y_3]_i^T$ , namely,

$$sol_{ro1} = [0.549981, 0.835177, 0.0929369, -0.995672, -0.96023, 0.279209]^{T}$$

$$sol_{ro2} = [-0.549981, -0.835177, -0.0929369, 0.995672, 0.96023, -0.279209]^{T}$$

$$sol_{ro3} = [0.310112, -0.9507, -0.99944, -0.0334597, 0.348137, 0.937444]^{T}$$

$$sol_{ro4} = [-0.310112, 0.9507, 0.99944, 0.0334597, -0.348137, -0.937444]^{T}$$

$$sol_{ro5} = [-0.99013, 0.14015, -0.984355, 0.176199, -0.994658, 0.103228]^{T}$$

$$sol_{ro6} = [0.99013, -0.14015, 0.984355, -0.176199, 0.994658, -0.103228]^{T}$$

$$sol_{ro7} = [0.985306, -0.170797, -0.482835, -0.875711, -0.190261, 0.981734]^{T}$$

$$sol_{ro8} = [-0.985306, 0.170797, 0.482835, 0.875711, 0.190261, -0.981734]^{T}$$

The formulation based on Eq. (5.90) is also conducted, which leads to

$$-58.7167\rho^4 - 109.331\rho^3 + 243.303\rho^2 + 83.8462\rho + 6.70696 = 0$$
 (5.99)

with the solutions  $\rho = 1.51856$ , -0.141547, -0.173344, -3.06567, from which eight values of  $\alpha_1$  can be obtained, which do correspond to the solutions in Eq. (5.98).

The corresponding position vector  $\mathbf{c}$  of the operation point, denoted  $\text{sol}_{tri} = [c_1, c_2, c_3]^T$ , are found as

$$sol_{tr1} = [0.507908, 0.119128, 0.825462]^{T}, \quad sol_{tr2} = [1.20758, 1.17601, 0.929398]^{T}$$

$$sol_{tr3} = [0.363044, 0.977219, 0.641]^{T}, \quad sol_{tr4} = [1.26536, 1.06529, 1.60808]^{T}$$

$$sol_{tr5} = [0.855996, 0.945059, 0.894451]^{T}, \quad sol_{tr6} = [0.581321, 0.681459, 0.642581]^{T}$$

$$sol_{tr7} = [0.905586, 1.49944, 1.34846]^{T}, \quad sol_{tr8} = [0.811763, 0.529586, 0.151661]^{T}$$

The corresponding configurations are plotted in Figs. 5.9, where the intermediate and distal links of the different limbs are displayed in different colours. It is readily shown that these configurations do share the same set of input design parameters; however, some of these layouts exceed the joint limits, and hence, are not feasible.

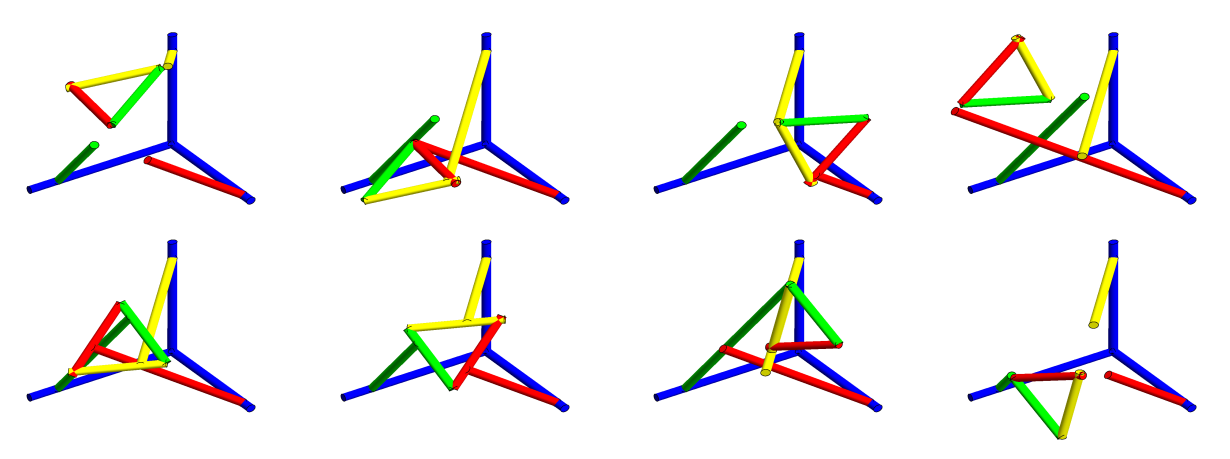


**Figure 5.9:** The layouts corresponding to those solutions in the case study of the forward kinematics.

# 5.4 Singularity Analysis

Since translation and rotation are usually coupled in a six-dof PKM, the corresponding singularity set is usually a five-dimensional surface in the six-dimensional space, whose evaluation or representation is quite challenging. However, it will be shown that the different types of singularity of the 3-CCC PKM are all dependent on the MP orientation only, which is quite advantageous, because the corresponding singularity locus becomes a two-dimensional surface within the three-dimensional orientation workspace, thereby simplifying dramatically its representation and evaluation. Hence, we can represent the singularity locus in the orientation workspace. Various orientation representation schemes have been proposed, such as Euler angles, tilt and torsion angles, quaternions, roll-pitch-yaw angles, axis and angle of rotation, etc. [105]. Among these representations, the Euler-Rodrigues representation [64] is found to be quite advantageous in the representation of orientation workspace, since this formulation provides a one-to-one mapping between the Euler-Rodrigues parameters (ERP) and the orientation, which is singularity-free; moreover, the graph plotted in terms of ERP entails a clearer geometric meaning, compared to the other representation schemes. Hence, this representation is adopted in this dissertation.

The Euler-Rodrigues parameters are defined as [64]

$$\mathbf{r} = \sin(\phi/2)\mathbf{e}, \quad r_0 = \cos(\phi/2), \quad \text{with } ||\mathbf{r}||^2 + r_0^2 = 1$$
 (5.101)

where  $\phi$  and  $\mathbf{e}$  represent the angle and the axis of rotation,  $\phi \in [0, \pi]$ ; the corresponding

rotation matrix is then expressed as

$$\mathbf{Q} = (r_0^2 - \mathbf{r} \cdot \mathbf{r})\mathbf{1} + 2\mathbf{r}\mathbf{r}^T + 2r_0\mathbf{R}$$
(5.102)

where **R** is the *cross-product matrix* [64] of **r**. For the purpose of graphic representation, we can substitute  $r_0$  with  $\sqrt{1-||\mathbf{r}||^2}$ , matrix **Q** then becoming a three-parameter function in terms of **r** and the singularity surface is composed of all the points whose position vector **r** yields singularity.

#### 5.4.1 Limb Singularity

In order to gain more insight into the limb Jacobian, we recall the relations derived in Subsection 5.1.1, and reorder the limb joint rates and the limb-twist relation in the form

$$\mathbf{J}_i \dot{\boldsymbol{\theta}}_i = \mathbf{t} \tag{5.103}$$

where

$$\mathbf{J}_{i} = \begin{bmatrix} \mathbf{a}_{i} & \mathbf{r}_{i} & \mathbf{b}_{i} & \mathbf{0} & \mathbf{0} & \mathbf{0} \\ \mathbf{a}_{i} \times \mathbf{p}_{ai} & \mathbf{r}_{i} \times \mathbf{p}_{ri} & \mathbf{b}_{i} \times \mathbf{p}_{bi} & \mathbf{a}_{i} & \mathbf{r}_{i} & \mathbf{b}_{i} \end{bmatrix}, \quad \boldsymbol{\theta}_{i} = \begin{bmatrix} \theta_{ia}, \theta_{ir}, \theta_{ib}, r_{ia}, r_{ir}, r_{ib} \end{bmatrix}^{T}$$
(5.104)

It is apparent that the limb Jacobian is block lower-triangular with two identical diagonal blocks; hence, its limb singularity is encountered when and only when its diagonal block becomes singular, which happens when  $\mathbf{a}_i$ ,  $\mathbf{b}_i$  and  $\mathbf{r}_i$  are coplanar, for any i = 1, 2, 3. There are three sets of limb singularity, one for each limb.

When the *i*th limb encounters a singularity, we have  $\mathbf{a}_i \parallel \mathbf{b}_i$ , i.e.,

$$\mathbf{a}_i \cdot \mathbf{b}_i = \mathbf{a}_i \cdot (\mathbf{Q} \mathbf{b}_{i0}) = \pm 1 \tag{5.105}$$

with  $\mathbf{Q}$  given in Eq. (5.102), which expands to

$$\mathbf{a}_{i} \cdot \mathbf{b}_{i} = (r_{0}^{2} - \mathbf{r} \cdot \mathbf{r}) \mathbf{a}_{i} \cdot \mathbf{b}_{i0} + 2(\mathbf{r} \cdot \mathbf{a}_{i})(\mathbf{r} \cdot \mathbf{b}_{i0}) + 2r_{0}(\mathbf{r} \times \mathbf{b}_{i0}) \cdot \mathbf{a}_{i}$$

$$= 2(\mathbf{r} \cdot \mathbf{a}_{i})(\mathbf{r} \cdot \mathbf{b}_{i0}) - 2r_{0}(\mathbf{a}_{i} \times \mathbf{b}_{i0}) \cdot \mathbf{r} = 2(\mathbf{r} \cdot \mathbf{a}_{i})(\mathbf{r} \cdot \mathbf{b}_{i0}) - 2r_{0}\mathbf{r}_{i0} \cdot \mathbf{r} = \pm 1$$

$$(5.106)$$

where  $\mathbf{b}_{i0}$  represents the direction of  $\mathbf{b}_i$  at the reference posture, and  $\mathbf{r}_{i0}$  is the unit vector parallel to the common perpendicular of  $\mathbf{a}_i$  and  $\mathbf{b}_{i0}$ . This theoretically represents two surfaces

within the orientation space. However, it will be shown that the limb singularity corresponding to the *i*th limb is, in fact, not a surface, but degenerates into two elliptic curves when represented in terms of the ERP, for i = 1, 2, 3. It is noteworthy that  $\mathbf{a}_i$ ,  $\mathbf{b}_{i0}$ ,  $\mathbf{r}_{i0}$  form a right-handed orthonormal basis, defining frame  $\mathcal{F}_{Li}$ , for i = 1, 2, 3; if we express vector  $\mathbf{r}$  in  $\mathcal{F}_{Li}$ , we obtain

$$\mathbf{r} = r_{ai}\mathbf{a}_i + r_{bi}\mathbf{b}_{i0} + r_{ri}\mathbf{r}_{i0} \tag{5.107}$$

where  $r_{ai}$ ,  $r_{bi}$ ,  $r_{ri}$  represent the components of  $\mathbf{r}$  about these three axes, respectively; then, Eq. (5.106) simplifies to

$$2r_{ai}r_{bi} - 2r_0r_{ri} = \pm 1 \tag{5.108}$$

from which  $r_0$  can be solved for as

$$r_0 = (2r_{ai}r_{bi} \mp 1)/(2r_{ri}) \tag{5.109}$$

Moreover,

$$\|\mathbf{r}\|^2 + r_0^2 = r_{ai}^2 + r_{bi}^2 + r_{ri}^2 + \left[ (2r_{ai}r_{bi} \mp 1)/(2r_{ri}) \right]^2 = 1$$
 (5.110)

which is quadratic in  $r_{ai}$ . After simplification,

$$(r_{ri}^2 + r_{bi}^2)r_{ai}^2 \mp r_{ai}r_{bi} + \frac{1}{4} - r_{ri}^2(1 - r_{ri}^2 - r_{bi}^2) = 0$$
 (5.111)

whose discriminant is calculated as

$$\Delta_{i} = r_{bi}^{2} - 4(r_{ri}^{2} + r_{bi}^{2})\left[\frac{1}{4} - r_{ri}^{2}(1 - r_{ri}^{2} - r_{bi}^{2})\right] = -r_{ri}^{2} + 4r_{ri}^{2}(r_{ri}^{2} + r_{bi}^{2})(1 - r_{ri}^{2} - r_{bi}^{2})$$

$$= -r_{ri}^{2}\left[2(r_{ri}^{2} + r_{bi}^{2}) - 1\right]^{2} \le 0$$
(5.112)

indicating that the quadratic equation has real solutions if and only if  $\Delta_i$  vanishes, in which case the equation has only one real solution for each of the two equations  $\mathbf{a}_i \cdot \mathbf{b}_i = \pm 1$ , namely,

$$r_{ai} = \frac{\pm r_{bi}}{2(r_{ri}^2 + r_{bi}^2)} \tag{5.113}$$

the  $\pm$  sign appears since  $\mathbf{a}_i \cdot \mathbf{b}_i = \pm 1$ , which has two possible values. Moreover, the above solution is valid only when  $\Delta_i = 0$ , namely,

$$r_{ri}^2 + r_{bi}^2 = \frac{1}{2} \quad \text{or} \quad r_{ri} = 0$$
 (5.114)

If  $r_{ri}^2 + r_{bi}^2 = 1/2$ , we have

$$r_{ai} = \pm r_{bi}, \ r_{ri}^2 + r_{bi}^2 = 1/2, \ r_{ai}^2 + r_{ri}^2 + r_{bi}^2 \le 1$$
 (5.115)

When viewed in frame  $\mathcal{F}_{Li}$ , the second equation is a cylinder whose axis is  $\mathcal{A}_i$ , while the first equation characterizes two planes passing through the origin, their intersection being two ellipses. The two principal semi-axes of the ellipses are found to be  $\sqrt{2}/2\mathbf{r}_{i0} = [0, 0, \sqrt{2}/2]^T$  and  $\mathbf{v}_i = [1/\sqrt{2}, \pm 1/\sqrt{2}, 0]^T$  in frame  $\mathcal{F}_{Li}$ ; moreover, it is simple to verify that an arbitrary point on the ellipses is given by the position vector

$$\chi_i = \mathbf{v}_i \cos \eta_i + \sqrt{2}/2\mathbf{r}_{i0} \sin \eta_i \tag{5.116}$$

where  $\eta_i$  is an arbitrary scalar. It is apparent that the two ellipses lie within in the unit sphere which satisfies the norm constraint naturally.

When  $r_{ri} = 0$ , from Eq. (5.113), we have

$$r_{ai} = \pm \frac{1}{2r_{bi}} \tag{5.117}$$

which has only four solutions that do not violate the norm constraint, namely,  $[r_{ai}, r_{bi}] = [\pm 1/\sqrt{2}, \pm 1/\sqrt{2}]$ . It is a simple matter to verify that these points satisfy Eqs. (5.115) as well. As a result, the singularity loci for each limb singularity yields two ellipses, characterized by Eq. (5.116).

So far we have found an expression for the singularity curve of the *i*th limb in  $\mathcal{F}_{Li}$ ; we now need to express it in the global orientation workspace frame. We assume the three axes of the global orientation workspace frame to be parallel to those of the BP frame. Since  $\mathcal{F}_{Li}$  is fixed to the BP frame (i.e., the global orientation workspace frame), it is simple to express the singularity curves in the BP frame: Their expressions are again provided by Eq. (5.116),

the only difference is that we need to express the direction vectors  $\mathbf{v}_i$  and  $\mathbf{r}_{i0}$  in the BP frame, which is straightforward. Finally, the singularity conditions of the three limbs yield six ellipses.

#### 5.4.2 The Singularity of the Forward Jacobian Matrix

Since **K**, the forward Jacobian, is a block lower-triangular matrix, it becomes singular if and only if one of its diagonal blocks is singular, which happens iff the triad  $\{\mathbf{s}_i\}_1^3$  becomes coplanar. This condition is characterized by

$$(\mathbf{s}_1 \times \mathbf{s}_2) \cdot \mathbf{s}_3 = 0 \tag{5.118}$$

where

$$\mathbf{s}_i = \mathbf{b}_i \times \mathbf{r}_i \parallel \mathbf{b}_i \times (\mathbf{a}_i \times \mathbf{b}_i) = (\mathbf{b}_i \cdot \mathbf{b}_i) \mathbf{a}_i - (\mathbf{b}_i \cdot \mathbf{a}_i) \mathbf{b}_i = \mathbf{a}_i - (\mathbf{a}_i \cdot \mathbf{b}_i) \mathbf{b}_i = \mathbf{a}_i - \mathbf{b}_i \cos \alpha_i$$
 (5.119)

Then, the singularity condition can be obtained upon plugging Eq. (5.119) into Eqs. (5.118). Moreover, if we consider only the case of PKMs with a continuous set of isotropy, then,  $\{\mathbf{a}_i\}_{1}^{3}$  forms an orthonormal basis and  $\{\mathbf{b}_i\}_{1}^{3}$  becomes coplanar. The singularity condition can be further derived as

$$[(\mathbf{a}_{1} - \cos \alpha_{1} \mathbf{b}_{1}) \times (\mathbf{a}_{2} - \cos \alpha_{2} \mathbf{b}_{2})] \cdot (\mathbf{a}_{3} - \cos \alpha_{3} \mathbf{b}_{3}) = 1 - \cos \alpha_{1}^{2} - \cos \alpha_{2}^{2} - \cos \alpha_{3}^{2} + b_{12} \cos \alpha_{1} \cos \alpha_{2} \mathbf{n} \cdot \mathbf{a}_{3} + b_{31} \cos \alpha_{1} \cos \alpha_{3} \mathbf{n} \cdot \mathbf{a}_{2} + b_{23} \cos \alpha_{2} \cos \alpha_{3} \mathbf{n} \cdot \mathbf{a}_{1}$$

$$(5.120)$$

where **n** represents the unit vector normal to  $\{\mathbf{b}_i\}_{1}^{3}$ ,  $\cos \alpha_i$  is calculated as  $\mathbf{a}_i \cdot \mathbf{b}_i$ , and coefficients  $b_{ij}$  are defined below

$$\mathbf{b}_i \times \mathbf{b}_j = b_{ij}\mathbf{n}, \quad i \neq j \tag{5.121}$$

which is constant for a given MP. Apparently, the singularity of  $\mathbf{K}$  is also depending only on the MP orientation.

## 5.4.3 The Singularity Analysis of the Inverse Jacobian

Its is apparent that the inverse Jacobian matrix **D** becomes singular when  $\mathbf{s}_i \cdot \mathbf{a}_i = (\mathbf{b}_i \times \mathbf{r}_i) \cdot \mathbf{a}_i = 0$ , for any i = 1, 2, 3, i.e., when  $\mathbf{a}_i$ ,  $\mathbf{r}_i$  and  $\mathbf{b}_i$  become coplanar, for any

i = 1, 2, 3. This is the same as the singularity condition of the limb singularity, so there is no need to investigate it again.

#### 5.4.4 Case Study

We use the same set of design parameters for the forward-displacement problem. Moreover, we represent the orientation in terms of its ERP parameters. The corresponding limb-singularity is shown in Figs. 5.10(a), and a combination with that of **K** is shown in Fig. 5.10(b).

From these figures, it is apparent that the singularity occurs only when the MP is rotated for large angles: it is found that the minimum distance from the origin to an arbitrary point on the singularity surface is around 0.664, which means that the MP can rotate about any direction for at least an angle of  $-83.2^{\circ}$  to  $83.2^{\circ}$  before encountering a singularity; when rotated about the majority of directions, the robot will never encounter a singularity. Moreover, since the singularity of the 3-CCC robot is only dependent on the orientation of the MP, the above conclusion is valid regardless of the location of the MP; hence, the proposed robot is unlikely to encounter a singularity without exceeding the joint limits or encountering link interference. As a result, singularity detection is not needed in real-time control in most cases, which greatly simplifies the control algorithm.

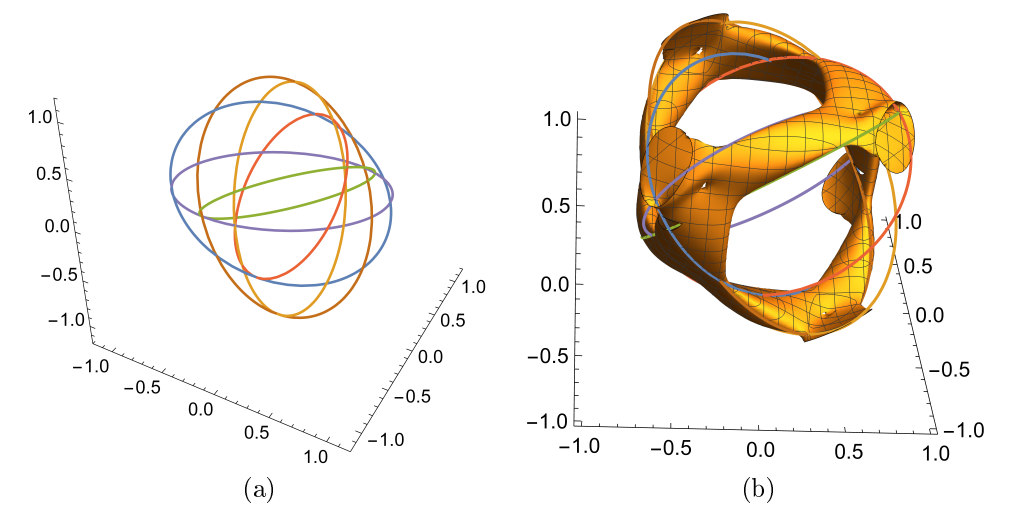


Figure 5.10: Singularity of the 3- $\underline{C}CC$  PKM (a) the curve for limb singularity (b) the limb singularity and that of K

# 5.5 Workspace Analysis

#### 5.5.1 The Geometrical Method for Workspace Quantification

In this section the fixed-orientation position workspace of the proposed robot is analyzed. We neglect the interference and only consider the limits of the active and passive joints. We propose the use of a geometrical method to calculate the fixed-orientation workspace, similar to the one used for the SDelta Robot [75], which allows us to obtain the workspace efficiently. The method follows:

Firstly, we derive the feasible workspace region of the MP upon regarding the latter as the end-effector of a serial robot, formed by the joints and links of the *i*th limb (i.e., we disconnect the MP from the two other limbs), denoted as  $W_i$ ; then, the workspace of the MP can be obtained as the intersection of  $\{W_i\}_{1}^{3}$ .

Next, we describe the process of obtaining the workspace region  $W_i$ . Let us denote the intersection of  $\mathcal{B}_i$  and  $\mathcal{R}_i$  as  $U_{i0}$  at the reference pose; furthermore, the point on the MP that coincides with  $U_{i0}$  at the reference posture is denoted as  $M_i$ , its position vector as  $\mathbf{m}_i^9$ ; it is then apparent that the shape of the translational workspace region of  $M_i$  is the same as

<sup>&</sup>lt;sup>9</sup>It is noteworthy that  $M_i$  does not necessarily coincide with  $U_i$  when the robot is not at the reference posture, since  $U_i$  is not a fixed point on the MP, due to the translational degree of freedom of the distal cylindrical joints.

that of the operation point C, while the region of the latter can be obtained simply through a pure translation of the former by the constant vector  $\overrightarrow{M_iC}$ . Furthermore, it can be readily verified that once the orientation of the MP is fixed, the directions of all the links in the three limbs are fixed. As a result, only the three translational degrees of freedom remain in each limb, and hence, the workspace region of point  $M_i$  is simply a parallelepiped, whose edges are parallel to  $\mathcal{A}_i$ ,  $\mathcal{R}_i$  and  $\mathcal{B}_i$ , respectively, the length of the edges equal to the stroke of the corresponding three C joints in the *i*th limb.

#### 5.5.2 Case Study

Next, the fixed orientation workspace is analyzed for the robot with the same set of design parameters as those of the forward-displacement problem. We assume that all the three C joints in each limb find themselves at the middle of their strokes at the reference posture, and the strokes of the first two C joints in each limb are specified as

$$d_{ia_{min}} = 0.5\ell, d_{ia_{max}} = 0.9\ell, r_{min} = 0.5\ell, r_{max} = 0.93\ell$$
 (5.122)

where  $d_{ia_{min}}$  and  $d_{ia_{max}}$  represent the minimum and maximum distances from  $L_i$  to the corresponding frame plane (Y-O-Z, Z-O-X, X-O-Y), for i=1,2,3, respectively,  $r_{min}$  and  $r_{max}$  represent the minimum and maximum length of the intermediate limbs, while the stroke of the distal C joint is prescribed to be roughly 0.8 times the length of the edge of the MP, namely, 0.45 $\ell$ . This layout, although slightly increasing the footprint, as shown in Fig. 5.11, avoids interference near the origin among the C-Drives. The workspace under several different orientations is plotted in Figs. 5.11, yielding volume values of  $0.049\ell^3$ ,  $0.024\ell^3$ ,  $0.024\ell^3$  and  $0.010\ell^3$ , respectively. The workspace shapes for Figs. 5.11(b) and 5.11(c) are the same, except that their orientations are different, which should be expected, due to symmetry. The workspace volume is generally large; for example, if we regard the above volume values with those of cubes, the length of the edge will be  $0.366\ell$ ,  $0.288\ell$ ,  $0.288\ell$ ,  $0.218\ell$ . It is noteworthy that the design parameters used above are arbitrarily chosen; better results can be achieved if we conduct an optimization of the workspace volume.

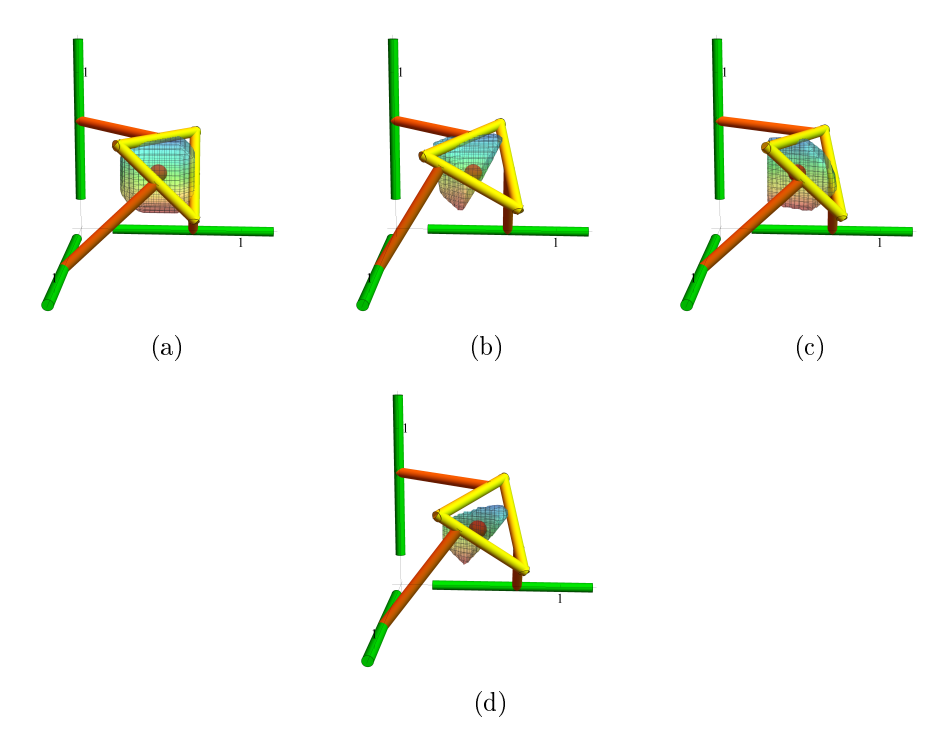


**Figure 5.11:** The workspace of the 3-<u>C</u>CC PKM (a) under the reference orientation (b) with the orientation  $\mathbf{e} = [1,0,0]^T$  and  $\phi = 15^\circ$  (c)  $\mathbf{e} = [0,0,1]^T$  and  $\phi = 15^\circ$  (d)  $\mathbf{e} = [1/\sqrt{3},1/\sqrt{3},1/\sqrt{3}]^T$  and  $\phi = 15^\circ$ 

# 5.6 Forward-Displacement, Singularity and Workspace Analyses—A Discussion

According to the forward-displacement, singularity and workspace analyses of the 3-<u>C</u>CC PKM, it is found that this class of PKM bears various interesting features: The forward-displacement analysis reveals that the rotation and translation degrees of freedom of the MP are decoupled not only at the velocity level but also at the displacement level, which significantly simplifies its analysis and control. The subproblems of rotation and translation are studied separately, both yielding a simple formulation that lead to minimal polynomials. A quartic resolvent polynomial is derived, which can be solved in closed form, and hence, all the solutions can be obtained precisely and simultaneously without resorting to an iterative method, which might converge to other branches of solutions, and even diverge. This feature is very rare for six-dof PKMs, probably the first time that is found in a six-dof PKM to the best of the author's knowledge, which is quite advantageous in control, especially when the robot operates near a singular configuration, where an iterative approach is likely to fail.

Singularity is shown to be dependent only on the orientation of the MP; it is possible to reduce the dimension of the singularity surface from five (for a six-dof PKM) to two, thereby greatly simplifying its singularity analysis and detection; moreover, the singularity loci are represented and visualized in terms of the Euler-Rodrigues parameters in the orientation workspace, which shows that the proposed robot will not encounter a singularity until it is rotated through a minimum of  $\pm 83.2^{\circ}$  about any axes, for the given parameters, which hardly happens without encountering link interference or joint limits. The singularity problem is thus not severe for the robot under study, which is quite advantageous. Finally, workspace analysis indicates that the robot has a reasonably large workspace volume with a more regular shape when compared with that of the Stewart-Gough Platform. These features indicate that the robot has great potential in highly demanding applications, such as those requiring high speed, high frequency or high amplitude.

We have completed the last topic of this dissertation, namely, the design and analyses of the 3-CCC PKM class.

# CLOSING REMARKS AND RECOMMENDATIONS FOR FUTURE RESEARCH

#### 6.1 Conclusions

PKMs with all the motors mounted on the base are quite advantageous, greatly reducing the inertia load of the system, capable of providing large accelerations, yielding better load-carrying capacity and a better dynamic response than the state of the art. These features make them quite suitable for shaking operations, which can be used, e.g., for inertia-parameter identification. With the growing demand for high-speed and high-precision operations, the accurate information of the inertia properties of a rigid body is becoming more and more important, which can be used in many applications such as model-based control. Moreover, small-amplitude high-frequency shaking operations about all six directions of the specimen motion are quite advantageous due to their capacity of providing sufficient excitation and generating data over a broad frequency range, which are essential for increasing the accuracy of the identification. In this vein, two classes of three-limb six-dof PKMs are proposed, bearing some common features, e.g., they both have a three-limb architecture, yielding less interference and larger workspace; all their motors are on the base, thus quite suitable for the shaking operations.

This dissertation covers three topics: Firstly, the kinematics, singularity and workspace analyses of the 3-CPS PKM, dubbed the SDelta robot, is investigated. SDelta features a symmetric structure; its forward-displacement analysis leading to a system of three quadratic equations in three unknowns, which admits up to eight solutions, or half the number of those admitted by the SGP. The kinematic analysis, undertaken with a geometrical method based on screw theory, leads to two Jacobian matrices, whose singularity conditions are investigated.

Instead of using the determinant of a  $6 \times 6$  matrix, we derive one simple expression that characterizes the singularity condition. This approach is also applicable to a large number of parallel robots whose six actuated-wrench axes intersect pairwise, such as the SGP and three-limb parallel robots whose limbs include, each, a passive spherical joint. Next, the workspace is analyzed via a geometric method. Furthermore, the six actuated wrenches bear a special form, i.e., they intersect pairwise. Based on this feature, we find the inverse of the robot forward Jacobian matrix symbolically, which is quite useful in singularity analysis, design for isotropy and optimal control. Finally, we formulate an optimization problem of the robot, based on its condition number, for maximum dexterity. Drawing from the optimization results, we offer some guidelines on choosing the optimum design parameters. It is shown that the SDelta can achieve a local minimum condition number close to unity. The above results indicate that the given robot has the potential to offer both large workspace and good dexterity with a proper choice of design variables.

The second topic is the design for isotropy of a large class of six-dof parallel-kinematics machines whose six actuated-wrench axes intersect pairwise; this feature covers a large number of PKMs. It is found that the inverse derived for the SDelta applies to this large class of PKMs, which has a significant theoretical value, quite useful in singularity analysis, design for isotropy and optimization. We have included a chapter to elaborate on its application in the optimum design of this large class of PKMs. Based on this expression, we analyzed their isotropy condition, where the location of the operation point can be chosen freely. It is shown that isotropy can be achieved only when the MP bears an equilateral triangle shape; however, the operation point need not be the centroid of this triangle. Moreover, for a MP with an acute-triangular shape, there can exist configurations that we call quasi isotropic, under which the condition number is close to unity, while the six rows of the Jacobian matrix are orthogonal; hence, the performance under such configurations is close to isotropy. This greatly increases the range of choices of the shape of the MP and the location of the operation point, which is required, e.g., when a tool is attached to the MP triangle.

The last topic is the kinematics, singularity, workspace analyses and the optimization for the second architecture, the 3-CCC PKM. It is found that, upon proper embodiment and

dimensioning, the 3-CCC PKM, with all actuators mounted on the base, exhibit interesting features, not found elsewhere. One is the existence of an isotropy locus, as opposed to isolated isotropy points in the workspace, thereby guaranteeing the accuracy and the homogeneity of the motion of the MP along the six directions of the motion space within a significantly large region of their workspace. The conditions leading to such a locus are discussed in depth; several typical isotropic designs are brought to the limelight. Moreover, the forwarddisplacement analysis reveals that the rotation and translation degrees of freedom of the MP are decoupled not only at the velocity level but also at the displacement level, significantly simplifying the analysis and control of this class of PKMs. Furthermore, the associated forward-displacement problem is formulated in such a way that it can be solved in closed form, which feature is rare in six-dof PKMs; hence, all the solutions can be obtained precisely and simultaneously, quite advantageous in simulation and control. Singularity is shown to be dependent only on the orientation of the MP, greatly simplifying its singularity analysis and detection. It is shown that the proposed robot will not encounter a singularity until the MP is rotated through a large angle. Finally, the proposed robot has a large workspace volume with a more regular shape when compared with the Stewart-Gough Platform.

The special features of the proposed architectures, especially the second, make them not only quite suitable for high-speed operations and the major application we target—shaking operations for inertia-parameter identification—but also in many other applications such as motion simulation, micro-manipulation, machining, and robotics-assisted surgery.

# 6.2 Recommendations for Future Research

Finally, some research directions are recommended for future work:

• For the design of the SDelta, alternative layouts of the three C-Drives can be explored, such as those with three vertical axes, three intersecting orthogonal axes or three skew orthogonal axes. As found during the analysis and optimization of the SDelta, there is a compromise to be made in the choice of the distance from the centroid of the MP to the BP plane between the requirement of high dexterity and large positioning workspace in the current design of the SDelta, though the dexterity is generally reasonably low. These

alternative layouts have the potential to provide a larger singularity-free orientation (and position) workspace together with a good dexterity.

- For the 3-CCC PKM, even though its workspace is already large, it can be further extended if we change the physical realization of the intermediate limbs. Currently, the three limbs are composed of three bars, which limits the stroke of the intermediate links. Other realizations of the limbs could be explored; for example, the links used by the Agile Eye [106] could be used here, upon replacing the R joints with C joints. This should increase the workspace volume of the proposed robot significantly. The same idea can be used for increasing the workspace volume of the SDelta, as well.
- This dissertation focuses on the kinematics of the robots under study. However, for the inertia-parameter identification task, the dynamics analysis of the proposed PKMs is also required; control algorithms must also be developed.
- According to the optimization results of the SDelta and the 3-CCC PKM, both allow infinitely many choices of the design parameters, thus leaving ample room for the optimization of other indices. Optimization should be conducted to maximize the dynamic performance of the PKMs, e.g., in terms of stiffness and frequency response.
- Due to the special features of the proposed structures, especially the second, they are promising in many other applications. These potential applications should be explored.

### REFERENCES

- [1] Griffis, M. and Duffy, J., "A forward displacement analysis of a class of stewart platforms," *Journal of Robotic Systems*, Vol. 6, No. 6, 1989, pp. 703–720.
- [2] Kong, X. and Gosselin, C., Type Synthesis of Parallel Mechanisms, Vol. 33, Springer, 2007.
- [3] Merlet, J.-P., Parallel Robots, Vol. 128, Springer, 2006.
- [4] Stewart, D., "A platform with six degrees of freedom," *Proceedings of the Institution of Mechanical Engineers*, Vol. 180, No. 1, 1965, pp. 371–386.
- [5] Fichter, F., "A Stewart platform-based manipulator general-theory and practical construction," *International Journal of Robotics Research*, Vol. 5, No. 2, 1986, pp. 157–182.
- [6] Podhorodeski, R. P. and Pittens, K. H., "A class of parallel manipulators based on kinematically simple branches," ASME Journal of Mechanical Design, Vol. 116, No. 3, 1994, pp. 908–914.
- [7] Yang, G., Chen, I. M., Chen, W., and Lin, W., "Kinematic design of a six-dof parallel-kinematics machine with decoupled-motion architecture," *IEEE Transactions on Robotics*, Vol. 20, No. 5, 2004, pp. 876–884.
- [8] Behi, F., "Kinematic analysis for a six-degree-of-freedom 3-PRPS parallel mechanism," *IEEE Journal of Robotics and Automation*, Vol. 4, No. 5, 1988, pp. 561–565.
- [9] Kim, J., Park, F. C., Ryu, S. J., Kim, J., Hwang, J. C., Park, C., and Iurascu, C. C., "Design and analysis of a redundantly actuated parallel mechanism for rapid machining," *IEEE Transactions on Robotics and Automation*, Vol. 17, No. 4, 2001, pp. 423–434.
- [10] Sorli, M., Ferraresi, C., Kolarski, M., Borovac, B., and Vukobratovic, M., "Mechanics of Turin parallel robot," *Mechanism and Machine Theory*, Vol. 32, No. 1, 1997, pp. 51–77.
- [11] Chen, C., Gayral, T., Caro, S., Chablat, D., Moroz, G., and Abeywardena, S., "A six degree of freedom epicyclic-parallel manipulator," *ASME Journal of Mechanisms and Robotics*, Vol. 4, No. 4, 2012, pp. 041011.

- [12] Liu, X. J. and Wang, J. S., "Some new parallel mechanisms containing the planar four-bar parallelogram," *International Journal of Robotics Research*, Vol. 22, No. 9, 2003, pp. 717–732.
- [13] Monsarrat, B. and Gosselin, C. M., "Workspace analysis and optimal design of a 3-leg 6-dof parallel platform mechanism," *IEEE Transactions on Robotics and Automation*, Vol. 19, No. 6, 2003, pp. 954–966.
- [14] Jin, Y., Chen, I. M., and Yang, G. L., "Kinematic design of a family of 6-dof partially decoupled parallel manipulators," *Mechanism and Machine Theory*, Vol. 44, No. 5, 2009, pp. 912–922.
- [15] Azulay, H., Mahmoodi, M., Zhao, R., Mills, J. K., and Benhabib, B., "Comparative analysis of a new 3xPPRS parallel kinematic mechanism," *Robotics and Computer-Integrated Manufacturing*, Vol. 30, No. 4, 2014, pp. 369–378.
- [16] Fu, J., Gao, F., Pan, Y., and Du, H., "Forward kinematics solutions of a special six-degree-of-freedom parallel manipulator with three limbs," Advances in Mechanical Engineering, Vol. 7, No. 5, 2015, pp. 1687814015582118.
- [17] Wu, Y. N. and Gosselin, C. M., "Synthesis of reactionless spatial 3-dof and 6-dof mechanisms without separate counter-rotations," *International Journal of Robotics Research*, Vol. 23, No. 6, 2004, pp. 625–642.
- [18] Harada, T., Friedlaender, T., and Angeles, J., "The development of an innovative two-DOF cylindrical drive: Design, analysis and preliminary tests," 2014 IEEE International Conference on Robotics and Automation (ICRA), May 31-June 5 2014, pp. 6338–6344.
- [19] Schedlinski, C. and Link, M., "A survey of current inertia parameter identification methods," *Mechanical systems and signal processing*, Vol. 15, No. 1, 2001, pp. 189–211.
- [20] Almeida, R. A. B., Urgueira, A. P. V., and Maia, N. M. M., "Identification of rigid body properties from vibration measurements," *Journal of Sound and Vibration*, Vol. 299, No. 4-5, 2007, pp. 884–899.
- [21] Almeida, R. A. B., Urgueira, A. P. V., and Maia, N. M. M., "Evaluation of the performance of three different methods used in the identification of rigid body properties," Shock and Vibration, Vol. 15, No. 3-4, 2008, pp. 467–479.
- [22] Barreto, J. and Muñoz, L. E., "Inertia parameter identification using a stewart platform," Robotics (ISR), 2010 41st International Symposium on and 2010 6th German Conference on Robotics (ROBOTIK), VDE, 2010, pp. 1–8.

- [23] Tian, T., Jiang, H., Tong, Z., He, J., and Huang, Q., "An inertial parameter identification method of eliminating system damping effect for a six-degree-of-freedom parallel manipulator," *Chinese Journal of Aeronautics*, Vol. 28, No. 2, 2015, pp. 582–592.
- [24] Raghavan, M., "The stewart platform of general geometry has 40 configurations," *ASME Journal of Mechanical Design*, Vol. 115, No. 2, 1993, pp. 277–282.
- [25] Wampler, C., Morgan, A., and Sommese, A., "Numerical continuation methods for solving polynomial systems arising in kinematics," *Journal of Mechanical Design*, Vol. 112, No. 1, 1990, pp. 59–68.
- [26] Faugère, J.-C. and Lazard, D., "Combinatorial classes of parallel manipulators," *Mechanism and Machine Theory*, Vol. 30, No. 6, 1995, pp. 765–776.
- [27] Innocenti, C. and Parenticastelli, V., "Direct position analysis of the Stewart platform mechanism," *Mechanism and Machine Theory*, Vol. 25, No. 6, 1990, pp. 611–621.
- [28] Gan, D., Dias, J., and Seneviratne, L., "Unified kinematics and optimal design of a 3rRPS metamorphic parallel mechanism with a reconfigurable revolute joint," *Mechanism and Machine Theory*, Vol. 96, 2016, pp. 239–254.
- [29] Merlet, J. P., "Solving the forward kinematics of a Gough-type parallel manipulator with interval analysis," *International Journal of Robotics Research*, Vol. 23, No. 3, 2004, pp. 221–235.
- [30] Boudreau, R. and Turkkan, N., "Solving the forward kinematics of parallel manipulators with a genetic algorithm," *Journal of Robotic Systems*, Vol. 13, No. 2, 1996, pp. 111–125.
- [31] McAree, P. R. and Daniel, R. W., "A fast, robust solution to the stewart platform forward kinematics," *Journal of Robotic Systems*, Vol. 13, No. 7, 1996, pp. 407–427.
- [32] Wang, Y. F., "A direct numerical solution to forward kinematics of general stewart-gough platforms," *Robotica*, Vol. 25, 2007, pp. 121–128.
- [33] Hunt, K. H., Kinematic Geometry of Mechanisms, Clarendon Press Oxford, 1978.
- [34] Kumar, V., "Instantaneous kinematics of parallel-chain robotic mechanisms," ASME Journal of Mechanical Design, Vol. 114, No. 3, 1992, pp. 349–358.
- [35] Merlet, J. P., "Singular configurations of parallel manipulators and Grassmann geometry," *International Journal of Robotics Research*, Vol. 8, No. 5, 1989, pp. 45–56.

- [36] Park, F. and Kim, J. W., "Singularity analysis of closed kinematic chains," *Journal of Mechanical Design*, Vol. 121, No. 1, 1999, pp. 32–38.
- [37] Zlatanov, D., Fenton, R. G., and Benhabib, B., "Identification and classification of the singular configurations of mechanisms," *Mechanism and Machine Theory*, Vol. 33, No. 6, 1998, pp. 743–760.
- [38] Bohigas, O., Zlatanov, D., Ros, L., Manubens, M., Porta, J. M., and IEEE, "Numerical computation of manipulator singularities," 2012 IEEE International Conference on Robotics and Automation (ICRA), 2012, pp. 1351–1358.
- [39] Notash, L., "Uncertainty configurations of parallel manipulators," *Mechanism and Machine Theory*, Vol. 33, No. 1-2, 1998, pp. 123–138.
- [40] Yang, G., Chen, I.-M., Lin, W., and Angeles, J., "Singularity analysis of three-legged parallel robots based on passive-joint velocities," *IEEE Transactions on Robotics and Automation*, Vol. 17, No. 4, 2001, pp. 413–422.
- [41] Kong, X. W. and Gosselin, C. M., "Uncertainty singularity analysis of parallel manipulators based on the instability analysis of structures," *International Journal of Robotics Research*, Vol. 20, No. 11, 2001, pp. 847–856.
- [42] Downing, D. M., Samuel, A. E., and Hunt, K. H., "Identification of the special configurations of the octahedral manipulator using the pure condition," *International Journal of Robotics Research*, Vol. 21, No. 2, 2002, pp. 147–159.
- [43] Ebert-Uphoff, I., Lee, J. K., and Lipkin, H., "Characteristic tetrahedron of wrench singularities for parallel manipulators with three legs," *Proceedings of the Institution of Mechanical Engineers Part C-Journal of Mechanical Engineering Science*, Vol. 216, No. 1, 2002, pp. 81–93.
- [44] Ben-Horin, P. and Shoham, M., "Singularity condition of six-degree-of-freedom three-legged parallel robots based on Grassmann-Cayley algebra," *IEEE Transactions on Robotics*, Vol. 22, No. 4, 2006, pp. 577–590.
- [45] Wen, J. T. and O'Brien, J. F., "Singularities in three-legged platform-type parallel mechanisms," *IEEE Transactions on Robotics and Automation*, Vol. 19, No. 4, 2003, pp. 720–726.
- [46] Ben-Horin, P. and Shoham, M., "Singularity analysis of a class of parallel robots based on Grassmann-Cayley algebra," *Mechanism and Machine Theory*, Vol. 41, No. 8, 2006, pp. 958–970.

- [47] Gosselin, C. and Angeles, J., "Singularity analysis of closed-loop kinematic chains," *IEEE Transactions on Robotics and Automation*, Vol. 6, No. 3, 1990, pp. 281–290.
- [48] Bonev, I. A. and Gosselin, C. M., "A geometric algorithm for the computation of the constant-orientation workspace of 6-rus parallel manipulators," *Proceedings of the 2000 ASME Design Engineering Technical Conferences*, 2000.
- [49] Masory, O. and Wang, J., "Workspace evaluation of Stewart platforms," *Advanced Robotics*, Vol. 9, No. 4, 1995, pp. 443–461.
- [50] Majid, M. Z. A., Huang, Z., and Yao, Y. L., "Workspace analysis of a six-degrees of freedom, three-prismatic-prismatic-spheric-revolute parallel manipulator," *Interna*tional Journal of Advanced Manufacturing Technology, Vol. 16, No. 6, 2000, pp. 441– 449.
- [51] Dash, A. K., Chen, I. M., Yeo, S. H., and Yang, G. L., "Workspace generation and planning singularity-free path for parallel manipulators," *Mechanism and Machine Theory*, Vol. 40, No. 7, 2005, pp. 776–805.
- [52] Jo, D. Y. and Haug, E. J., "Workspace analysis of closed loop mechanisms with unilaterial constraints," Advances in Design Automation 1989, September 17, 1989 September 21, 1989, Vol. 19-3 of American Society of Mechanical Engineers, Design Engineering Division (Publication) DE, Publ by American Soc of Mechanical Engineers (ASME), 1989, pp. 53-60.
- [53] Adkins, F. A. and Haug, E. J., "Operational envelope of a spatial Stewart platform," *ASME Journal of Mechanical Design*, Vol. 119, No. 2, 1997, pp. 330–332.
- [54] Haug, E., Luh, C.-M., Adkins, F., and Wang, J.-Y., "Numerical algorithms for mapping boundaries of manipulator workspaces," *ASME Journal of Mechanical Design*, Vol. 118, No. 2, 1996, pp. 228–234.
- [55] Gosselin, C., "Determination of the workspace of 6-dof parallel manipulators," ASME Journal of Mechanical Design, Vol. 112, No. 3, 1990, pp. 331–336.
- [56] Merlet, J.-P., "Geometrical determination of the workspace of a constrained parallel manipulator," Advances in Robot Kinematics, Ferrare, Italy, Sept., 1992, pp. 7–9.
- [57] Kumar, V., "Characterization of workspaces of parallel manipulators," ASME Journal of Mechanical Design, Vol. 114, No. 3, 1992, pp. 368–375.

- [58] Merlet, J. P., "Determination of 6d workspaces of Gough-type parallel manipulator and comparison between different geometries," *International Journal of Robotics Research*, Vol. 18, No. 9, 1999, pp. 902–916.
- [59] Bohigas, O., Manubens, M., and Ros, L., "A complete method for workspace boundary determination on general structure manipulators," *IEEE Transactions on Robotics*, Vol. 28, No. 5, 2012, pp. 993–1006.
- [60] Johnson, A., Kong, X., and Ritchie, J., "Determination of the workspace of a three-degrees-of-freedom parallel manipulator using a three-dimensional computer-aided-design software package and the concept of virtual chains," *Journal of Mechanisms and Robotics*, Vol. 8, No. 2, 2016, pp. 024501.
- [61] Snyman, J. A. and du Plessis, L. J., "An optimization approach to the determination of the boundaries of manipulator workspaces," ASME Journal of Mechanical Design, Vol. 122, No. 4, 2000, pp. 447–456.
- [62] Moreno, H. A., Saltaren, R., Carrera, I., Puglisi, L., and Aracil, R., "Performance indices for robotic manipulators: A review of the state of the art," Revista Iberoamericana de Automatica e Informatica Industrial, Vol. 9, No. 2, 2012, pp. 111–122.
- [63] Patel, S. and Sobh, T., "Manipulator Performance Measures—A Comprehensive Literature Survey," Journal of Intelligent & Robotic Systems, 2014, pp. 1–24.
- [64] Angeles, J., Fundamentals of Robotic Mechanical Systems. Theory, Methods, Algorithms, Springer, New York, 4th ed., 2014.
- [65] Angeles, J. and López-Cajún, C. S., "Kinematic isotropy and the conditioning index of serial robotic manipulators," *International Journal of Robotics Research*, Vol. 11, No. 6, 1992, pp. 560-571.
- [66] Salisbury, J. K. and Craig, J. J., "Articulated hands: Force control and kinematic issues," *The International Journal of Robotics Research*, Vol. 1, No. 1, 1982, pp. 4–17.
- [67] Khan, W. A. and Angeles, J., "The kinetostatic optimization of robotic manipulators: the inverse and the direct problems," *Journal of Mechanical Design*, Vol. 128, No. 1, 2006, pp. 168–178.
- [68] Zanganeh, K. E. and Angeles, J., "Kinematic isotropy and the optimum design of parallel manipulators," *International Journal of Robotics Research*, Vol. 16, No. 2, 1997, pp. 185–197.

- [69] Fassi, I., Legnani, G., and Tosi, D., "Geometrical conditions for the design of partial or full isotropic hexapods," *Journal of Field Robotics*, Vol. 22, No. 10, 2005, pp. 507–518.
- [70] Legnani, G., Fassi, I., Giberti, H., Cinquemani, S., and Tosi, D., "A new isotropic and decoupled 6-dof parallel manipulator," *Mechanism and Machine Theory*, Vol. 58, 2012, pp. 64–81.
- [71] Tsai, K. and Lee, T., "Synthesis of 6-DOF 3-chain isotropic parallel manipulators," Reconfigurable Mechanisms and Robots, 2009. ReMAR 2009. ASME/IFToMM International Conference on, IEEE, 2009, pp. 215–220.
- [72] Ben-Horin, R., Shoham, M., IEEE, IEEE, and IEEE, A six-degree-of-freedom parallel manipulator with three planarly actuated links, Iros '97 proceedings of the 1997 IEEE/rsj international conference on intelligent robot and systems: Innovative robotics for real-world applications, vols 1-3, 1996.
- [73] Kumagai, M. and Hollis, R. L., "Development and control of a three DOF spherical induction motor," *Robotics and Automation (ICRA)*, 2013 IEEE International Conference on, IEEE, 2013, pp. 1528–1533.
- [74] Clavel, R., "Device for the Movement and Positioning of an Element in Space," Dec. 11 1990, US Patent 4,976,582.
- [75] Li, W. and Angeles, J., "A Novel Three-Loop Parallel Robot With Full Mobility: Kinematics, Singularity, Workspace, and Dexterity Analysis," ASME Journal of Mechanisms and Robotics, Vol. 9, No. 5, 2017, pp. 051003–051003–10.
- [76] French, M., Form, structure and mechanism, Springer-Verlag, New York, 1992.
- [77] Hunt, K. H., "Special configurations of robot-arms via screw theory," *Robotica*, Vol. 4, 1986, pp. 171–179.
- [78] Gibson, C. G. and Hunt, K. H., "Geometry of screw systems—1. Screws genesis and geometry," *Mechanism and Machine Theory*, Vol. 25, No. 1, 1990, pp. 1–10.
- [79] Nanua, P., Waldron, K. J., and Murthy, V., "Direct kinematic solution of a Stewart platform," *IEEE Transactions on Robotics and Automation*, Vol. 6, No. 4, 1990, pp. 438–444.
- [80] Parenti-Castelli, V. and Innocenti, C., "Direct displacement analysis for some classes of spatial parallel mechanisms," *Proc. of the 8th CISM-IFToMM Symp. on Theory and Practice of Robots and Manipulators*, 1990, pp. 126–133.

- [81] Salmon, G., Higher algebra, Chelsea Publishing Co., New York, 5th ed., 1964.
- [82] Di Gregorio, R., "Analytic formulation of the 6-3 fully-parallel manipulator's singularity determination," *Robotica*, Vol. 19, No. 6, 2001, pp. 663–667.
- [83] FarzanehKaloorazi, M., Masouleh, M. T., and Caro, S., "Collision-free workspace of parallel mechanisms based on an interval analysis approach," *Robotica*, 2016, pp. 1–14.
- [84] Khan, W. A. and Angeles, J., "A novel paradigm for the qualitative synthesis of simple kinematic chains based on complexity measures," *Journal of Mechanisms and Robotics*, Vol. 3, No. 3, 2011, pp. 031010.
- [85] Yoshikawa, T., "Manipulability of robotic mechanisms," The International Journal of Robotics Research, Vol. 4, No. 2, 1985, pp. 3–9.
- [86] Dahlquist, G. and Björck, Å., Numerical Methods, Prentice-Hall, Englewood Cliffs, NJ, 1974.
- [87] Tsai, K. Y. and Huang, K. D., "The design of isotropic 6-dof parallel manipulators using isotropy generators," Mechanism and Machine Theory, Vol. 38, No. 11, 2003, pp. 1199–1214.
- [88] Tsai, K. Y., Lee, T. K., and Jang, Y. S., "A new class of isotropic generators for developing 6-DOF isotropic manipulators," *Robotica*, Vol. 26, 2008, pp. 619–625.
- [89] Roth, B., "Screws, motors, and wrenches that cannot be bought in a hardware store," Robotics Research: The First International Symposium, Vol. 8, Chapter, 1984, pp. 679–693.
- [90] Klein, C. A. and Miklos, T. A., "Spatial robotic isotropy," *The International journal of robotics research*, Vol. 10, No. 4, 1991, pp. 426–437.
- [91] Li, W. and Angeles, J., "Full-Mobility Three-CCC Parallel-Kinematics Machines: Kinematics and Isotropic Design," *Journal of Mechanisms and Robotics*, Vol. 10, No. 1, 2018, pp. 011011–011011–11.
- [92] Daniali, H. R. M., Zsombor-Murray, P. J., and Angeles, J., "The kinematics of spatial double-triangular parallel manipulators," ASME Journal of Mechanical Design, Vol. 117, No. 4, 1995, pp. 658–661.
- [93] Daniali, H. M., Zsombor-Murray, P., and Angeles, J., "Direct kinematics of double-triangular parallel manipulators," *Mathematica Pannonica*, Vol. 79, 1996, pp. 96.

- [94] Daniali, H. R. M., Contributions to the kinematic synthesis of parallel manipulators, Ph.D. thesis, McGill University, 1996.
- [95] Gan, D. M., Liao, Q. Z., Dai, J. S., and Wei, S. M., "Design and kinematics analysis of a new 3CCC parallel mechanism," *Robotica*, Vol. 28, 2010, pp. 1065–1072.
- [96] Toz, M. and Kucuk, S., "Dimensional optimization of 6-DOF 3-CCC type asymmetric parallel manipulator," *Advanced Robotics*, Vol. 28, No. 9, 2014, pp. 625–637.
- [97] Duffy, J., Analysis of mechanisms and robot manipulators, Edward Arnold London, 1980.
- [98] Brand, L., Advanced Calculus: an introduction to classical analysis, Courier Corporation, 2006.
- [99] Gosselin, C. M., Sefrioui, J., and Richard, M. J., "On The Direct Kinematics of 3-degree-of-freedom Parallel Manipulators with a Coplanar Platform," *Journal of Mechanical Design*, Vol. 116, No. 2, 1994, pp. 587–593.
- [100] Gosselin, C. and Gagné, M., "A closed-form solution for the direct kinematics of a special class of spherical three-degree-of-freedom parallel manipulators," Computational KinematicsâĂŹ 95, Springer, 1995, pp. 231–240.
- [101] Gosselin, C. M., Sefrioui, J., and Richard, M. J., "On the Direct Kinematics of Spherical Three-Degree-of-Freedom Parallel Manipulators of General Architecture," *Journal of Mechanical Design*, Vol. 116, No. 2, 1994, pp. 594–598.
- [102] Selby, S. M., "Standard mathematical tables," Standard mathematical tables, Chemical Rubber, 1970.
- [103] Angeles, J., "The application of dual algebra to kinematic analysis," Computational methods in mechanical systems, Springer, 1998, pp. 3–32.
- [104] Huang, Z., Zhao, Y., and Zhao, T., Advanced Spatial Mechanism Theory (in Chinese), Higher Education Press, Beijing, 2006.
- [105] Jiang, Q. M. and Gosselin, C. M., "Determination of the maximal singularity-free orientation workspace for the Gough-Stewart platform," *Mechanism and Machine Theory*, Vol. 44, No. 6, 2009, pp. 1281–1293.
- [106] Bonev, I. A. and Gosselin, C. M., "Analytical determination of the workspace of symmetrical spherical parallel mechanisms," *IEEE Transactions on Robotics*, Vol. 22, No. 5, 2006, pp. 1011–1017.

# APPENDICES

# A.1 The Three-Cosine Theorem

The three-cosine theorem—needed for deriving Eq. (4.26)—is recalled below for quick reference. Let us assume that a line  $\mathcal{L}$  and a plane  $\Pi$  intersect at point O, as shown in Fig. A.1; moreover, the orthogonal projection of  $\mathcal{L}$  onto  $\Pi$  is  $\mathcal{L}'$ , while  $\mathcal{M}$  is an arbitrary line in  $\Pi$  that passes through O. Finally, the angle between  $\mathcal{L}'$  and  $\mathcal{M}$  is denoted  $\alpha_1$ , while the angle between  $\mathcal{L}$  and  $\mathcal{L}'$  and that between  $\mathcal{L}$  and  $\mathcal{M}$  are denoted  $\alpha_2$  and  $\alpha_3$ , respectively. Then, the three-cosine theorem states that these three angles obey the relation

$$\cos \alpha_3 = \cos \alpha_1 \cos \alpha_2 \tag{A.1}$$

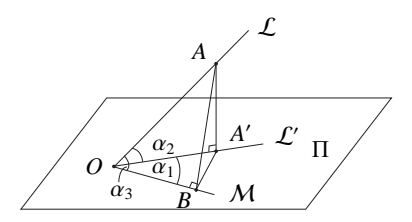


Figure A.1: The illustration of the three-cosine theorem

# A.2 The Coefficients of the Resultant Polynomial for the Forward-Kinematics of the 3-CCC PKM

The derivation of the coefficients of Eq. (5.90) is provided below. Firstly, we notice that Eq. (5.90) is obtained upon dividing both sides of Eq. (5.89) by  $\sin \alpha_1^4$ ; moreover, all the

factors of Eq. (5.89)— $\{H_i\}_0^2$ , N and D—are homogeneous in  $\alpha_1$ . Hence, if we introduce the substitution

$$\sin \alpha_1 = 1, \cos \alpha_1 = \rho \tag{A.2}$$

in Eqs. (5.82) and (5.84), and revise the expressions for  $\{G_i\}_0^2$ ,  $\{H_i\}_0^2$ , N and D accordingly, then Eq. (5.89) naturally becomes a quartic equation in  $\rho$ , which is the same as Eq. (5.90) using the procedure described in subsection 5.3.1. Hence, we adopt this substitution to simplify the derivation.

Firstly, the coefficients given in Eqs. (5.82) and (5.84) are rewritten as

$$E_{s2} = \epsilon_1, \ E_{c2} = \epsilon_2, \ E_{s1} = \epsilon_3, \ E_{c1} = \epsilon_4, \ E_0 = \epsilon_5 \rho^2 + \epsilon_6, \ F_1 = \varphi_1, \ F_0 = \varphi_2 \rho + \varphi_3$$
 (A.3)

Then,  $\{G_i\}_0^2$  and  $\{H_i\}_0^2$  can be obtained as

$$G_{2} = \epsilon_{2} - \epsilon_{1} \equiv \lambda_{1}, G_{1} = \varphi_{1}\epsilon_{3} + \epsilon_{4} \equiv \lambda_{2}$$

$$G_{0} = (\epsilon_{1} + \epsilon_{5}) \rho^{2} + \varphi_{2}\epsilon_{3}\rho + \varphi_{3}\epsilon_{3} + \epsilon_{1} + \epsilon_{6} \equiv \lambda_{3}\rho^{2} + \lambda_{4}\rho + \lambda_{5}$$

$$H_{2} = \varphi_{1}^{2} + 1 \equiv \mu_{1}, H_{1} = 2\varphi_{1}\varphi_{2}\rho + 2\varphi_{1}\varphi_{3} \equiv \mu_{2}\rho + \mu_{3}$$

$$H_{0} = (\varphi_{2}^{2} - 1) \rho^{2} + 2\varphi_{2}\varphi_{3}\rho + \varphi_{3}^{2} - 1 \equiv \mu_{4}\rho^{2} + \mu_{5}\rho + \mu_{6}$$

$$(A.4)$$

while N and D can be derived as

$$N = (\lambda_1 \mu_4 - \lambda_3 \mu_1) \rho^2 + (\lambda_1 \mu_5 - \lambda_4 \mu_1) \rho - \lambda_5 \mu_1 + \lambda_1 \mu_6 \equiv \nu_2 \rho^2 + \nu_1 \rho + \nu_0$$

$$D = -\lambda_1 \mu_2 \rho + \lambda_2 \mu_1 - \lambda_1 \mu_3 \equiv \sigma_1 \rho + \sigma_0$$
(A.5)

where  $\{\lambda_i\}_1^5$ ,  $\{\mu_i\}_1^6$ ,  $\{\nu_i\}_0^2$  and  $\{\sigma_i\}_0^1$  are intermediate results introduced to reduce computational cost. Finally, the coefficients of Eq. (5.90) can be derived as

$$\zeta_{4} = \mu_{2}\nu_{2}\sigma_{1} + \mu_{1}\nu_{2}^{2} + \mu_{4}\sigma_{1}^{2}, \quad \zeta_{3} = \mu_{2}\nu_{1}\sigma_{1} + \mu_{3}\nu_{2}\sigma_{1} + \mu_{2}\nu_{2}\sigma_{0} + 2\mu_{1}\nu_{1}\nu_{2} + \mu_{5}\sigma_{1}^{2} + 2\mu_{4}\sigma_{0}\sigma_{1}$$

$$\zeta_{2} = \mu_{2}\nu_{1}\sigma_{0} + \mu_{3}\nu_{1}\sigma_{1} + \mu_{3}\nu_{2}\sigma_{0} + \mu_{2}\nu_{0}\sigma_{1} + \mu_{1}\nu_{1}^{2} + 2\mu_{1}\nu_{0}\nu_{2} + \mu_{4}\sigma_{0}^{2} + \mu_{6}\sigma_{1}^{2} + 2\mu_{5}\sigma_{0}\sigma_{1}$$

$$\zeta_{1} = \mu_{2}\nu_{0}\sigma_{0} + \mu_{3}\nu_{1}\sigma_{0} + \mu_{3}\nu_{0}\sigma_{1} + 2\mu_{1}\nu_{0}\nu_{1} + \mu_{5}\sigma_{0}^{2} + 2\mu_{6}\sigma_{1}\sigma_{0}, \quad \zeta_{0} = \mu_{3}\nu_{0}\sigma_{0} + \mu_{1}\nu_{0}^{2} + \mu_{6}\sigma_{0}^{2}$$
(A.6)